Aalborg Universitet

AALBORG UNIVERSITY
DENMARK

Multi-Cell Uplink Radio Resource Management. A LTE Case Study

Zheng, Naizheng

Publication date:
2011

Document Version
Publisher's PDF, also known as Version of record

[Link to publication from Aalborg University](#)

Citation for published version (APA):
Zheng, N. (2011). *Multi-Cell Uplink Radio Resource Management. A LTE Case Study*. Department of Electronic Systems, Aalborg University.

Multi-Cell Uplink Radio Resource Management

A LTE Case Study

Naizheng Zheng

PhD Thesis
2011, Ålborg, Denmark

Supervisors:
Professor Preben E. Mogensen, PhD
Aalborg University, Denmark

Co-supervisors:
Jeroen Wigard, PhD
Nokia Siemens Networks, Aalborg, Denmark
Klaus I. Pedersen, PhD
Nokia Siemens Networks, Aalborg, Denmark
Istvan Z. Kovacs, PhD
Nokia Siemens Networks, Aalborg, Denmark

Abstract

Long Term Evolution (LTE) is the next generation mobile broad-band network and its standardization has been finalized by 3rd Generation Partnership Project (3GPP) in Release 8 (Rel'8). In order to ensure the long-term competitiveness for the next decade and beyond, the study item on LTE-Advanced (LTE-A) has been started as the next evolution step to investigate how LTE can become a real Fourth Generation (4G) network.

This study explores the enhancement of LTE network in the Uplink (UL) direction at system level. In the earlier literature, most of the studies were focused on the single-cell Radio Resource Management (RRM) optimization, where the performance of multi-cell RRM is being less investigated. The inter-cell interference is the major concern in the LTE network. By exploiting the multi-cell solution, the impact of inter-cell interference can be limited, and the overall network performances can be further enhanced.

Antenna downtilting is an efficient way to reduce the inter-cell interference in both UL and Downlink (DL) direction. With a certain optimal antenna downtilting angle, the received signal power is improved within its own serving cell and the inter-cell interference to the other neighboring cells is also reduced. However, if the antenna is downtilted too aggressively, it may result in insufficient coverage and mobility support. In this study, the mechanical antenna downtilting is firstly investigated in the UL LTE and the interaction of antenna downtilting together with UL Fractional Power Control (FPC) is also analyzed.

Based on the antenna downtilting study, it can be foreseen that the User Equipment (UE)s who are close to the cell-border still suffer from the degradation of high level of inter-cell interference and the low signal quality due to the propagation loss. To solve this problem, the Coordinated Multi-Point (CoMP) solution is investigated. CoMP is an advanced technique for interference mitigation which is proposed in the LTE-A as one of the features to further reduce

the impact of inter-cell interference. Theoretically by applying CoMP, the inter-cell interference could be converted into the useful signal and being completely eliminated. For the UL LTE application, the UL CoMP in the form of both macro diversity reception and joint reception are investigated in this study. The joint effort of UL CoMP reception together with Interference Cancellation (IC) technique and UL FPC are thoroughly analyzed. Besides, the multi-cell Coordinated Packet Scheduling (CPS) is also investigated in this study based on the UL CoMP joint reception, where a simple CPS algorithm is studied for a cluster of neighboring cells to jointly allocate the UEs served in their cells.

Handover (HO) is another effective technique to mitigate the inter-cell interference. A simple HO decision algorithm is being proposed in this study by utilizing Reference Signal Received Power (RSRP) measurement in the DL LTE. The performance is compared with the traditional Power Budget (PBGT) algorithm, where the proposed integrator algorithm has the advantages of requiring less parameter setup for the realistic application.

Dansk Resumé

[1]Long Term Evolution (LTE) er seneste version af mobilt bredbånd, hvor standardisering af første version af 3rd Generation Partnership Project (3GPP) netop er afsluttet- kaldet 3GPP Version 8. For at sikre en fortsat konkurrence inden for bredbånds standard, har 3GPP startet arbejdet med LTE-Advanced (LTE-A), som i nogle tilfælde også kaldes Fourth Generation (4G).

Dette studium har fokus på systemforbedringer og ydeevne af LTE og LTE-A af linket fra mobilen til antennemasten. I den eksisterende litteratur har tidligere studier primært fokuseret på undersøgelser med uafhængig "radio resource management (RRM)" per mobil celle, hvorfor multi-celle RRM aspekter stadig kræver nye studier. Specielt er interferensen mellem celler vigtig for LTE. Det er f.eks muligt at begrænse den totale interferens i et netværk ved at udnytte brugen af multi-celle RRM.

Antenne tilting er en effektiv metode til at begrænse effekten af interferens mellem celler. Ved at optimere antenne tilt vinklen er det muligt at optimere den modtagne effekt fra de ønskede mobiler, mens interferensen fra andre mobiler minimeres. Men hvis antenne tilt vinklen bliver for stor, opnås den modsatte effekt, hvor der opnås et tab i stedet for en gevinst. I dette studium er mekanisk antenne tilt blevet undersøgt for LTE i kombination med effektiv kontrol af mobilers transmissionseffekt.

Baseret på førnævnte antenna tilt studier blev det observeret, at mobiler på grænsen mellem to celler typisk oplever meget interferens. For at løse dette problem er løsninger baseret på multi-celle koordineret modtagelse af signaler fra mobiler undersøgt - også kaldet CoMP med engelsk forkortelse. CoMP er en forholdsvis avanceret teknik, som også undersøges for mulig standardisering til LTE-A. Brugen af CoMP kombineret med avancerede modtagere med aktiv

---

[1]Translated by Klaus I. Pedersen, Nokia Siemens Network (NSN) - Aalborg, Denmark

interferens-undertrykkelse og koordinerede transmissioner i naboceller er blevet undersøgt. Algoritmer af forskellig kompleksitet er blevet udviklet og undersøgt, og resultater er genereret, som viser fordele ved brug af sådanne teknikker.

Brug af optimeret "Handover (HO)" er en anden effektiv teknik, som kan bruges til at kontrollere interferensen mellem naboceller. En simpel HO beslutningsalgoritme er foreslået i dette studium, baseret på mobil-målinger af modtaget effekt fra forskellige celler. De opnåede resultater viser, at den foreslåede algoritme er attraktiv, da den har et mindre antal parametre, som skal konfigureres i forhold til mange andre algoritmer i litteraturen.

Preface and Acknowledgments

This dissertation is the result of a three years research project carried out at the Radio Access Technology (RATE) section, Institute of Electronic Systems (ES), Aalborg University, Denmark. The study is under the supervision and guidance of Professor Preben E. Mogensen (Aalborg University, Denmark), Dr. Jeroen Wigard (Nokia Siemens Networks, Aalborg, Denmark), Dr. Klaus I. Pedersen (Nokia Siemens Networks, Aalborg, Denmark) and Dr. Istvan Z. Kovacs (Nokia Siemens Networks, Aalborg, Denmark).

First, I would like to thank my supervisors for their advice, guidance and patience. It has been an honor for me to work with a group of supervisors who are not only technically knowledgeable, but also very understanding when it comes to personal issues. Every one of them has contributed significantly to this work.

Further, I would like to thank the colleagues and secretaries from both Aalborg University and Nokia Siemens Networks Aalborg. Thanks for their inspiring discussions, friendly assistance and collaboration. Our friendship will be marked in my memory forever.

Of course, the current work cannot be accomplished without the strong support and understanding from my parents, my parents in-law, my wife Qi Zhao, my lovely daughters DanYu Zheng and XiYu Zheng. Thanks for their constant love and affection.

Naizheng Zheng
Aalborg, Denmark, December 2010

Abbreviations

Abbreviations used in the thesis are listed below for quick reference. The abbreviations are additionally defined at their first occurrence.

Acronyms

2-D	2-Dimensional
2G	2nd Generation
3-D	3-Dimensional
3G	3rd Generation
3GPP	3rd Generation Partnership Project
4G	Fourth Generation
aGW	Access Gateway
AC	Admission Control
ACK	Acknowledgement
AMC	Adaptive Modulation and Coding
AMI	Average Mutual Information
ARPU	Average Revenue per User
ARQ	Automatic Repeat ReQuest
ATB	Adaptive Transmission Bandwidth
AVI	Actual Value Interface
AWGN	Additive White Gaussian Noise
BLER	BLock Error Rate

BS	Base Station
CA	Carrier Aggregation
CAPEX	Capital Expenditures
CAZAC	Constant Amplitude Zero Auto-Correlation
CB	Coordinated Beamforming
CC	Chase Combining
CDMA	Code Division Multiple Access
CDF	Cumulative Density Function
CLPC	Close-Loop fractional Power Control
CN	Core Network
CoMP	Coordinated Multi-Point
CP	Cyclic Prefix
CPS	Coordinated Packet Scheduling
CRC	Cyclic Redundancy Check
CSI	Channel State Information
CWS	Combining Window Size
dB	Decibel
dBm	Decibel relative to $1\,mW$
DL	Downlink
DMRS	DeModulation Reference Signal
eNB	Evolved NodeB
EESM	Exponential Effective SINR Metric
EGC	Equal Gain Combining
EPS	Evolved Packet System
FDPS	Frequency-Domain Packet Scheduling
FFT	Fast Fourier Transform
FTB	Fixed Transmission Bandwidth
FPC	Fractional Power Control
GA	Gaussian Approximation
GSM	Global System for Mobile Communication
HARQ	Hybrid Automatic Repeat reQuest
HO	Handover
HOM	Handover Margin
HPBW	Half Power Beam Width
HSDPA	High-Speed Downlink Packet Access
HSPA	High-Speed Packet Access

HSUPA	High-Speed Uplink Packet Access
IC	Interference Cancellation
ICIC	Inter-Cell Interference Coordination
IIR	Infinite Impulse Response
IMT-**A**	International Mobile Telecommunication-Advanced
IoT	Interference over Thermal noise
IP	Internet Protocol
IPS	Independent Packet Scheduling
IR	Incremental Redundancy
ISD	Inter-Site Distance
ITU	International Telecommunication Union
JP	Joint Processing
KPI	Key Performance Indicator
LA	Link Adaptation
LLR	Log Likelihood Ratio
LOS	Line of Sight
LTE	Long Term Evolution
LTE-**A**	LTE-Advanced
ms	Millisecond
MAC	Medium Access Control
MAI	Multiple Access Interference
MCS	Modulation and Coding Scheme
MIMO	Multiple Input Multiple Output
MISO	Multiple Input Single Output
ML	Maximum-Likelihood
MME	Mobility Management Entity
MMSE	Minimum Mean Square Error
MRC	Maximal Ratio Combining
MU-**MIMO**	Multi-User MIMO
MUD	Multi-User Detection
NACK	Negative Acknowledgement
OFDM	Orthogonal Frequency Division Multiplexing
OFDMA	Orthogonal Frequency Division Multiple Access
OI	Overload Indicator
OLLA	Outer Loop Link Adaptation
OLPC	Open-Loop fractional Power Control

OPEX	Operating Expenses
PAPR	Peak-to-Average Power Ratio
PBGT	Power Budget
PC	Power Control
PDCP	Packet Data Convergence Protocol
PDU	Protocol Data Unit
PF	Proportional Fair
PHY	Physical Layer
PIC	Parallel Interference Cancellation
PL	Path Loss
PRB	Physical Resource Block
PS	Packet Scheduling
PUSCH	Physical Uplink Shared Channel
RAT	Radio Access Technology
RoF	Radio over Fiber
RS	Reference Symbol
QoS	Quality of Service
QPSK	Quadrature Phase Shift Keying
RAN	Radio Access Network
Rel'8	Release 8
RLC	Radio Link Control
RN	Relaying Nodes
RR	Round Robin
RRC	Radio Resource Control
RRM	Radio Resource Management
RS	Reference Symbols
RSRP	Reference Signal Received Power
RTT	Round-Trip Time
SAE	System Architecture Evolution
SC	Selection Combining
SC-FDMA	Single-Carrier Frequency Division Multiple Access
SIC	Successive Interference Cancellation
SIMO	Single Input Multiple Output
SNR	Signal-to-Noise Ratio
SU-MIMO	Single-User MIMO
SINR	Signal-to-Interference-plus-Noise Ratio

SNR	Signal-to-Noise Ratio
SRS	Sounding Reference Signal
TDPS	Time-Domain Packet Scheduling
TTI	Transmission Time Interval
TTT	Time-to-Trigger
TU	Typical Urban
UE	User Equipment
UL	Uplink
UMTS	Universal Mobile Telecommunications System
UTRAN	Universal Terrestrial Radio Access Network
VoIP	Voice over Internet Protocol
WCDMA	Wideband Code Division Multiple Access

Symbol Notations

A	Gain of Antenna Radiation Pattern
a	Receive Antenna Index
b	Index of Serving eNB
D	Distance to Boresight Cell Border
d	Distance between BS and UE
$\mathbf{f_c}$	Carrier Frequency
H	Channel Matrix
h	Complex Channel Gain
$\mathbf{h_{BS}}$	Height of Base Station
$\mathbf{h_{UE}}$	Height of User Equipment
I	Received Interference Power
$\mathbf{I_{PSD}}$	Interference Spectral Density
$\mathbf{\bar{I}}$	Average of Received Interference Power
i	Index of User Equipment
L	UE Measured PL from DL RS
$\mathbf{N_t}$	Number of Transmit Antenna
$\mathbf{N_r}$	Number of Receive Antenna
$\mathbf{N_{HARQ}}$	Number of HARQ Transmissions
$\mathbf{N_{i\&q}}$	Number of In-phase and Quadrature Representation
$\mathbf{N_{PRB}}$	Number of Assigned PRB to one User

$\mathbf{N_{prb}}$	Thermal Noise of one PRB
$\mathbf{N_{PSD}}$	Noise Spectral Density
$\mathbf{N_{resolution}}$	Number of Quantized Resolution
$\mathbf{N_{subcarrier}}$	Number of OFDM Sub-carrier per PRB
$\mathbf{N_{symbol}}$	Number of OFDM Symbol per PRB
$\mathbf{N_u}$	Number of Users Transmitting on the same PRB
$\mathbf{P_{tx}}$	UE Transmission Power
$\mathbf{P_{rx}}$	eNB Received Power
$\mathbf{P_{max}}$	Maximum UE Transmission Power
$\mathbf{P_0}$	Cell or User-specific Parameter for Fractional Power Control
$\mathbf{p}$	Index of Sounded PRB
$\mathbf{q}$	q-th HARQ Transmission
$\mathbf{R}$	Set of Simultaneously Sounded PRBs or CSI Resolution
$\mathbf{r}$	Received Signal Vector
$\mathbf{r'}$	Element of CSI Resolution
$\mathbf{S}$	Received Power of Sounding Reference Signal
$\mathbf{s}$	Transmit Signal
$\mathbf{T}$	Acknowledged Throughput
$\widehat{T}$	Estimated Achievable Throughput
$\overline{T}$	Averaged Acknowledge Throughput
$\mathbf{t}$	Index of Instant Time
$\mathbf{v}$	Index of User Equipment
$\mathbf{W}$	Detector Weight
$\mathbf{x}$	x-axis
$\mathbf{y}$	y-axis
$\mathbf{z}$	z-axis
α	Cell or User-specific PL Compensation Factor
ρ	CSI Forgetting Factor
ξ	PF Filter Coefficient
ϵ	CSI Measurement Error
σ_{CSI}	Standard Deviation of CSI Measurement Error
Δ_i	CLPC Commands Signaled from eNB to UE
Δ_{mcs}	MCS-dependent Power Offset set by eNB
ϕ	Angle between Direction of Interest and Antenna Boresight
θ	Angle Deviation from the Horizontal Plane
ω	Interference plus Noise Vector
γ	SINR Output

Contents

Thesis Introduction

The purpose of this initial chapter is to give an overview of the whole PhD study and the thesis. In Section 1.1, an overview of 3G cellular communication system is presented. As the main focus in this PhD study, the Long Term Evolution (LTE) network is described in Section 1.2. The requirements for LTE-Advanced network are defined and proposed key technologies to achieve them are discussed in Section 1.3. Interference management is one of the important issues for further optimizing the LTE network and it is discussed in Section 1.4. In Section 1.5, the objectives and scope of this PhD study are specified while the employed scientific method is described in Section 1.6. The novelty and main contributions of the PhD study are described in Section 1.7, and finally the organization of the thesis is presented.

1.1 Preliminaries

Nowadays, more and more people become mobile subscribers. The global economy recession did not stop people from using the mobile communication services. Until the year 2009, the number of worldwide mobile subscribers has reached 4.3 billion and it is estimated that there will be 5.8 billion mobile subscribers by 2013 globally [1]. Mobile phones have become an important part of everybody's daily live. Voice service through the mobile phone is not the only function anymore. In recent years, more and more mobile subscribers start checking their email, surfing the web, downloading music and even playing real-time games on their wireless devices [2]. So there is a rapid growth in demand of broadband wireless data service. The operator assessment in [3] has shown that data traffic has increased to a level more than 10 times over the voice traffic in the year 2009 as shown in Figure 1.1 and the analyst forecast report shows that, because of
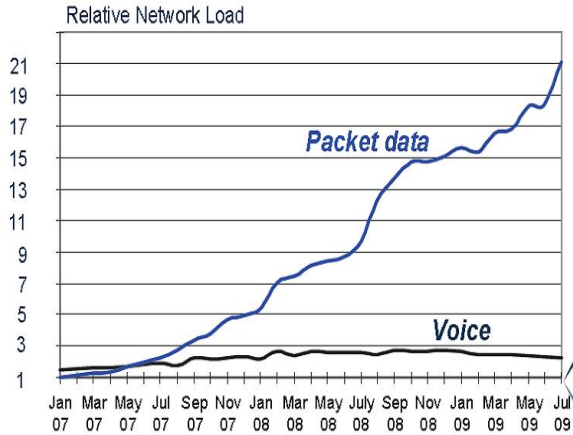
Figure 1.1: Mobile Traffic Growth [3]

increasing competition and price reduction, the declines in mobile voice Average Revenue per User (ARPU) will continue in the year 2010. However, the progress in broadband data service will ensure that the total ARPU grows [4]. In order to meet the requirements of serving mobile subscribers, the mobile operators must develop their short and long term technology strategies based on new and innovative mobile data services.

Right now in the wireless industry, there are several paths or solutions which can lead the mobile operator to the future mobile broadband. Each mobile operator will take one path over the other depending on their own business strategies and timetables. But one ultimate goal has been agreed that the new technology should be an efficient Internet Protocol (IP) wireless network capable of supporting voice, video, messaging and data services [5]. LTE is such a promising technology which can meet the needs of future IP-based services [6], and more and more mobile operators have converged on the LTE technology, as they believe that LTE will offer them and their customers the most benefits and the best interests.

LTE evolved from the first 3rd Generation (3G) network, Universal Mobile Telecommunications System (UMTS), which comes after the 2nd Generation (2G) Global System for Mobile Communication (GSM) specifications and is standardized by the 3GPP since 1998 [7]. In the first release (Release 99), a new Radio Access Network (RAN), which is called Universal Terrestrial Radio Access Network (UTRAN), was introduced together with a new air interface called Wideband Code Division Multiple Access (WCDMA). WCDMA is a wideband spread spectrum air interface that utilizes code division multiple access, and sometimes it is used as a synonym for UMTS [7]. As shown in Figure 1.2,
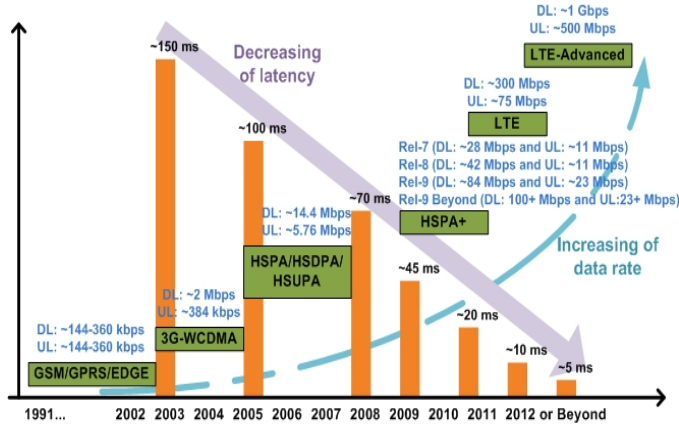
Figure 1.2: Evolution of 3GPP Family

WCDMA enables DL peak data rate of 2 Mbit/s and UL peak data rate of 384 kbit/s with latency of 150 ms on a common 5 MHz bandwidth. In order to preserve the future competitiveness compared to the other technologies, the 3GPP standardization body started the evolution of WCDMA technology by introducing the 3.5G network High-Speed Packet Access (HSPA), which includes the DL evolution High-Speed Downlink Packet Access (HSDPA) in Release 5 and the UL evolution High-Speed Uplink Packet Access (HSUPA) in Release 6 [8]. HSDPA improves the DL peak data rate to 14.4 Mbit/s and reduces the network latency to around 100 ms. HSUPA further enhances the UL peak data rate to 5.7 Mbit/s and reduce another 30 ms network latency. The continuing evolution of HSPA in Release 7, Release 8, Release 9 and beyond[1] named HSPA+ or HSPA evolved, provides even higher data rate, lower latency and higher spectral efficiency. As shown in Figure 1.2, HSPA+ in Release 9 can achieve the DL peak data rate up to 84 Mbit/s and UL peak data rate of 23 Mbit/s on 10 MHz bandwidth. Meanwhile, the round trip time latency is reduced below 50 ms [10].

HSPA+ and LTE will probably coexist in parallel for many years. Many UMTS or HSPA operators have decided to use the HSPA+ as an upgrade path to the future LTE, because the HSPA+ can deliver remarkable data rate to meet

---

[1]HSPA+ in Rel-8 reaches 42 Mbit/s by combining 2x2 Multiple Input Multiple Output (MIMO) and high order modulation (64QAM) in 5 MHz bandwidth or by utilizing high order modulation and multi-carrier in 10 MHz bandwidth. HSPA+ in Rel-9 combines multi-carrier and MIMO in 10 MHz to reach 84 Mbit/s peak rates. Uplink multi-carrier double the uplink peak data rate to 23 Mbit/s. For HSPA+ in Releases beyond Rel-9, it may expand multi-carrier to 20 MHz and utilize combinations of multi-carrier and MIMO to reach peak data rates exceeding 100 Mbit/s in the DL and 23 Mbit/s in the UL [9]

the current needs of advanced mobile subscribers with simple, affordable, and incremental cost to the existing HSPA network. However, when the mobile operators reach their network capacity limits with all the available technologies, the deployment of the LTE network is definitely required in order to provide much higher data capacity in the future. [4][11].

1.2   Long Term Evolution - LTE

LTE was firstly introduced and specified by the 3GPP in Release 8. It enables the mobile operators to operate network in scalable bandwidth up to 20 MHz, i.e. 1.4, 3, 5, 10, 15 and 20 MHz [12][13]. With 20 MHz bandwidth, LTE enables the peak data rates exceeding 300 Mbit/s (4x4 MIMO) in the downlink and 75 Mbit/s (64 QAM) in the uplink with significantly reduced round trip delay around 10 ms [14][15]. In order to achieve such a challenging improvement, LTE introduces a new radio access technology together with MIMO technology in the physical layer and a simple radio network architecture for the higher layer [16].

Orthogonal Frequency Division Multiple Access (OFDMA) has been selected as the radio interface in the DL LTE [17]. OFDMA can be regarded as an extension of the OFDM to the multiuser scenarios, in which, instead of assigning all the available sub-carriers to one user, a subset of sub-carriers is allocated by the base station exclusively to each user in order to accommodate multiple user transmissions simultaneously. The frequency selectivity enabled multiuser diversity is an intrinsic advantage of OFDMA over other multiple access methods [18]. Therefore, by applying the radio resource management in the OFDMA systems, such as a variety of sub-carrier assignment, modulation coding scheme selections and power allocation, it can provide the Quality of Service (QoS) guarantees [19]. Concerning the UE transmit power efficiency, Single-Carrier Frequency Division Multiple Access (SC-FDMA) has been selected as the radio interface in the UL LTE. Because the overall SC-FDMA transmit signal is a single carrier signal, its Peak-to-Average Power Ratio (PAPR) is relatively low compared to the case of OFDMA which produces a multi-carrier signal [19]. Besides, the SC-FDMA maintains most benefits of OFDMA and improved coverage. However, as discussed in [20] and also specified in UL LTE, the sub-carrier of SC-FDMA need to be allocated continuously to a single user in order to minimize the effect of frequency offset. This constraint will be a very challenging criteria when designing radio resource allocation schemes [19].

MIMO is one of the technologies which can provide better radio link reliability and/or higher data rate without using extra bandwidth or transmission power

[21]. In general, MIMO schemes include diversity, multiplexing and beamforming. The diversity improves the reliability of the unpredictable wireless channel. By transmitting or receiving the same signal multiple times in the frequency selective channel, the signals are getting faded at the same time are very rare. So the average received signal quality can be improved. At rich scattering environment and high Signal-to-Interference-plus-Noise Ratio (SINR) with good channel estimation, the multiplexing can transmit independent signals in different antennas to boost the data transmission rate. If the antennas are quite correlated, the channels in different antennas are behaving almost the same. The beamforming can tune the antenna beam to the expected user. So the signal quality of the expected user can be increased and interference to the other users is reduced. Compared with the conventional Single-user MIMO for improving of per user data rate, the Multi-user MIMO leverage multiple users as spatially distributed resources to increase the average cell throughput. The nature of LTE adopted OFDMA and SC-FDMA is also very well suited for the MIMO operation because it simplifies the MIMO channel equalization in the frequency selective environment [22]. In order to limit the feedback overhead in real application, a codebook-based MIMO is specified in the LTE Release 8 [12][13]. In the DL direction, OFDMA-MIMO schemes, such as transmit diversity, spatial multiplexing (SU-MIMO and MU-MIMO with 2x2 or 4x4 configuration) and dedicated reference signal-based beamforming, are supported. Considering the power consumptions in the mobile side, with the configuration of 1 transmit antenna and 2 or 4 receive antennas, so far only the MU-MIMO schemes are supported in the UL direction.

LTE comes hand in hand with System Architecture Evolution (SAE), an evolution of the Core Network (CN) towards a flat, packet only and all-IP based architecture. As presented in Chapter 2 and shown in Figure 2.1, the flat network is composed of only two node types, the Evolved NodeB (eNB) and the Access Gateway (aGW). The RRM functionalities are performed independently in each eNB in a distributed manner. The eNBs are interconnected with each other by means of the X2 interface. It is assumed that there always exist an X2 interface between the eNBs that need to communicate with each other, e.g. for support of handover of UEs.

1.3   Further Evolution of LTE - LTE-Advanced

LTE is commonly considered as 3.9G network since it does not fully comply with the International Mobile Telecommunication-Advanced (IMT-A) next generation mobile network requirement [23] specified by the International Telecommunication Union (ITU) [24]. In order to maintain the long-term competitiveness

of LTE, the 3GPP is now working on further evolving the LTE towards 4G LTE-A network. 3GPP has set its own requirements for LTE-A [25]. It aims at reaching or even exceeding the IMT-A requirements as well as its own defined requirements.

- Peak Data Rate: 1 Gbit/s in DL and 500 Mbit/s in UL

- Latency: Control Plane from Idle to Connect less than 50 ms and User Plane less than 10 ms

- Peak Spectrum Efficiency: 30 bit/s/Hz in DL and 15 bit/s/Hz in UL with MIMO configuration 8x8 and 4x4 respectively

- Average Spectrum Efficiency: 2.6 bit/s/Hz in DL and 2.0 bit/s/Hz in UL with MIMO configuration 4x2 and 2x4 respectively

- Cell-edge Spectrum Efficiency: 0.09 bit/s/Hz in DL and 0.07 bit/s/Hz in UL with MIMO configuration 4x2 and 2x4 respectively

- Mobility: Support mobility across the cellular network for various mobile speeds up to 350km/h or perhaps even up to 500km/h depending on the frequency band

- Compatibility: Backward compatible with the Release 8 LTE, so that both Release 8 terminals can work in an LTE-A network and an LTE-A terminal can operate in a Release 8 LTE network [26][27].

- Spectrum Allocation: Extended bandwidth support up to 100 MHz

In order to meet the above challenging targets, several potential technologies, such as Carrier Aggregation (CA), advanced MIMO , Coordinated Multi-Point (CoMP) and Relaying Nodes (RN), are being investigated in 3GPP as part of the study item [26]. To reach the high peak data rate targets as shown in above, the transmission bandwidth is being extended from the maximum 20 MHz up to 100 MHz. Considering the backwards compatibility requirements with Rel-8 LTE, CA is being considered as the method to extend the bandwidth, where multiple component carriers are aggregated to provide the necessary bandwidth. LTE terminals receive/transmit on one component carrier, whereas LTE-A terminals may receive/transmit on multiple component carriers simultaneously to reach the higher bandwidths [28]. In addition to wider bandwidth, advanced MIMO with 8x8 antenna configuration in the DL and 4x4 in the UL allow the peak spectral efficiency exceeding the requirement. Co-channel interference limits the system capacity, especially the cell-edge data rate. To mitigate the interference, CoMP is being extensively discussed within the context of LTE-A. The basic idea behind CoMP is to apply tight coordination at different

cell sites to reduce the co-channel interference floor, thereby improving the cell edge user performance [26]. The targeted high data rates by LTE-A requires a tighter infrastructure. The deployment of RN can improve the signal strength and extend the cell coverage. As no wired backhaul is required, RNs provide an attractive, simple to install and cost-efficient solution for dense cell deployments [26]. In this PhD study, UL CoMP issues are explored. They are described and presented in the later chapters.

1.4   Interference Management Issues

Unlike the WCDMA network, where the intra-cell interference and the near-far effect issue are the main interest, in the LTE network the frequency domain orthogonality ideally removes the intra-cell interference. The inter-cell interference becomes the major concern, which is typically due to the small frequency reuse factor for obtaining higher spectrum efficiency [29], namely the reuse factor of 1 when all frequencies are utilized in every cell. The inter-cell interference hinders the LTE network performances, especially for the users at the cell-edges or at bad coverage locations. Also with the tendency of decreasing macro-cell Inter-Site Distance (ISD) for the same number of UEs per cell, limiting the inter-cell interference from each cell becomes more and more important.

In general, there are mainly three approaches which can be used for UL interference mitigation. These are interference randomization, interference cancellation, and interference coordination [30]. Interference randomization does not really reduce the interference, but rather randomizes the interferences for example in the time or frequency domain and achieves the diversity gain. The interference cancellation is used to cancel the strongest interference. The conventional interference cancellation technique is based on the advanced signal processing in the transceiver with/without multiple antennas. The interference coordination minimizes the interference level by taking advantage of the efficient RRM techniques to coordinate the frequency band allocation, transmission power assignment or antenna parameter settings in the nearby cells. Besides, in the UL LTE, the UL power control is the most important interference management technique. The power control is changed to provid the required SINR while at the same time controlling the inter-cell interference. The optimal operation of UL power control is very important for achieving good UL LTE performance.

CoMP is an advanced interference mitigation technique proposed in LTE-A for further optimizing the overall performance of LTE network. CoMP coordinate multiple network nodes with distributed and/or centralized structures [26]. The coordination requires control or even user data information to be exchanged

among the cooperating nodes through dedicated communication links. The availability of these links, together with their capacity and latency, determines the feasible type of coordination. CoMP is a multi-cell multi-user solution which involves the techniques such as Joint Processing (JP) and Coordinated Packet Scheduling (CPS)/Coordinated Beamforming (CB). The JP coherent joint DL transmission/UL reception to/from geographically separated antennas. With CPS/CB, the decisions for packet scheduling/selection of beams in one cell also considers interference situation in neighboring cells. So an even more dynamic and adaptive inter-cell interference coordination can be achieved. Based on the Release 8 LTE, specifications are required in the DL CoMP for both eNB and UE, while less specification effort is foreseen to have support for UL CoMP [26][28].

1.5   Study Objectives and Scope

The object of the PhD study is to investigate some potential multi-cell RRM techniques for limiting the impact of inter-cell interference in the UL LTE and further enhance the overall LTE network performances. As discussed in the previous section, the interference management is an important issue in the LTE network. In this study, the developed multi-cell RRM techniques focus on the system level solution and their performance evaluation.

The eNB antenna downtilting is one of the conventional multi-cell solutions to relieve the effect of inter-cell interference. By downtilting the eNB antenna, both cell-edge and system throughput are expected to be improved with increasing signal strength in the serving cell and decreasing received inter-cell interference from the neighboring cells. The potential of antenna downtilting in the UL LTE is investigated first and the optimal antenna downtilting angle need to be identified, which is used for the later studies. Meanwhile, as stated earlier, UL power control is an important technique to achieve the good UL LTE performance. The interaction of antenna downtilting with UL power control should be studied in order to find the optimal power control parameter setup.

Based on the antenna downtilting study, it can be foreseen that the UEs close to the cell-border still suffer from the degradation of high level of inter-cell interference and the low signal quality due to the propagation loss. In order to solve this problem, the potential benefits of using CoMP techniques are investigated. The performance of UL CoMP receptions in the form of both macro diversity combining and joint schemes are studied respectively. With CoMP macro diversity reception, the serving and coordination cell received signals of CoMP UEs are processed separately and macro-combined in the serving cell. Whereas

for the CoMP joint reception, the serving and coordination cell received signals are jointly processed in the serving cell. By applying the multi-cell coordinated Packet Scheduling (PS) together with the CoMP joint reception scheme, the performance gain of combined effort need to be evaluated compared with the standing alone solution. As presented earlier, the CoMP technique is a newly proposed promising candidate for efficient interference management in LTE-A network. Several interesting issues need to be studied, such as how to utilize the CoMP technique in the LTE network, how much gain the CoMP scheme can achieve, and how feasible the CoMP solutions to be implemented in the future LTE-A product are, e.g. the impact on the existing LTE backhaul requirements. All these questions will be investigated in this PhD study.

Of course, this PhD study cannot cover all the aspects of interesting research. A certain study delimitation has been defined. LTE/LTE-A based network in the UL direction is the main focus in this Ph.D study. In order to make the study realistic, the LTE framework and design guidelines are employed in the analysis. The algorithm design and evaluation of the multi-cell RRM techniques at system-level is the main concern.

1.6 Scientific Methods Employed

The system-level performance of LTE network depends on a large number of parameters and the complicated interaction among the system entities makes it too complex or sometimes impossible to formulate a theoretical framework. Therefore, the computer-aided simulation approach is adopted in this PhD study. The basic idea of computer-aided design is to use a computer model to design networks and new features for networks. Features as well as parameter settings can be simulated before actually implementing them in the network [31]. The accuracy of using simulation approach depends on the network function modeling and radio environment modeling. A good modeling can be build to express more realistic and valid LTE network with less simplifying assumptions. An important aspect of this study is to modeling and verification of modeling assumptions. It involves work on mathematical modeling and deriving abstraction models applied in the simulator.

A semi-static UL system-level simulator was employed in this study, where the system models applied in the simulator take the 3GPP recommended modeling assumptions and guidelines for LTE into account, as described in [32]. The system models contain the detailed implementation of Link Adaptation (LA) based on Adaptive Modulation and Coding (AMC), explicit PS together with the Hybrid Automatic Repeat reQuest (HARQ) process, concrete fractional

power control and link-to-system mapping technique suitable for SC-FDMA.
The traffic type, such as 3GPP-recommended infinite/full buffer and realistic
finite buffer, is also implemented. The simulation results presented in this PhD
thesis have been generated and analyzed through massive computer simulations
by using the developed system models and implemented system-level simulator
features during the period of the PhD study. Besides, the final results and
conclusions have also been examined with other similar or 3GPP studies for
accuracy comparison.

1.7   Novelty and Contributions

The main contribution of this PhD study is the analysis, understanding and
further improvement of UL multi-cell RRM techniques in terms of interference
management issues in the LTE network. Especially, the investigating and de-
signing work related to the UL LTE CoMP study, which provides the contribu-
tions not only from the academic's point of view but also from the industry's
interests. The corresponding evaluation work involves the conceptual design,
system modeling, software development and performance analysis. One impor-
tant contribution of the study is the system-level simulator development. A
lot of time have actually spend on the modeling, implementing and testing of
features in the simulator. Several topics are addressed in this PhD study period
as presented in the following.

The first topic of the study is the investigation of mechanical antenna downtilt-
ing scheme in the UL LTE network. In the open literature, antenna tilting has
been studied a lot on the Code Division Multiple Access (CDMA)-based sys-
tems [33][34]. However, the utilization of antenna tilting depends on the applied
radio access technology. WCDMA uses soft handover and cell breathing, there-
fore require a different antenna downtilting strategy than the LTE network. In
this study, the network-based antenna tilting was evaluated together with the
3GPP agreed UL open-loop power control scheme. The optimal antenna down-
tilting angle has been investigated for different inter-site-distances ranging from
500 meters to 1732 meters. The parameters of open-loop power control were
evaluated and used as reference for the later investigations. This contribution
has been published in:

- Naizheng Zheng, Per-Henrik Michaelsen, Jens Steiner, Claudio Rosa and
  Jeroen Wigard, "Antenna Tilt and Interaction with Open Loop Power
  Control in Homogeneous Uplink LTE Networks", in *Proceedings of the
  IEEE International Symposium on Wireless Communication Systems, pp.
  693-697, Reykjavik, Iceland, October, 2008*

The second topic of the study is the UL CoMP related, where the UL CoMP in the form of macro diversity reception was first investigated. In the existing literature, [35] had the similar study which was conducted with the 2-Dimensional (2-D) antenna pattern. Stronger inter-cell interference is expected with 2-D antenna pattern which results in higher CoMP performance gain. In this study, the performance of UL CoMP macro diversity reception was investigated with the 3-Dimensional (3-D) antenna pattern. The mechanical antenna downtilting is applied with the optimal angle based on the previous study. The study also presents, by combination of interference cancellation and UL close-loop power control schemes, the overall UL LTE network can be further optimized in both CoMP Intra-Site and Inter-Site scenarios. This contribution has been published in:

- Naizheng Zheng, Malek Boussif, Claudio Rosa, Istvan Z. Kovacs, Klaus I. Pedersen, Jeroen Wigard and Preben E. Mogensen, "Uplink Coordinated Multi-Point for LTE-A in the Form of Macro-Scopic Combining", in *Proceedings of the IEEE Vehicular Technology Conference (VTC), pp.1-5, Taipei, China, May, 2010*

The third topic of the study evaluates the UL CoMP joint reception. Most of the published articles of CoMP joint reception were concentrate on the theoretical research [36][37][38] and DL CoMP investigations [39][40][41]. Based on the assumption of full network cooperation, tremendous CoMP gain has been reported in the theoretical CoMP studies [36]. However, it is practically infeasible to cooperate network over a large scale due to the implementation challenges, such as constrained network backhaul and imperfect channel estimations. In this study, the performance of UL CoMP joint reception was investigated in the CoMP scenario with limited cooperation area and compared with the UL CoMP macro diversity reception. The requirements of LTE X2-interface for both applications were also analyzed. The application of coordinated packet scheduling has also been studied in the Intra-Site scenario with UL CoMP joint reception to further optimize the overall network performance. This study is based on the realistic Minimum Mean Square Error (MMSE)/Successive Interference Cancellation (SIC) receiver and investigated with different cooperation scenarios. Besides, the recommendations have also given for the Inter-Site scenario from the future industrial implementation interests. The work is planned to be submitted to:

- Naizheng Zheng, Gilberto Berardinelli, Claudio Rosa, Istvan Z. Kovacs, Klaus I. Pedersen, Jeroen Wigard and Preben E. Mogensen, "The performance of UL CoMP with Joint Reception in the LTE-Advanced networks"

- Naizheng Zheng, Claudio Rosa, Istvan Z. Kovacs, Klaus I. Pedersen, Jeroen Wigard and Preben E. Mogensen, "Joint Reception of Uplink Coordinated Multi-Point with Coordinated Packet Scheduling"

The last topic of the study is about HO issue in the DL LTE. This topic is independent from the other UL studies because of changing research fundings. But the handover technology itself is another multi-cell solution to combat the inter-cell interference. Hard HO has been standardized in the DL LTE Rel'8. The traditional HO decision method has been studied a lot in the GSM-based network [42]. LTE network requires seamless mobility services, therefore it needs a faster decision algorithm and can be easily utilized in the future deployment. In this study, a hard HO algorithm is proposed based on the LTE RSRP measurements. Compared with the traditional algorithm, it requires less HO setup parameters, but provides identical overall performance in the DL LTE. The results of this study have been published in:

- Naizheng Zheng and Jeroen Wigard, "On the Performance of Integrator Handover Algorithm in LTE Networks", in *Proceedings of the IEEE Vehicular Technology Conference (VTC), pp.1-5, Calgary, Canada, September, 2008*

1.8 Thesis Outline

The PhD thesis is organized as follows:

- Chapter 2: *Radio Resource Management in Uplink LTE* - This chapter presents an overview of the LTE system architecture and general descriptions of the RRM functionalities in the UL LTE.

- Chapter 3: *Antenna Tilting in Homogeneous LTE* - This chapter presents the multi-cell interference mitigation technique by applying the mechanical antenna tilting in the homogeneous UL LTE networks. The interactions of antenna downtilting with the open-loop fractional power control scheme have also been investigated.

- Chapter 4: *Uplink CoMP in the form Macro-Scopic Combining* - This chapter presents the basic UL CoMP structure and the UL CoMP reception by use of macro diversity combining. The study is based on the Maximal Ratio Combining (MRC) receiver. With the combination of ideal IC and close-loop FPC, the upper bound of UL CoMP in the form of macro diversity reception can be studied.

- Chapter 5: *Joint Uplink CoMP Reception* - This chapter presents the UL CoMP with multi-cell multi-user joint detection. The evaluation results are compared with the corresponding CoMP macro diversity scheme based on the realistic MMSE/SIC receiver. And the requirements of LTE X2-interface have also been analyzed for both applications from the future practical application interests.

- Chapter 6: *Coordinated Packet Scheduling for Joint Uplink CoMP* - This chapter presents a multi-cell coordinated packet scheduling algorithm which can further improve the performance of the UL CoMP joint reception in the Intra-Site scenario compared with the studies conducted in Chapter 5.

- Chapter 7: *Main Conclusion and Future Work* - The chapter provides a summary of the overall study and discusses future research issues.

- Appendix A: *Performance of Integrator Handover Algorithm* - This chapter evaluates the performance of a proposed hard handover algorithm in the DL LTE based on the RSRP measurement for different handover parameters.

- Appendix B: *Quasi-dynamic System Level Simulator Description* - This appendix provides the detailed description of the implemented UL system level simulator.

Radio Resource Management in Uplink LTE

This chapter outlines the study related Radio Resource Management (RRM) entities in the UL LTE network, where the functionality and modeling issue of each entity is briefly described and the interactions among the entities are also discussed.

In Section 2.1, the flat LTE network architecture together with the corresponding protocols in each stack is introduced. Following the protocol layers with bottom up approach in eNB, in Section 2.2, the signaling used for the higher layer UL RRM is first presented. In Section 2.3, Hybrid Automatic Repeat reQuest (HARQ) process is described. Link Adaptation (LA) functionality which includes Fractional Power Control (FPC), Adaptive Modulation and Coding (AMC) and Outer Loop Link Adaptation (OLLA) is discussed in Section 2.4. In Section 2.6, the dynamic Packet Scheduling (PS) issue is presented. Finally, in Section 2.7, the interaction works among different RRM entities are also illustrated.

2.1 System Architecture of LTE

In order to meet the low latency constraints in LTE, 3GPP has specified a simple, flat and IP-based network architecture as part of the SAE effort. The new flat architecture only contains two node types [43], which are the eNB and the Mobility Management Entity (MME)/aGW, as shown in Figure 2.1. It reduces the number of network elements in the access path which saves the time it takes to access the radio and core network resources. From the cost saving's
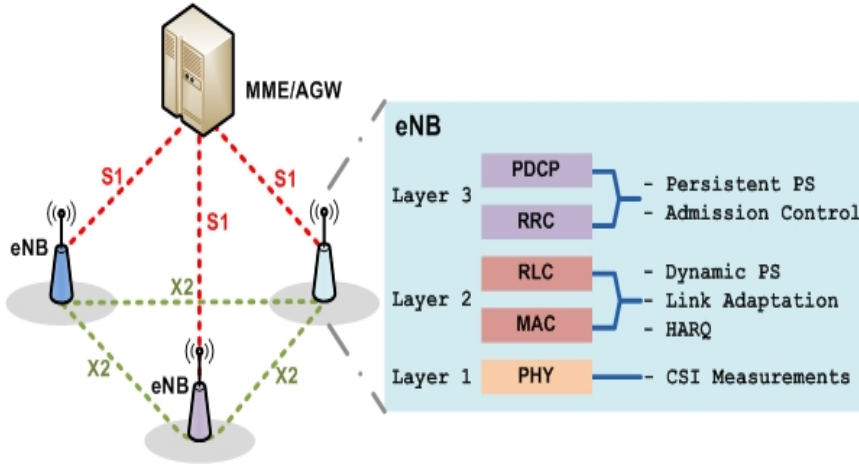
Figure 2.1: LTE Flat Architecture and Protocol Stacks in eNB

aspect, the LTE-SAE architecture reduces both Operating Expenses (OPEX) and Capital Expenditures (CAPEX), which means that only the two node types must scale in capacity in order to accommodate large increases in data volumes [44].

As shown in Figure 2.1, the eNBs are connected to the core network over the so-called S1-interface and the X2-interface is specified for connections between the eNBs. The X2-interface is the key interest in this study for the CoMP application. The basic functionalities of X2-interface include error message handling, load management and mobility support[19]. The error message handling allows reporting of general error situations. The load management used by eNBs to indicate resource status or counteract traffic load imbalance between neighboring cells with the aim of improving the overall system capacity. The mobility support allows the eNB to handover a certain UE to another eNB, where forwarding of user plane data, status transfer, and UE context release function are parts of the mobility support [45][46][47][48].

The UTRAN eNB is interfacing with the UE. As shown in Figure 2.1, it hosts protocol layers, such as Physical Layer (PHY), Medium Access Control (MAC), Radio Link Control (RLC), and Packet Data Convergence Protocol (PDCP) to the user-plane. Correspondingly it also offers Radio Resource Control (RRC) functionality to the control-plane [16]. The eNB contains many RRM entities which include HARQ, LA, dynamic PS, Admission Control (AC), persistent PS and HO [19]. In the following sections, the functionality and modeling issue of the study related UL RRM entities are briefly described.

2.2   Signaling and Support for Uplink RRM

Buffer status reports and power headroom reports are the main signalings used for the UL RRM, where the UE buffer status reports provide the knowledge of UE buffer status to the eNB scheduler to make sure enough resource allocation to the UE and the power headroom reports transfer the UE transmit power information to the eNB for performing correct RRM decisions at eNB, e.g. allocating correct transmission format including bandwidth and modulation and coding scheme to the UE. The Channel State Information (CSI) is extracted from the UL Reference Symbols (RS) and utilized by the PS and LA entities to support the channel-aware scheduling and the AMC respectively. In this section, CSI is presented in detail and the readers are referred to [19] for further readings about the buffer status report and power headroom report issues.

The CSI can be seen as the SINR measurement of Sounding Reference Signal (SRS) [49], where SRS is introduced in the UL LTE as a wider band RS typically transmitted in the last SC-FDMA symbol of a 1ms subframe. User data transmission is not allowed in this block, which results in about 7 percent reduction in UL capacity [50]. Practically, the SRS is an optional feature which can be turned off in a cell. Users with different transmission bandwidth can then share this sounding channel in the frequency domain. The received SRS is estimated in the eNB and provide information on UL channel quality. SRS can be transmitted over a fractional or full scheduling bandwidth. By applying the Constant Amplitude Zero Auto-Correlation (CAZAC) sequences and the UL synchronous transmission, the orthogonality guarantee the simultaneous transmission of SRS among the users using the same transmission bandwidth without interfering with each other. In the UL LTE, the orthogonal CAZAC sequences only apply to the users in the same cell or intra-cell users [19]. For the real application, the SRS parameter setup, such as SRS bandwidth, period, duration and sub-band hopping sequence will impact the accuracy of the corresponding SINR measurements [19].

In this study, it is assumed that, in every Transmission Time Interval (TTI), the CSI of each active user in the corresponding cell is available at the eNB over the entire scheduling bandwidth. Assume the MRC combining method, the CSI estimation of user i on Physical Resource Block (PRB)[1] p at instant time t is

---

[1]PRB in LTE is defined as the minimum time and frequency domain scheduling granularity which consists of 12 consecutive OFDM sub-carriers and 14 OFDM symbols. Since no Exponential Effective SINR Metric (EESM) model is used in the simulator, the fast fading resolution in the frequency domain is on a PRB basis and not on a sub-carrier basis.

modeled as [49]:

$$CSI_{i,p,t} = \sum_{a=1}^{N_r} \left(\frac{\sum\limits_{r' \in R} S_{i,a,r',t}}{\sum\limits_{r' \in R} (\bar{I}_{b(i),a,r',t} + N_{prb})} \right) \cdot 10^{\frac{\epsilon_{p,t}}{10}} \qquad (2.1)$$

where:

- N_r is the number of receive antennas at the eNB b where user i is served

- R is the set of simultaneously sounded PRBs within the CSI resolution of PRB i. The size of R is the so-called CSI resolution.

- $S_{i,a,r',t}$ is the SRS power received from user i at time t on PRB r' and antenna a.

- $\bar{I}_{b(i),a,r',t}$ is the averaged interference signal power received at eNB b, at instant time t, on PRB r' and antenna a. The CSI interference component is calculated via the exponential averaging over a certain time window as shown in Equation 2.2, which is due to the dynamic scheduling and variability of the instantaneous interference conditions in the UL LTE. It has been shown in [51] that it is beneficial for the UL channel estimation and overall performance.

$$\bar{I}_{b(i),a,r',t} = \rho \cdot I_{b(i),a,r',t} + (1 - \rho) \cdot \bar{I}_{b(i),a,r',t-1} \qquad (2.2)$$

In Equation 2.2, ρ is a system parameter that can be used to control the averaging period of the interference used in CSI measurements.

- N_{prb} represents the thermal noise of one PRB

- $\epsilon_{p,t}$ is the introduced CSI measurement error which is a zero mean Gaussian distribution random variable with standard deviation of σ_{CSI}. The random variables $\epsilon_{p,t}$ and $\epsilon_{p,t+a}$ are uncorrelated for $a \neq 0$. The CSI resolution is directly related to the standard deviation of the expected measurement errors. Based on the previous study [52], with CSI resolution of 2 to 3 PRBs, it is reasonable to have a standard deviation of the measurement error of approximately 1 dB.

2.3   Hybrid Automatic Repeat Request - HARQ

In order to combat the data transfer errors, the LTE supports two levels of re-transmissions for providing reliability, the MAC layer HARQ and RLC layer Automatic Repeat ReQuest (ARQ). In general, the HARQ gives the additional information to the receiver that enables it to prevent a certain amount of errors if the initial transmission cannot be avoided, and the ARQ is required to handle the residual errors that are not corrected by the HARQ [19].
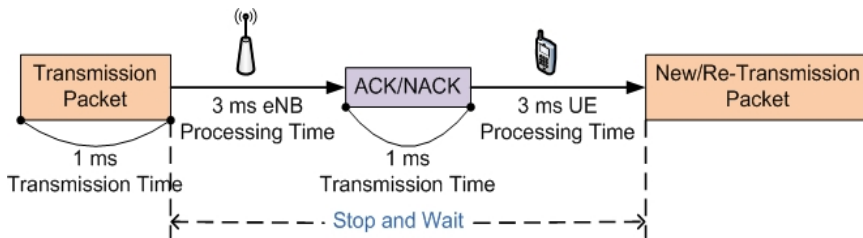

Figure 2.2: LTE HARQ Timing for a single Uplink Packet

The HARQ in LTE is based on the use of a stop-and-wait procedure. An example of the UL HARQ process is shown in Figure 2.2. As it can be seen, once the UL packet is transmitted from the UE, the eNB will decode it and provide the feedback with either an Acknowledgement (ACK) or a Negative Acknowledgement (NACK). If a NACK is received in the UE, a re-transmission will be triggered, either in the form of Incremental Redundancy (IR) or Chase Combining (CC), otherwise a new UL packet will be sent out. A so-called synchronous HARQ re-transmission is applied in the UL LTE study [49], which means that the re-transmission of HARQ block occurs at a pre-defined periodic interval. By doing so, no explicit signaling is required to inform the receiver about the re-transmission schedule. The HARQ can also be utilized in LTE either adaptively or non-adaptively, where the adaptive means the possibility of changing transmission parameters, e.g. resource allocation and Modulation and Coding Scheme (MCS), in the subsequent re-transmissions [49].

As also shown in Figure 2.2, the whole HARQ process takes roughly about 8 ms, where around 3 ms is estimated for the eNB/UE processing time and 1 ms for the transmission delay [19]. In Chapter 5 UL CoMP study, it can be foreseen that the 3 ms eNB processing time brings a big challenge for the CoMP operation with limited X2-interface latency.

In this study, the HARQ process with ideal Chase Combining is considered, and

the SINR after HARQ combining is modeled as [53]:

$$SINR_{N_{HARQ}} = \sum_{q=1}^{N_{HARQ}} SINR_q \qquad (2.3)$$

where $SINR_{N_{HARQ}}$ represents the combined SINR after N_{HARQ} transmissions and $SINR_q$ denotes the SINR of the q-th transmission. In this study, the HARQ allows a maximum of three retransmissions before discarding a transmission block, i.e. $N_{HARQ} = 4$.

2.4   Link Adaptation

To respond to the fast variation of wireless channel and maximize the spectrum efficiency, LTE includes a collection of techniques which are referred to as Link Adaptation (LA). It contains the adaptation mechanisms such as AMC, OLLA and FPC [19].

2.4.1   Adaptive Modulation and Coding

The basic function of AMC is to select the most suitable MCS for transmissions according to the changing channel environments. There are a lot of studies related to the AMC, as shown in [54]. With better channel quality or at high SINR region, higher order of MCS can be utilized to provide higher spectral efficiency. As shown in Figure 2.3, with a certain pre-defined or expected BLock Error Rate (BLER) target at the first transmission (i.e. 20% BLER) and the UE experienced SINR value, the MCS schemes can be selected in order to maximize the expected throughput. The AMC can be applied either on a fast or a slow basis. In this study, the TTI-based fast AMC is used, where it has been shown in [51] that, because the fast AMC can better explore the fast variation channel by allocating a higher order MCS, the fast AMC has much better performance than slow AMC in terms of average cell throughput.

2.4.2   Outer-Loop Link Adaptation

OLLA is required to compensate for the fast AMC errors, where the errors are typically due to the CSI measurement, link adaptation delay and interference
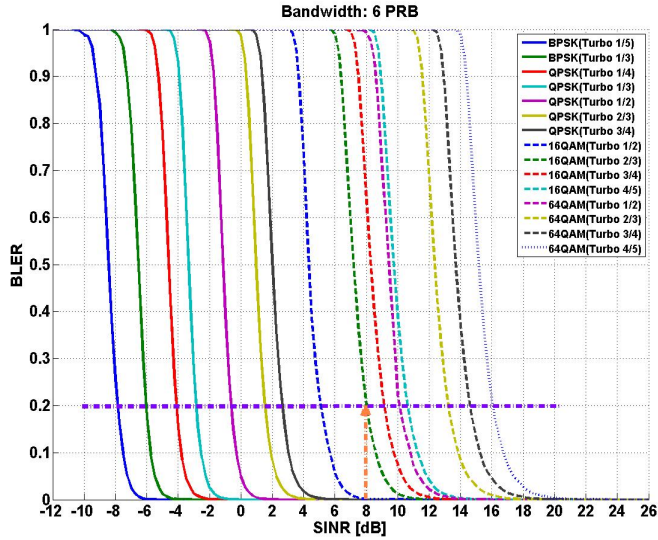
Figure 2.3: SINR vs BLER

variability. These errors cause the experienced BLER at first transmission to deviate from the predefined target [55]. In LTE, the application of OLLA is not standardized but rather vendor specific. The advantages of introducing OLLA have already been shown for both HSDPA [56] and LTE DL [57]. In this study, a simple OLLA algorithm is utilized in the UL LTE [58], where by monitoring the received ACK/NACK of each user, an offset parameter is utilized and used as an input to the AMC to stabilize the overall LA performance as shown in Equation 2.4.

$$CSI_{i,final} = CSI_i - OLLA_{off} \tag{2.4}$$

It should be noted that the same offset $OLLA_{off}$ is applied to all the CSI reports of a given UE across the frequency domain. In order to avoid saturation as a result of unexpected errors, the dynamic range of the offset parameter is defined within a certain interval. In this study, the OLLA offset is equal to 0.5 Decibel (dB) for all the UEs and the the OLLA offset range is within $[-4.0, 4.0]$ dB.

2.5   Fractional Power Control

The main role of power control in UL LTE is to limit inter-cell interference while respecting minimum SINR requirements [19]. It has been agreed in the 3GPP meeting to utilize the FPC scheme in the UL LTE [59] as expressed in Equation 2.5 in *dBm*:

$$P_{tx} = \min\{P_{max}, \underbrace{P_0 + 10 \cdot log_{10} N_{PRB} + \alpha \cdot L}_{\substack{\textbf{Open-Loop} \\ \textbf{Component}}} + \underbrace{\Delta_{mcs} + f(\Delta_i)}_{\substack{\textbf{Close-Loop} \\ \textbf{Component}}}\} \qquad (2.5)$$

As it can be seen from the Equation 2.5, the FPC consists of two parts, which are the Open-Loop fractional Power Control (OLPC) component and the Close-Loop fractional Power Control (CLPC) component, where:

- P_{tx} is the UE transmit power,

- P_{max} is the maximum UE transmit power,

- P_0 is a broadcasted cell/user-specific parameter,

- N_{PRB} is the number of assigned PRB to a certain UE,

- α is the cell/user-specific Path Loss (PL) compensation factor,

- L is the PL of the DL RS measured in the UE,

- Δ_{mcs} is a UE-specific parameter signaled from the upper layer RRC,

- Δ_i is a user-specific correction value with a relative or absolute value depending on the $f(\cdot)$-function.

2.5.1   Open-Loop Fractional Power Control

If the CLPC component is not applied, the Equation 2.5 can be simplified as:

$$P_{tx} = \min\{P_{max}, P_0 + 10 \cdot log_{10} N_{PRB} + \alpha \cdot L\} \qquad (2.6)$$

From Equation 2.6, it can be seen the UE transmission power is strongly dependent on the selected open-loop power control parameters (P_0 and α) and the propagation scenario, i.e. path loss distribution. The transmission power has an

impact on the received interference level and consequently on the distribution of the scheduled SINR, which on the other hand directly impacts the system and user spectral efficiency. As a result the choice of parameters P_0 and α are very important when trying to find a optimum operation point considering both coverage and cell throughput performance.

Basically, the OLPC can be operated at either full or fractional compensation of the PL. With full compensation of the PL, by applying the α value equal to 1.0 in Equation 2.6, the same SINR will be received at the eNB for all the UEs unless the P_{max} constraint takes effect. In order to fight for the inter-cell interference in the UL LTE, fractional compensation of the PL can be utilized by applying the α value for example equal to 0.6 or 0.8 in Equation 2.6. The scheme allows compensation part of the PL so that the UEs with higher PL will operate with a low SINR requirement and will likely generate less interference to the neighboring cells. Based on the previous study and presented in [29], in an interference-limited scenario, the cell coverage improves as the interference increases until the first cell-edge user start reaching the maximum transmit power. Then, to an increase of P_0 (and hence of interference) corresponds a decrease in coverage. From the coverage perspective, the optimal interference operating point is higher for lower α value. Generally a lower value of α improves the cell throughput performance up to approximately α=0.6 [29].

2.5.2 Close-Loop Fractional Power Control

The CLPC command can also be applied to combat the inter-cell interference or to correct the PL measurement errors. The general understanding is that CLPC is slow and a-periodic in the UL LTE. The 3GPP specifications allow 2 types of CLPC commands, which are:

- Absolute CLPC command: the UE applies the offset based on the latest OLPC command as reference.

- Cumulative CLPC command: the UE applies the offset based on the latest transmission power value as reference.

The application of the CLPC algorithm can be adopted with either the Intra-cell approach or the Inter-cell strategy. For the Intra-cell approach, the close-loop component simply adjusts the UE transmit power based on the measurements. By utilizing the Overload Indicator (OI) through the LTE X2-interface connections, the interference based inter-cell CLPC can be conducted [60]. In this

study, the inter-cell CLPC has also been utilized as presented in the later CoMP topic.

2.6   Dynamic Packet Scheduling

The goal of dynamic PS is to efficiently utilize the spectrum resources and maximize the cell capacity, while making sure that the minimum QoS requirements for the Evolved Packet System (EPS) bears are fulfilled [19]. In reality, the wireless channel is varying in both time and frequency scale. The dynamic PS exploits the multi-user diversity by multiplexing the UEs in both time and frequency domain and allocating the UE with the favorable conditions on a certain transmission resource.
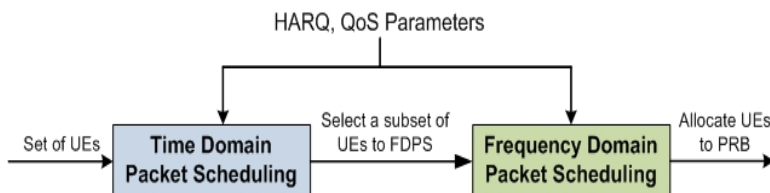
Figure 2.4: LTE Dynamic Packet Scheduling

The allocation algorithm of dynamic PS can be designed in many different ways. In this study, the allocation algorithm is divided into Time-Domain Packet Scheduling (TDPS) and Frequency-Domain Packet Scheduling (FDPS) as shown in Figure 2.4, where the TDPS indicates a phase of user selection, and the FDPS indicates a phase of PRB allocation. This two step structure is beneficial because of the low computational complexity, where the FDPS only has to consider a subset of UEs who are selected by the TDPS according to the selection criteria or metrics.

The selection criteria or metrics of TDPS and FDPS can be defined according to different provisions, such as the Round Robin (RR), Proportional Fair (PF), maximum CSI measurement or QoS requirement. With different scenarios, e.g. traffic type, number of UEs or even cell size, the performance of the selected metrics performs differently.

In the FDPS, the UE can be allocated with either Fixed Transmission Bandwidth (FTB) or Adaptive Transmission Bandwidth (ATB) based on the selection criteria metrics. With FTB, the number of PRBs assigned to every UE are identical. However, for the OFDM-based LTE network, bandwidth scalability is one

of the key features for improving the spectrum efficiency and providing QoS. The ATB exploits the bandwidth flexibility and takes, such as UE buffer status, traffic type, cell load and UE power limitation, into consideration by assigning different portions of bandwidths to different UEs. As presented in [49] with unbalanced cell load, in a Macro Case-1 scenario, the ATB-based PS guarantees a high bandwidth utilization which results in a higher cell throughput than FTB but lower outage user throughput because of increase noise level. In a Macro Case-3 scenario, the ATB is able to provide a gain in both average cell throughput and outage user throughput depends on the power settings. It is clear that ATB is the obvious choice for having the best scheduler. But the disadvantage of ATB is that there are many options/combinations to evaluate for deciding the best PRB allocation for each TTI. Therefore, for the sake of simple PS, the FTB is considered in this study.

2.7 Interaction of Related Uplink RRM Entities

As shown in Figure 2.5, the UL RRM entities do not work alone, but interact with each other. Especially there are a lot of interactions between the dynamic PS and other functionalities, e.g. signaling manager entities and LA entities.
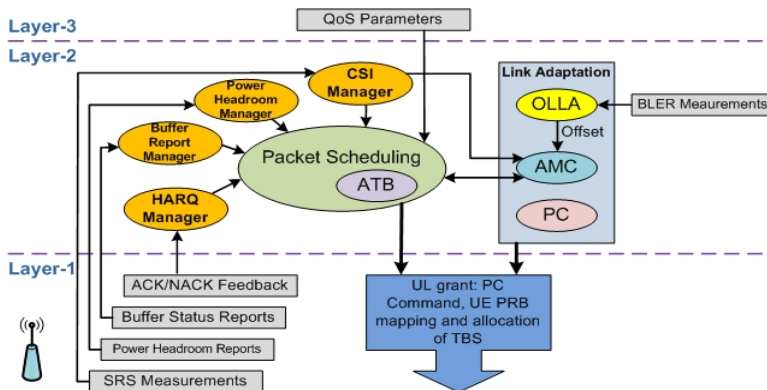

Figure 2.5: Interactions of Upink LTE RRM

- **Interaction of Dynamic PS with Signaling Manager Entities:** The signaling manager entities include the buffer status manager, power headroom manager, CSI manager, HARQ manager and QoS manager as shown in Figure 2.5. Some of the interactions between the signaling manager entities (e.g. the buffer status manager and the power headroom manager)

and the dynamic PS have already been briefly discussed in Section 2.2. If the dynamic PS utilizes the maximum CSI measurements as the selection criteria metrics in either TDPS or FDPS, it also has to directly interact with the CSI manager to acquire the CSI information for each UE per TTI on a certain PRB. For the synchronous HARQ in UL LTE, the dynamic PS needs to apply the information from HARQ manager in order to prioritize the pending HARQ re-transmissions over the other first transmission UEs. If the designed dynamic PS algorithm guarantees the QoS, the knowledge of QoS requirements should be provided from the QoS manager.

- **Interaction of Dynamic PS with LA Entities:** The fundamental part of the UL RRM is the interaction between dynamic PS and LA entity. In the UL LTE, the AMC is the link between the dynamic PS and the CSI manager as shown in Figure 2.5. It is responsible for providing the channel quality information to the dynamic PS for a given UE on a particular transmission bandwidth. Once the dynamic PS has assigned a specific UL resource to a UE, the AMC is also responsible for selecting the most appropriate MCS to the corresponding UE.

2.8   Summary

In this chapter the state of art background knowledge of RRM entities in the UL LTE network is introduced. The main functionalities of study related RRM entities, such as HARQ, LA, AMC, OLLA, FPC and PS, are briefly described. Besides, the signaling used for the UL LTE RRM and the interaction among different RRM entities are illustrated. The issues of system-level modeling in each entity are also presented and will be utilized in the later performance evaluation in this study.

Antenna Tilting in Homogeneous LTE

For LTE networks, the frequency domain orthogonality ideally removes the intra-cell interference. The inter-cell interference becomes the major concern from an overall interference point of view, typically due to the application of frequency reuse factor[1] 1 for obtaining higher spectrum efficiency. Antenna tilting is one of the inter-cell interference reduction techniques. A well defined antenna tilting scheme minimizes the interference in the cellular network without losing coverage. Dependent on the target, by tilting the BS antenna in an optimal manner, the mobile radio network can be optimized for coverage enhancement, capacity improvement, interference reduction, power consumption saving, and traffic/cell load balancing.

In this study, the mechanical antenna downtilting is being studied in the UL LTE. The optimal angle of mechanical antenna downtilting is identified, and the parameter settings for the Open-Loop fractional Power Control are selected. They are used as a baseline for the later simulation studies as well as a good guideline for the future practical LTE network applications.

In Section 3.1, the state of the art of antenna tilting is presented. The modeling issues of mechanical antenna downtilting are presented in Section 3.2. In Section 3.3, the influence of antenna tilting to the mobile network is illustrated, and the issues are briefly discussed together with the LTE FPC. In Section 3.4, the simulation assumptions for the mechanical downtilting study are described, and the simulation results are presented in Section 3.5. Finally, in Section 3.6, the conclusions for the mechanical downtilting study are made.

---

[1]Frequency reuse factor indicates how often the same frequency channel can be used in a given system. Smaller frequency reuse factor can be used to limit the co-channel interference.
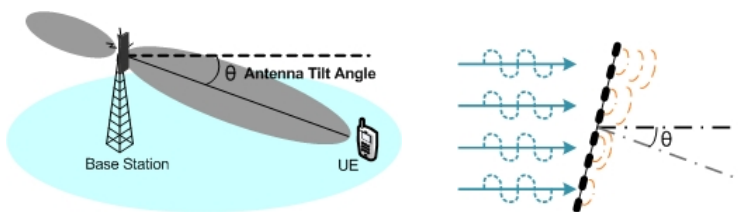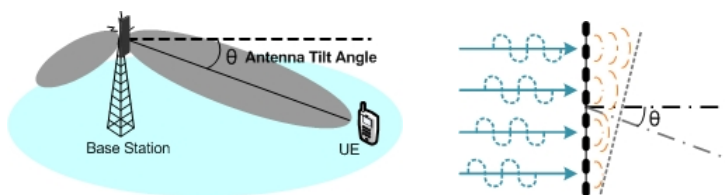
Figure 3.1: Mechanical Antenna Downtilting

Figure 3.2: Electrical Antenna Downtilting

3.1   Antenna Tilting

Antenna tilting or beam tilting is defined as the process of adjusting the angle
of antenna main beam below or above the horizontal (Azimuth) plane. Positive
and negative tuning angles are also referred to as antenna down-tilting and up-
tilting respectively. Fundamentally, the antenna tilting can be implemented in
two ways, mechanical tilting or electrical tilting.

In general, the mechanical tilting is to adjust the physical angle of the mounted
antenna brackets. As shown in Figure 3.1, with mechanical downtilting, it
lowers the angle of the antenna main lobe below the horizontal plane on one
side, and it also raises the antenna back lobe above the horizontal plane on
the other side. The effective mechanical downtilting angle corresponds to the
physical one exactly in the main lobe direction and decreases as a function
of horizontal direction, where the antenna radiation pattern is not changed
from the antenna side lobe direction [61]. With even higher downtilting angels,
the radiation pattern of mechanical downtilted antenna is shrinked from the
boresight direction and getting wider from the sides, as shown in Figure 3.3. In
comparison with the mechanical downtilting as shown in Figure 3.2 and Figure
3.3, the electrical downtilting does not change the physical angle of an antenna.
Instead it adjusts the antenna radiation pattern by utilizing the phase shifter to
lower the antenna lobes in all the geometrical horizontal directions. Practically,
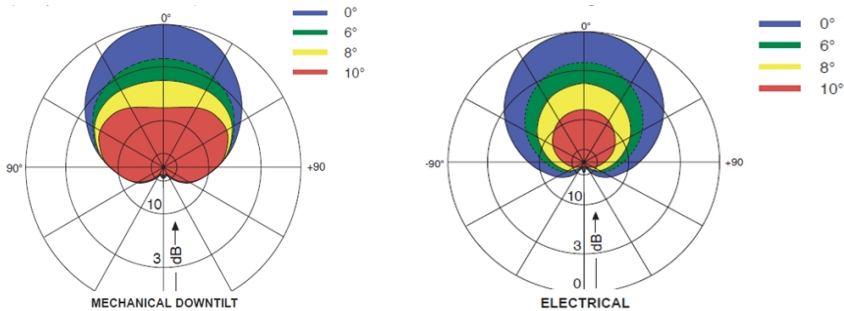
Figure 3.3: Practical Antenna Radiation Pattern [62]

the purely mechanical tilting and fixed electrical tilting can be implemented either independently or jointly.

In the open literature, antenna tilting has been studied a lot on the CDMA-based systems. Based on the simulation study in [63] the average tilting applied in WCDMA is about $10^o \sim 12^o$ for dense urban area and $6^o \sim 8^o$ for suburban area. The above studied tilting angle is generally larger than what is experienced in actual deployment because of simplified channel model applied in the analytical studies [64]. Concerning the gains from antenna tilting there is wide range of quoted values, ranging from ten to several hundred percent depending on the the reference used [65][66]. Typically the practical gain from antenna tilting is smaller than the simulation studies. From [33][34], the WCDMA capacity can be improved up to 20-30% for small macro cells with antenna downtilting. If using network-wide tilt, the gains is in the order of 10-20%, whereas cell based tilt optimization may provide 20-30% enhancement [67]. However, the use of antenna tilting depends on the applied radio technology. The Multiple Access Interference (MAI) and near-far problem are the main concern [68] for the asynchronous transmission in the UL CDMA. Whereas, in the UL LTE, the synchronous transmission preserves the intra-cell orthogonality and the co-channel inter-cell interference becomes the key aspect. WCDMA also uses soft handover and therefore require a different tilting strategy than the LTE that adopts hard handover. Besides, the cell breathing[1] utilized in the CDMA systems somewhat compensates for the changes in antenna titling and consequently requires quite large changes to observe an effect on the network [69].

---

[1]Cell breathing is defined as the constant change in the geographical area covered by the cell tower. When the cell becomes heavily loaded, it shrinks, and the lightly loaded neighboring cells expand. In this way, the user traffic from the overloaded cell is redirected to neighboring cells and the overall system is load balanced.

For the planning and deployment of real networks, the selection of a reasonable mechanical downtilting angle should be emphasized in order to maximize the overall network performances and guarantee the QoS. In this study, the mechanical antenna downtilting is being studied in UL LTE and used as a baseline for the later simulation studies.

3.2   Modeling of Mechanical Downtilting

When evaluating the benefits of different features in system-level simulations, it is important that the simulated cellular network represents a realistic network. For many system-level simulators, only the 2-D antenna pattern, the horizontal antenna pattern in the Azimuth plane, was considered [70]. The vertical antenna pattern in the Elevation plane was implicitly modeled via the maximum antenna gain pattern. However, numerous publications [71][72] have reported on the impact of modeling the vertical antenna pattern on the network capacity, coverage and interference. For the investigation of mechanical downtilting in this study, the vertical antenna pattern has a major influence on the received signal strength. So it is very important and necessary to introduce a 3-D antenna pattern to any advanced system-level simulator, which considers the influences of both horizontal and vertical patterns.

3.2.1   3-D Antenna Pattern Modeling

The adopted antenna pattern models in this study are characterized by the Half Power Beam Width (HPBW) and expressed in Equation 3.1 and 3.2 in dB [43]:

$$A\left(\phi\right) = -min\left[12\left(\frac{\phi}{\phi_{3dB}}\right)^2, A_{\phi,m}\right]\tag{3.1}$$

$$A\left(\theta\right) = -min\left[12\left(\frac{\theta}{\theta_{3dB}}\right)^2, A_{\theta,m}\right]\tag{3.2}$$

where ϕ, $-180 \leq \phi \leq 180$ is defined as the angle between the direction of interest and the antenna boresight, where the antenna boresight is specified as the direction in which the maximum antenna gain presents, ϕ_{3dB} represents the 3 dB horizontal HPBW in degrees and $A_{\phi,m}$ represents the maximum attenuation of horizontal pattern. For the vertical pattern, the same structure as the horizontal pattern is used, where θ, $-90 \leq \theta \leq 90$ is defined as the angle deviation

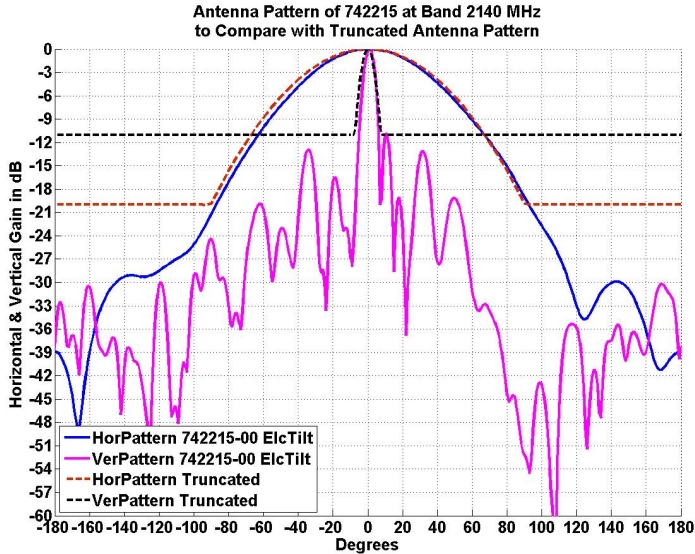**Antenna Pattern of 742215 at Band 2140 MHz to Compare with Truncated Antenna Pattern**

Figure 3.4: Antenna Gain Patterns: Measured vs. Model

from the horizontal plane, θ_{3dB} represents the vertical HPBW in degrees, and $A_{\theta,m}$ represents the maximum attenuation of the vertical pattern.

In Figure 3.4, the utilized antenna pattern models are compared with the practical antenna patterns, Kathrein 742215 , which are measured at 2140 MHz [62]. The adopted antenna pattern model better matches the practical antenna pattern in the main lobe direction and captures the main characteristics of the practical antenna. The horizontal HPBW ϕ_{3dB} is 70° (i.e. +/- 35° at -3 dB) with back lobe gain cutoff $A_{\phi,m}$ at -20 dB. The gain suppression at the theoretical cell border between sectors at 60° is -9 dB. The vertical gain pattern is a parabolic approximation of the practical pattern. It has a vertical HPBW θ_{3dB} around 10° (i.e. +/- 5° at -3 dB). The vertical back lobe gain is chosen to cutoff at the first side lobe null with $A_{\theta,m}$ of -11 dB.

Practically, the antenna can be described by the proposed model or even measured data along the horizontal and vertical pattern cuts[1] respectively. In order to describe the antenna gain with respect to the angle ϕ and θ in a given direction, a process of interpolation is needed. In the literature, different interpolation approaches have been investigated by trying to express the full-sphere

---

[1]Practically, the measurement of 3-D antenna pattern is done by measuring a number of 2-D patterns. The 2-D pattern is referred to as a pattern cut. Pattern cuts can be obtained by fixing azimuth pattern and varying elevation pattern or vice versa.

measurements as precise as possible or depicting the full-sphere gain with only a small set of parameters. As presented in [71][72] and [73], a certain weighting of the horizontal and vertical pattern models can improve the overall modeling accuracy. In order to make it simple and feasible for the system-level simulations, the two patterns can simply be added with equal unity weights as expressed in Equation 3.3 in dB:

$$A\left(\phi, \theta\right) = A\left(\phi\right) + A\left(\theta\right) \tag{3.3}$$

In order to restrict the extra attenuation introduced by the vertical pattern as shown in Figure 3.4, the maximum front to back ratio of $A\left(\phi, \theta\right)$ is limited by $max\left[A\left(\phi, \theta\right), A_{\phi, \theta, m}\right]$, where $A_{\phi, \theta, m}$ is equal to -25 dB according to the 3GPP agreement [43].

3.2.2 3-D Antenna Mechanical Tilting Modeling

The modeling of mechanical antenna tilting in the system-level simulator is done by rotating the patterns in the 3-D coordinate system. Theoretically, the rotation of the 3-D coordinate can be divided into a composition of the rotation of angle ϕ in the horizontal plane around the Z-axis and the rotation of angle θ in the vertical plane around the Y-axis. It can be expressed as:

$$\begin{bmatrix} x_{new} \\ y_{new} \\ z_{new} \end{bmatrix} = \begin{bmatrix} \cos\left(\phi\right)\cos\left(\theta\right) & \sin\left(\phi\right)\cos\left(\theta\right) & \sin\left(\theta\right) \\ -\sin\left(\phi\right) & \cos\left(\phi\right) & 0 \\ -\cos\left(\phi\right)\sin\left(\theta\right) & \sin\left(\phi\right)\sin\left(\theta\right) & \cos\left(\theta\right) \end{bmatrix} \begin{bmatrix} x_{orig} \\ y_{orig} \\ z_{orig} \end{bmatrix} \tag{3.4}$$

where x_{orig}, y_{orig}, and z_{orig} are the coordinate axis before the rotation, and x_{new}, y_{new} and z_{new} are the coordinate axis after the rotation.

If assumed that there is no rotation in the horizontal plane with the angle $\phi=0$, the above Equation 3.4 can be simplified to:

$$\begin{bmatrix} x_{new} \\ y_{new} \\ z_{new} \end{bmatrix} = \begin{bmatrix} \cos\left(\theta\right) & 0 & \sin\left(\theta\right) \\ 0 & 1 & 0 \\ -\sin\left(\theta\right) & 0 & \cos\left(\theta\right) \end{bmatrix} \begin{bmatrix} x_{orig} \\ y_{orig} \\ z_{orig} \end{bmatrix} \tag{3.5}$$

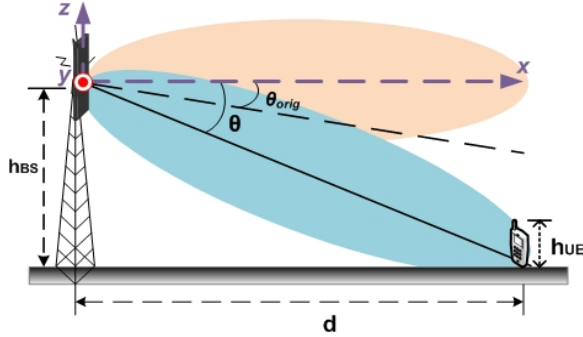According to the geometry rule, angle is measured anti-clockwise. Therefore, for

Figure 3.5: Model Of Mechanical Downtilting Rotation

the mechanical downtilting, which is measured as a clockwise angle, the rotation angle should be defined as $-\theta$ as shown in Equation 3.6:

$$
\begin{bmatrix} x_{new} \\ y_{new} \\ z_{new} \end{bmatrix} = \begin{bmatrix} \cos(\theta) & 0 & -\sin(\theta) \\ 0 & 1 & 0 \\ \sin(\theta) & 0 & \cos(\theta) \end{bmatrix} \begin{bmatrix} x_{orig} \\ y_{orig} \\ z_{orig} \end{bmatrix} \tag{3.6}
$$

Since the unit vector y_{orig} does not change, the x_{orig} and z_{orig} can then be expressed as $\cos(\theta_{orig})$ and $\sin(\theta_{orig})$, where θ_{orig} is defined as positive for downwards tilt and sometimes it is also called antenna vertical beamwidth factor. Because a certain antenna vertical beamwidth will influence the antenna downtilting angle. The above Equation 3.6 can be simplified to:

$$
\begin{bmatrix} x_{new} \\ z_{new} \end{bmatrix} = \begin{bmatrix} \cos(\theta) & -\sin(\theta) \\ \sin(\theta) & \cos(\theta) \end{bmatrix} \begin{bmatrix} \cos(\theta_{orig}) \\ \sin(\theta_{orig}) \end{bmatrix} = \begin{bmatrix} \cos(\theta + \theta_{orig}) \\ \sin(\theta + \theta_{orig}) \end{bmatrix} \tag{3.7}
$$

In a scenario, as shown in Figure 3.5, with Base Station (BS) antenna height h_{BS}, UE height h_{UE} and UE to BS distance d, the antenna mechanical downtilting angle θ can be expressed as shown in Equation 3.8:

$$
\theta = \arctan\left(\frac{h_{BS} - h_{UE}}{d}\right) - \theta_{orig} \tag{3.8}
$$

In Figure 3.6, the vertical antenna gain versus distance with different antenna downtilting angle θ has been shown. With downtilting angle $\theta = 0^o$, the max-
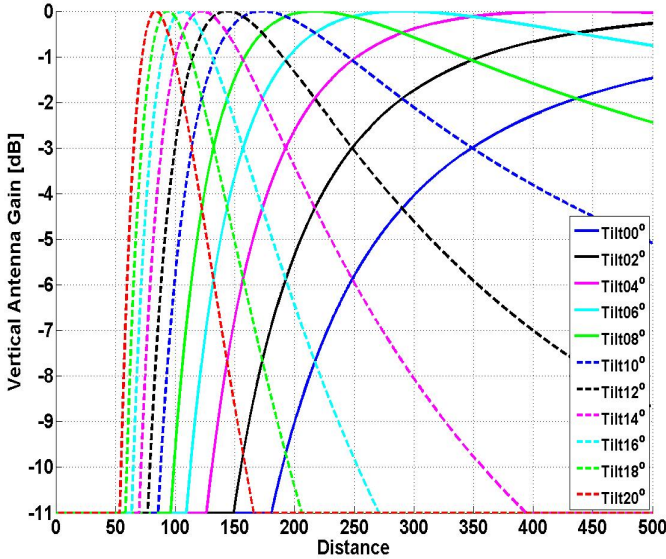
Figure 3.6: Vertical Antenna Gain versus Distance along x-axis ($\phi = 0$)

imum vertical antenna gain appears at infinite far away distance, and it is expected that the maximum vertical antenna gain value is shifted to the shorter distances with the increase of downtilting angles.

3.3 Influence of Antenna Downtilting

As shown in Figure 3.6, by ignoring the azimuth effects, the antenna gain is only dependent on the distance, which can be thought as an adjustment to the distance dependency of pathloss.

In the open environment, the effects of antenna downtilting can be fairly estimated by calculating the vertical angle between the base station antenna and the mobile antenna. However, in the urban area, the vertical angle is calculated by using the rooftop height instead of the mobile height in order to include the obstruction from the surrounding buildings. In [74], the prediction model by using the average building height proves better fit to measurements with different antenna downtilting angle. As a consequence, the impact of antenna tilting reduces and almost disappears if nearby buildings have almost equal height of

the BS antenna. In addition to this effect, the vertical antenna pattern is influenced by reflection and scattering from mounting structures, e.g. as presented in [75], the rooftop, which is a dielectric structure with finite conductivity, is much closer to the antenna and thus will have a significant influence on the radiation pattern. In this study a simplified model is applied in order to demonstrate the effect of antenna downtilting. Generally, analytical studies based on the simplified models lead to larger antenna tilting angles than experienced as best practice in actual deployment [76].

Considering the link budget of received signal power P_{rx} in dBm as:

$$P_{rx} = P_{tx} - PL_{dB} - SF_{dB} + A(\phi, \theta) \;\; [\text{dBm}] \tag{3.9}$$

where P_{tx} is the transmit power, PL is the propagation path loss, SF is the channel slow/shadowing fading, and $A(\phi, \theta)$ is the gain of antenna pattern.

For the vertical antenna downtilting, if the user is moving along the antenna boresight direction, there is no variation in the horizontal antenna gain $A(\phi)$. The total antenna gain variation only depends on the vertical antenna gain $A(\theta)$.

The modified Okumura-Hata model is adopted by 3GPP for the macro cellular simulation and it is also considered in this study. The model is described in detail in [77][78] and can be expressed as:

$$
\begin{aligned}
PL_{dB} &= 80 - 18 \cdot \log_{10}(h_{BS}) + 21 \cdot \log_{10}(f_c) \\
&\quad + \left(40 - 160 \cdot 10^{-3} \cdot h_{BS}\right) \cdot \log_{10}(d) & (3.10) \\
&= 128.1 + 37.6 \cdot \log_{10}(d) \;\; [\text{dB}] & (3.11)
\end{aligned}
$$

where f_c is the carrier frequency. And by setting $f_c = 2.0 \; GHz$ and $h_{BS} = 15$ m, the final distance dependent PL model in dB is shown in Equation 3.11.

In Figure 3.7, the vertical antenna gain $A(\theta)$ is added to the path propagation model for showing the signal strength in relation to the distance away from the BS for different antenna tilting angles. As it can be seen, with increasing downtilting angle, the $A(\theta)$ is increased at a distance close to the BS and decreased at far-away distances from the BS. This means that, with a certain optimal antenna downtilting angle, the received signal power becomes stronger within its own serving cell, and the inter-cell interference to the other neighboring cells is also reduced.
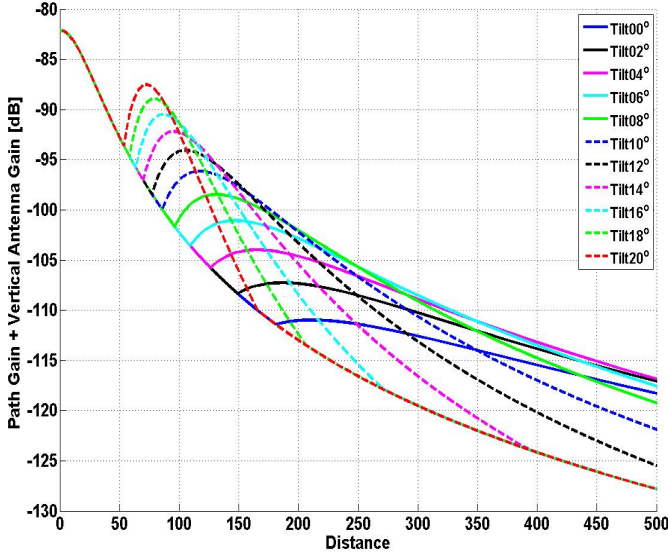
Figure 3.7: Path Gain plus Antenna Gain vs. Distance along x-axis ($\phi = 0$)

In this study, a simple antenna downtilting method is proposed for the practical LTE network application based on the simple 2-eNB scenario. As shown in Figure 3.8, UE-1 and UE-2 are served by eNB-1 and eNB-2 respectively. UE-2 acts as an interference to the UL UE-1 reception in the eNB-1 and it is located at the boresight border with distance $D = \frac{\text{ISD}}{\sqrt{3}}$ for the worst interference scenario. According to Equation 3.8, the vertical antenna gain at UE-1 and UE-2 can then be expressed as:

$$G_{\text{UE1}} = A(\arctan\left(\frac{h_{\text{BS}} - h_{\text{UE}}}{d}\right) - \theta_{\text{tilt}}) \qquad (3.12)$$

$$G_{\text{UE2}} = A(\arctan\left(\frac{h_{\text{BS}} - h_{\text{UE}}}{D}\right) - \theta_{\text{tilt}}) \qquad (3.13)$$

And based on Equation 3.11, the pathloss from the eNB-1 to UE-1 and UE-2 can be calculated as:

$$PL_{\text{UE1}} = 128.1 + 37.6 \cdot \log_{10}\left(\sqrt{(h_{\text{BS}} - h_{\text{UE}})^2 + d^2}\right) \; [\text{dB}] \qquad (3.14)$$
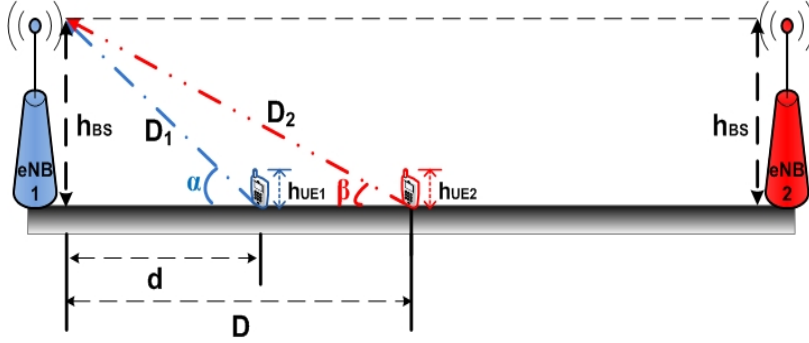
Figure 3.8: Antenna Downtilting of 2-eNB Scenario

$$\mathrm{PL_{UE2}} = 128.1 + 37.6 \cdot \log_{10}\left(\sqrt{(\mathrm{h_{BS}} - \mathrm{h_{UE}})^2 + \mathrm{D}^2}\right) \ [\mathrm{dB}] \qquad (3.15)$$

At different downtilting angle, the eNB-1 received SINR value of UE-1 with respect to distance, d, are shown in Figure 3.9 for Macro Case-1 scenario and with fixed BS and UE height it can be expressed as:

$$
\begin{aligned}
\mathrm{SINR_{UE1}}(\theta_{\mathrm{tilt}}, \mathrm{d}) \ = \ & \mathrm{PL_{UE1}(d)} + \mathrm{G_{UE1}}(\theta_{\mathrm{tilt}}, \mathrm{d}) \\
& - \mathrm{PL_{UE2}(D)} - \mathrm{G_{UE2}}(\theta_{\mathrm{tilt}}, \mathrm{D}) \qquad (3.16)
\end{aligned}
$$

For the Macro Case-1 scenario, the boresight cell border distance D = 288 m. As it can been seen from Figure 3.9, the SINR value around the cell border area is optimized at 14° downtilting. According to Figure 3.6, with 6° downtilting the main lobe of vertical antenna pattern points to the boresight cell border. To reach the optimal 14° downtilting, the eNB antenna needs to be further downtilted 8°, which is exactly the angle of the first notch in the vertical pattern as shown in Figure 3.4. So by pointing the first notch of vertical pattern to the boresight cell border, the performance of cell-edge UEs can be optimized. This method combines the geometry of cell sector with the knowledge of antenna pattern, which is also supported in the later system level simulation results as shown in Figure 3.17.

The system-level investigation of the mechanical antenna downtilting in the UL LTE will be presented in the following sections. One of the key interests of the study is the interaction of antenna downtilting with the UL FPC. As shown in the Equation 3.9, if no closed-loop FPC is applied for simplicity, the P_{tx} can
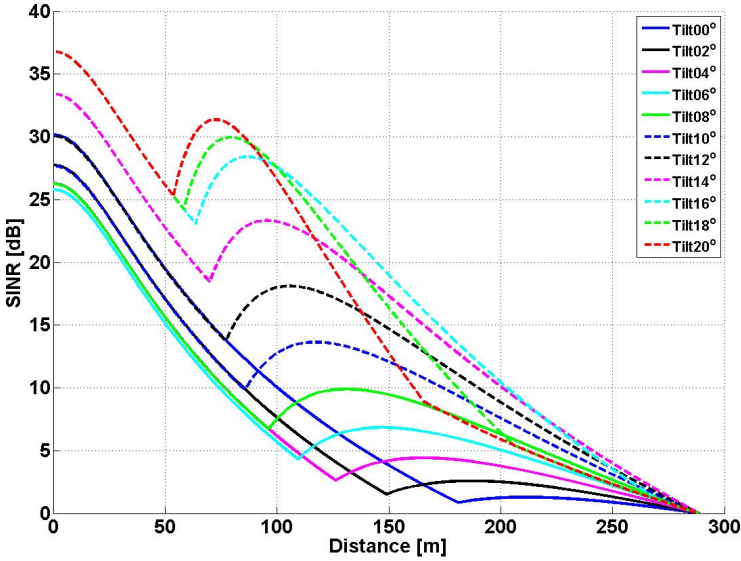
Figure 3.9: SINR vs. Distance along x-axis ($\phi = 0$)

be derived from the open-loop FPC algorithm as described in the Equation 2.6, where the Path Loss of the DL RS measured in the UE is a key component to determine the UE transmit power. By downtilting the BS antenna, the overall PL curve will be changed as shown in the Figure 3.7, which directly influences the open-loop FPC algorithm. Combining Equation 2.6 and Equation 3.9, the UE transmission power P_{tx} can be described as:

$$P_{tx} = min\{P_{max}, P_0 + 10 \cdot log_{10} N_{PRB} + \alpha \cdot L\left(A\left(\theta\right)\right)\} \qquad (3.17)$$

As shown in Equation 3.17, with constant P_0, α and the number of assigned PRB value N_{PRB}, the UE transmit power will be varied, and the network performance will be effected. This interaction between antenna downtilting and OLPC is investigated in Section 3.5.2.

3.4 Simulation Assumptions

The performance evaluation is done by using a multi-cell system-level simulator, which is developed by following the guidelines presented in [32] and described in Appendix B. The simulation assumptions and parameters related to the results discussed in this chapter are listed in Table 3.1, where the full list of default simulation parameters is presented in Table B.1.

Table 3.1: Simulation Assumptions of Mechanical Antenna Downtilting

Parameter	Assumptions
Number of UEs	10 UEs/cell
Deployment Scenario	Macro Case-1: ISD=500 m
	Macro Case-3: ISD=1732 m
HPBW	Horizontal: 70°
	Vertical: 10°
BS Antenna Gain	14 dBi
Antenna Downtilt Angle	0° to 20° with interval of 2°
P_0 and α value	Macro case-1: P_0=-58 dBm and α=0.6
	Macro case-1: P_0=-106 dBm and α=1.0
	Macro case-3: P_0=-64 dBm and α=0.6
Max UE Transmit Power	250 mW
Receiver Type	MRC
Minimum UE to BS Distance	35 m
UE Height	1.5 m
BS Height	32 m
Traffic Model	Full Buffer

As it can be seen, the simulations are carried out in the homogeneous scenario where all the UEs are uniformly distributed and balance loaded with 10 UEs/cell in the whole network area. Both the Macro case-1 and Macro case-3 scenarios are investigated in this study, where the Macro Case-1 scenario is characterized by a small cell radius with ISD of 500 m, and the Macro Case-3 scenario is indicated by a large cell radius with ISD of 1732 m. The antenna pattern of horizontal HPBW 70° and vertical HPBW 10° is utilized. All the BSs have the same height and are downtilted with the same angle from 0° to 20° with an interval of 2° in each simulation. The BS antenna is located at the roof top with the height of 32 m above ground, and the height of UEs is 1.5 m. The settings of open-loop FPC parameters are based on the previous work in [29], where the study is only considered the 2-D antenna pattern. A full or infinite buffer traffic model are applied in the study simulations, which means that the UEs always have data to transmit from their buffer.

3.5   System-Level Evaluations

In the following, the system-level evaluation of antenna downtilting in the UL LTE is presented. The Macro Case-1 scenario is first analyzed in detail, where both the open-loop Fractional Power Control parameters and the effect of vertical antenna beamwidth are thoroughly investigated in the Macro Case-1 scenario. The performance of antenna downtilting in the Macro Case-3 scenarios is also presented afterwards. In the following simulation results presented, in order to make it easy to be read the figures, only the curves with selected downtilting angles are presented.

3.5.1   Macro Case-1 Scenario

As shown in Figure 3.10, the Cumulative Density Function (CDF) of UE PL distribution is presented at different downtilting angles, where the PL for each UE contains the components of PL attenuation, slow channel fading and 3-D antenna pattern effects. By downtilting the antenna from 0° to 12°, because the downtilted antenna mainbeam is pointing toward its own cell, the PL attenuations are reduced for all the UEs. Since the cell-center UEs have better bearing of the downtilted beam, as seen from 4° to 12°, they show much better improvement than the cell-edge UEs. Further downtilting the antenna angle, as seen from 12° to 20°, the cell starts losing its coverage, which in terms of the UEs close to the cell-edge have increasing PL attenuations. However, there are still a small amount of the cell-center UEs who can benefit from the downtilted vertical beam.

The CDF of UE transmit power distribution is shown in Figure 3.11. Since only the open-loop component of FPC is utilized at different downtilting angle, the curve shape of UE transmit power distribution follows the UE PL distribution as presented in Figure 3.10. Because the maximum transmit power P_{max} is applied as shown in Equation 2.6, the UE transmit power is limited at 24 dBm ($10 \cdot log_{10} 250$ mw). At 0°, about 10% of the UEs are transmitted with maximum power. With downtilting angle to 12°, the UEs operated at saturated power are reduced to about 5%. However, by increasing the downtilting angle to 20°, more than 20% of the UEs are transmitted at maximum power because of the impact of shrinking cell coverage.

The CDF of eNB received signal power from each UE is shown in Figure 3.12. It presents the joint effect of UE PL together with UE transmit power. To compare with the previous two figures, it has to be realized that the representation of cell-edge UEs is now located at the lower left corner of the plot or 5% outage of
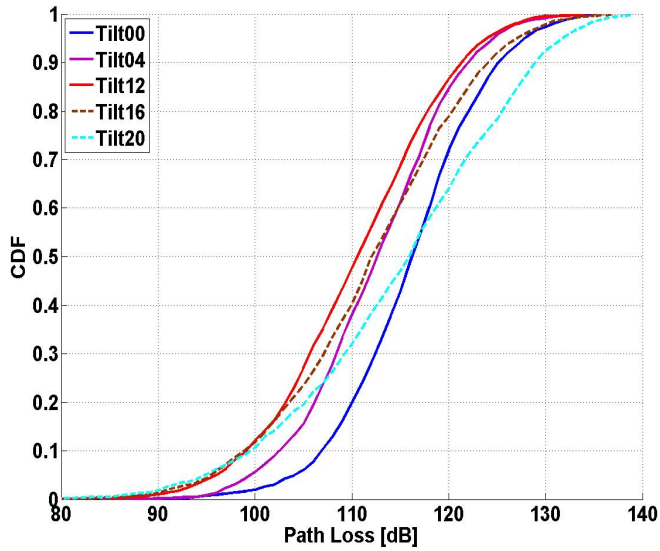
Figure 3.10: Case-1 Path Loss Distribution for fixed OLPC parameters $P_0 = -58$ and $\alpha = 0.6$
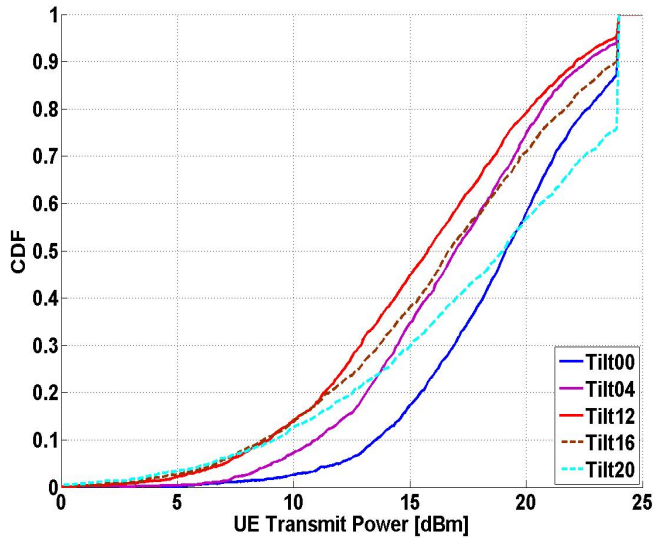

Figure 3.11: Case-1 UE Transmit Power Distribution for fixed OLPC parameters $P_0 = -58$ and $\alpha = 0.6$

the CDF curve, where in the previous two plots the cell-edge UEs are located at the upper right corner of the plot or 95% outage of the CDF curve.
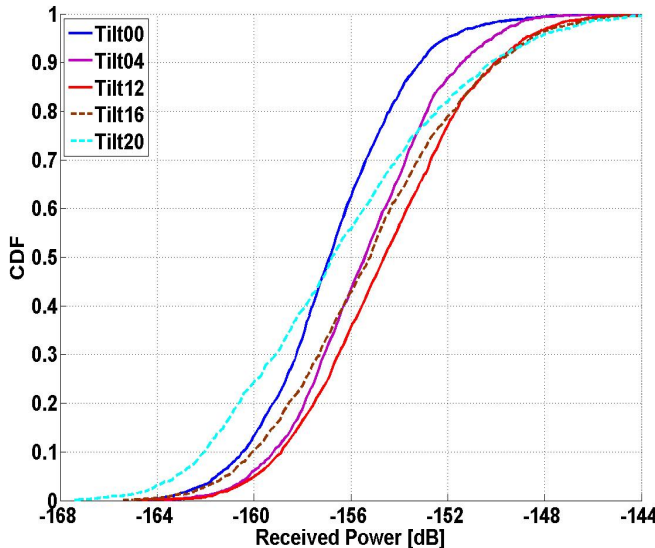

Figure 3.12: Case-1 Received Power Distribution for fixed OLPC parameters $P_0 = -58$ and $\alpha = 0.6$

Similar to the previous UE PL distribution, by increasing the antenna down-tilting angle, the average received signal power is increased until downtilting angle at 12°. For the cell-edge UEs who typically have poor signal quality, the average received signal power are working equally good for both 4° to 12°. But for the cell-center UEs, their performance can still be improved without losing the cell-edge UE performance because of better bearings of the vertical antenna gain and the average received signal power is maximized at 12°. When the downtilting angle is larger than 12°, the downtilting antenna beam is pointing to the area too close to the eNB, and a huge percentage of UEs cannot benefit from the vertical antenna gain any more, which leads to the decreased average received signal power.

In Figure 3.13, the CDF of Interference over Thermal noise (IoT) is shown, and the IoT is defined as [7]:

$$\mathrm{IoT} = \frac{(\mathrm{I_{PSD}} + \mathrm{N_{PSD}})}{\mathrm{N_{PSD}}} \tag{3.18}$$

where I_{PSD} is the interference spectral density, and N_{PSD} represents the noise spectral density. The IoT indicates the level of interference in the system assuming the noise as reference. In case there is no interference in the system, the IoT is equal to 1.0 in linear or 0.0 dB.

As expected in Figure 3.13, by increasing the downtilting angle, the IoT strength is decreased. To compare the non-downtilt case with downtilt angle at 12°, at 50% of the CDF, there is around 4 dB reduction of the IoT, and at 95% of the CDF there is around 2 dB reduction of the IoT.
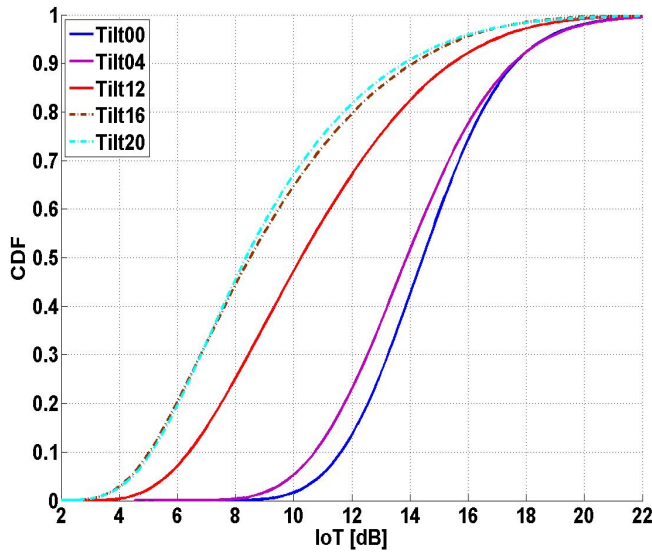
Figure 3.13: Case-1 Interference over Thermal Noise for fixed OLPC parameters $P_0 = -58$ and $\alpha = 0.6$

In Figure 3.14, the CDF of average UE SINR is plotted. At 50% of the CDF, for the downtilting angle at 12°, with the joint effect of increasing the received signal power and decreasing the received inter-cell interference strength as presented in above, there are about 5 dB increases of the SINR compared with the non-tilt case. For the downtilting angle at 16°, even though the average received signal power is about 0.6 dBm less than the downtilting angle at 12°, the average IoT strength is about 1.9 dB higher, and the SINR is still about 1.0 dB higher than the 12° case. For the cell-edge user at 5% outage, with the 16° case, the IoT reduction can not compensate for the decreased received signal power anymore, which makes the overall SINR performance worse than the 12° downtilting case.
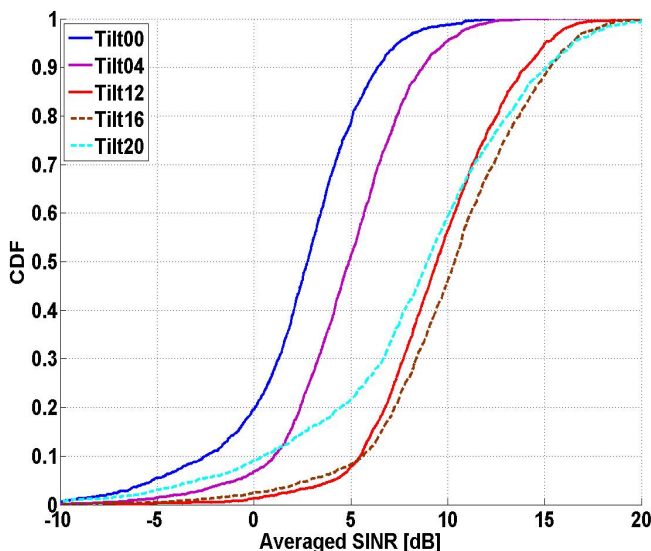
Figure 3.14: Case-1 Received SINR Distribution for fixed OLPC parameters $P_0 = -58$ and $\alpha = 0.6$

The CDF of average UE throughput is presented in Figure 3.15. At different downtilting angles, the UE throughput curves have the same trend as the average SINR curves presented in Figure 3.14. In order to improve the overall network performances for both cell-center and cell-edge UEs, the amount of antenna downtilting angle is always a trade-off between the cell coverage and capacity, where the cell coverage is defined as the CDF of UE throughput at 5% level.

In Figure 3.16, the cell coverage and cell capacity versus different antenna downtilting angles are shown respectively. As it can be seen, the cell coverage is maximized at 14°. With a further increase of the downtilting angle, the cell coverage starts shrinking, which results in a poor performance or lower SINR for the cell-edge UEs. For the cell capacity, it is still further improved and maximized at downtilting angle of 16°, because of the cell-center UEs better bearing of the downtilted antenna pattern. With a further increase of the downtilting angle above 16°, even the cell-center UEs cannot benefit much from the vertical antenna gain any more, which makes the cell capacity decrease.

Based on the above analysis, for the Macro Case-1 scenario, the optimal enhancement by downtilting angle at 14° is the best choice to achieve increased overall network performance.
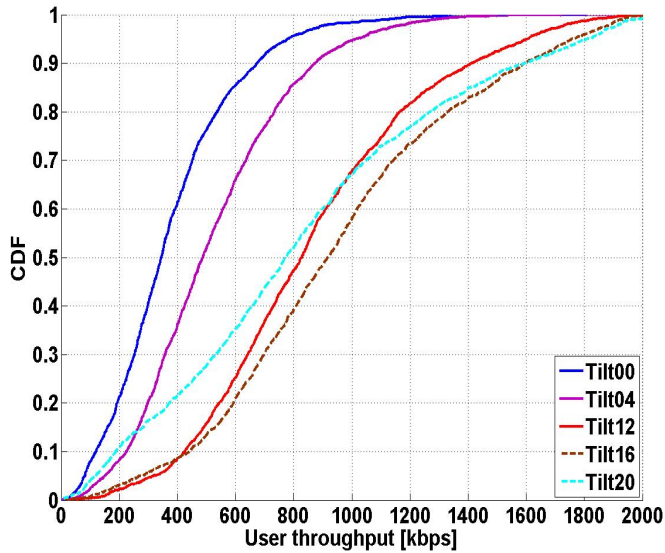
Figure 3.15: Case-1 UE Throughput Distribution for fixed OLPC parameters $P_0 = -58$ and $\alpha = 0.6$
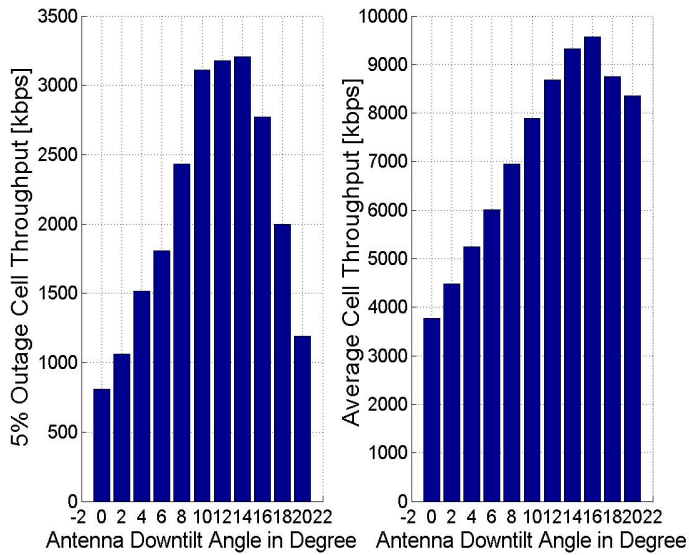

Figure 3.16: Case-1 Average Cell Throughput vs. Cell-edge Throughput with $\alpha = 0.6$

3.5.2   Interaction of Antenna Tilting with Open-Loop fractional Power Control - Case 1

In the previous section, the settings of open-loop FPC parameters are based on the work in [29], which only considered the 2-D antenna pattern. In this section, the chosen of open-loop FPC parameters are evaluated under the 3-D antenna pattern configuration.

In Figure 3.17 and 3.18, the interaction between antenna tilting and OLPC is shown with $\alpha = 0.6$ and $\alpha = 1.0$ in terms of average cell throughput and 5% outage cell throughput.
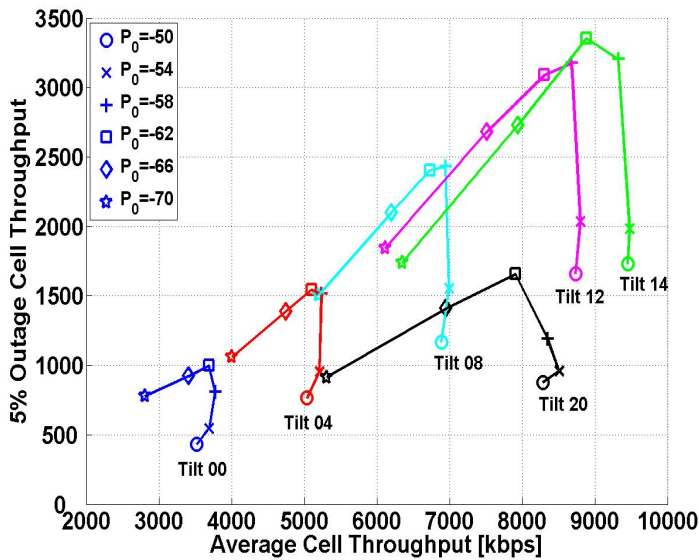

Figure 3.17: Case1 Average Cell Throughput vs. 5% Outage with $\alpha = 0.6$

As it can be seen from the $\alpha = 0.6$ case in Figure 3.17, different colored curve represents the antenna downtilting angles, and variation of P_0 value is shown for each individual downtilting angle. In general, both the 5% outage and average cell throughput is improving with the increasing P_0 value until a certain optimum point, i.e. -58 dBm at 12° case. This is due to the fact that both cell-edge and cell-center UEs can improve the received SINR by increasing of transmit power, and the optimum point can simply be estimated from the Equation 2.6, where by taking the 12° case as an example, with the simulation assumption of 6 PRBs and the total PL of 124 dB as shown in 95% outage of Figure 3.10, the
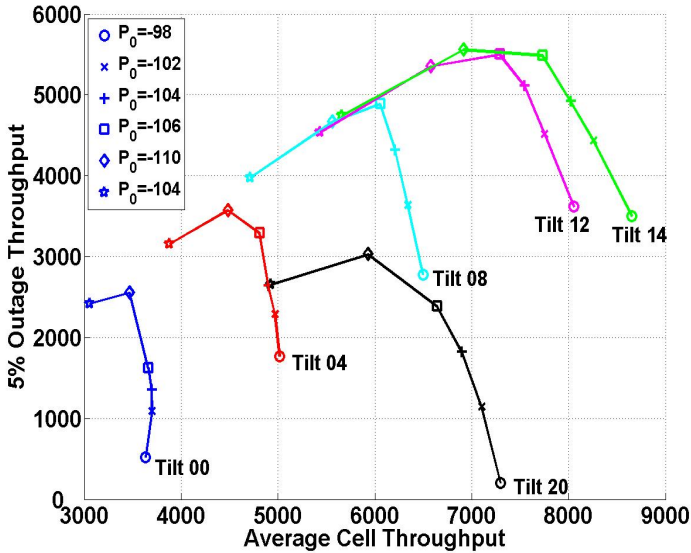
Figure 3.18: Case-1 Average Cell Throughput vs. 5% Outage with $\alpha = 1.0$

optimal P_0 value is equal to -58 dBm $(10 \cdot \log_{10} 250 - (10 \cdot \log_{10} 6 + 0.6 \cdot 124))$.

By further increasing the P_0 value over the optimal point, many cell-edge UEs start transmitting at the maximum power which generates higher interference to the other UEs. For the cell-center UEs in Figure 3.17, they can still benefit slightly from the increasing received power and result in average cell throughput gains. But for the 5% cell-edge UEs, their performance is decreased considerably by the increased interference, i.e. at 12° case the varying of P_0 value from -58 dBm to -50 dBm reduces the 5% outage throughput dramatically.

The plots with $\alpha = 1.0$ case are shown in Figure 3.18. As expected, both 5% outage and average cell throughput are enhanced with increase of downtilting angle until the optimal angle of 14° and the optimal P_0 value of -106 dBm $(10 \cdot \log_{10} 250 - (10 \cdot \log_{10} 6 + 1.0 \cdot 124))$. To compare with $\alpha = 0.6$, utilizing $\alpha = 1.0$ maximizes the cell-edge UE throughput by compromising the cell-center UE performances. At optimal downtilting angle of 14° with $\alpha = 1.0$ and $P0 = -106$ dBm, the 5% outage and average cell throughput is about 5.5 Mbps and 7.8 Mbps respectively as shown in Figure 3.17, whereas for $\alpha = 0.6$ with $P0 = -62$ dBm as shown in Figure 3.18, the 5% outage and average cell throughput is about 3.4 Mbps and 9.0 Mbps respectively.

3.5.3   Macro Case-3 Scenario

The antenna downtilting scheme has also been evaluated under the Macro Case-3 scenario. Compared with the interference-limited Macro Case-1 scenario, Macro Case-3 is more noise-limited with larger ISD. As discussed in Section 3.3, the vertical antenna downtilting scheme is an efficient inter-cell interference reduction technique, and as presented in the previous Section 3.5.1, both the 5% outage and average cell throughput can be enhanced with the optimal antenna downtilting in the Macro Case-1 scenario. So how much gain can the antenna downtilting help under the noise-limited scenario?
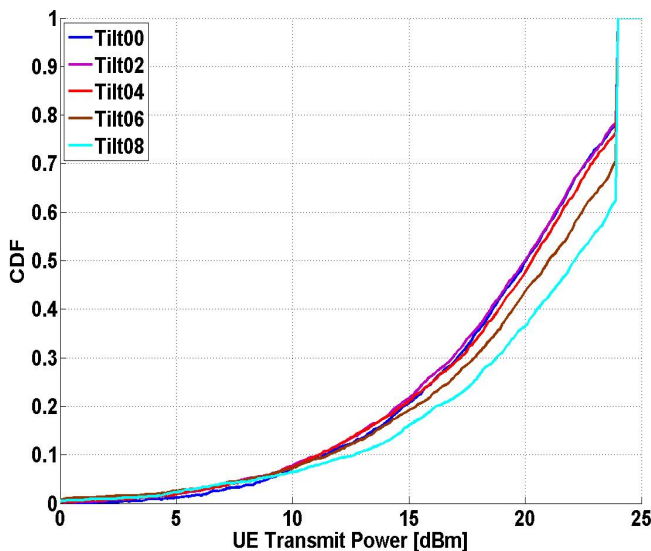

Figure 3.19: Case-3 UE Transmit Power Distribution for fixed OLPC parameters $P_0 = -64$ and $\alpha = 0.6$

In Figure 3.19, the CDF of UE transmit power is shown at different downtilting angle from 0° to 8° with interval of 2°. As it can be seen, with downtilting angle of 0°, about 20% of UEs are transmitted with maximum power. The further downtilting of antenna does not reduce the UE PL, but rather loses the cell coverage, where more UEs start operating at sacturated power in order to maintain their own performances. At downtilting angle of 8° there are nearly 40% maximum power UEs.

The CDF of IoT is shown in Figure 3.20, as expected under the noise-limited scenario, the average interference is already very small, i.e. at 50% the IoT is
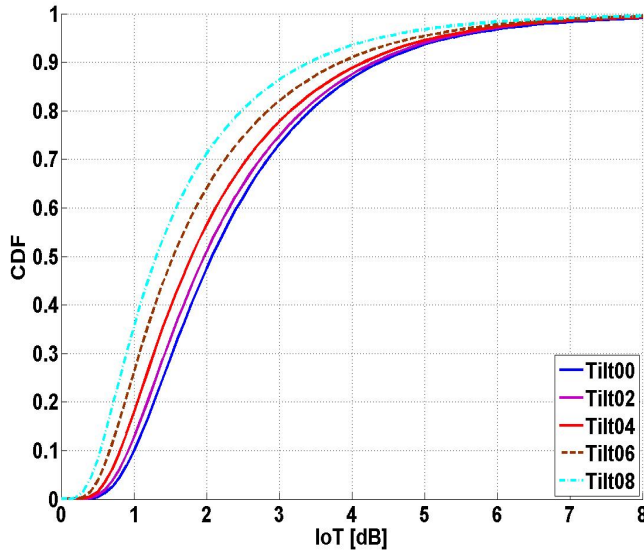
Figure 3.20: Case-3 Interference over Thermal Noise for fixed OLPC parameters $P_0 = -64$ and $\alpha = 0.6$

about 2 dB with dowtilting angle of 0°. By further downtilting the antenna, the reduced interference is very marginal, i.e. at downtilting of 8° there is about 1 dB reduction at 50%.

As discussed in Section 2.5, the FPC scheme partially compensates the PL, which means that not all the UEs have the same SINR requirements. In the Macro Case-1 scenario as presented in Section 3.5.2, the cell-edge UEs are able to meet the SINR requirements imposed by the FPC algorithm at different downtilting angles, since only a few cell-edge UEs (about 5%-10% of total users shown in Figure 3.11) are transmitted with maximum power as they are in an interference-limited scenario. However, when noise becomes the main constraint, with different downtilting angles as shown in Figure 3.19, the cell-edge UEs are in any case transmitting at maximum power so they tend to experience a similar SINR regardless of the PL compensation factor. This behavior predicts a less noticeable effect of the FPC algorithm with antenna downtilting on the 5%-outage performance in Macro Case-3 scenario.

Based on the above transmit power and interference analysis, the CDF of received SINR distributions is shown in Figure 3.21. It is no surprise that there is nearly no SINR improvement by using antenna downtilting under the Macro
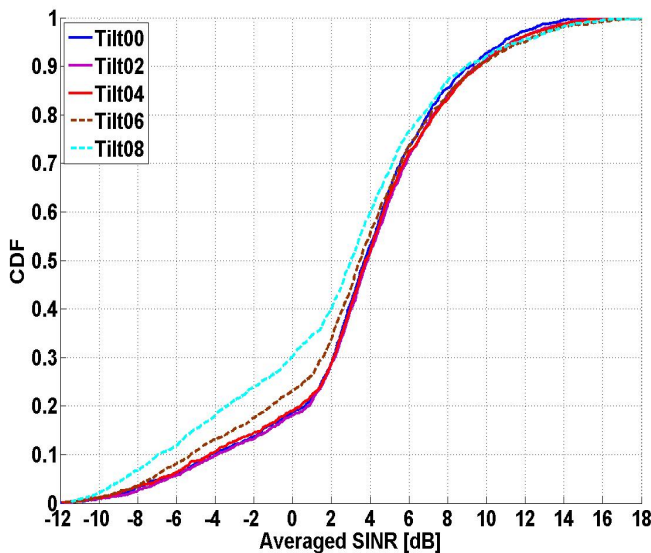
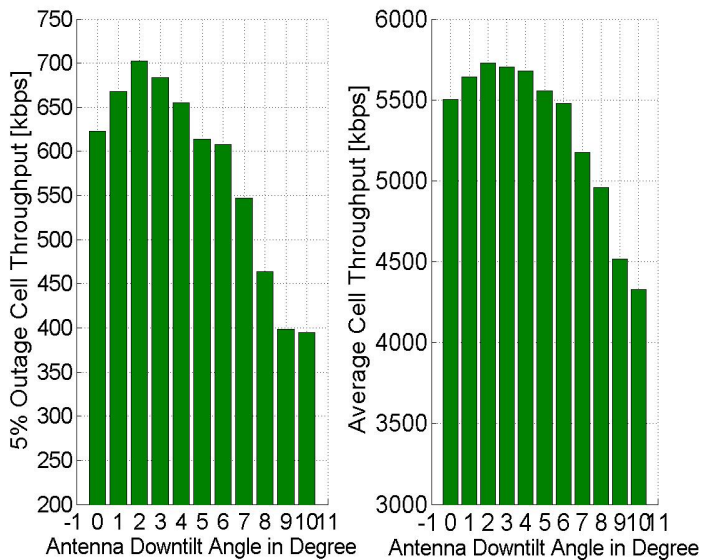Figure 3.21: Case-3 Received SINR Distribution for fixed OLPC parameters $P_0 = -64$ and $\alpha = 0.6$

Figure 3.22: Case-3 Average Cell Throughput vs. Cell-edge Throughput with $\alpha = 0.6$

Case-3 scenario. For each downtilting angle, the probability peaks in the curve between 20% and 40% range are caused by the cell-edge UEs operated at maximum transmit power, where the corresponding number of percentage for each angle can also be seen in the Figure 3.19.

The 5% outage and average cell throughput versus the antenna downtilting angle are shown in Figure 3.22. As it can be seen, the 2° is the optimal antenna downtilting angle for the Macro Case-3 scenario in terms of both cell-edge and average UE throughput.

3.5.4   Effect of Antenna Beamwidth

The effect of different vertical antenna HPBW has also been evaluated in this study under the Macro Case-1 scenario.
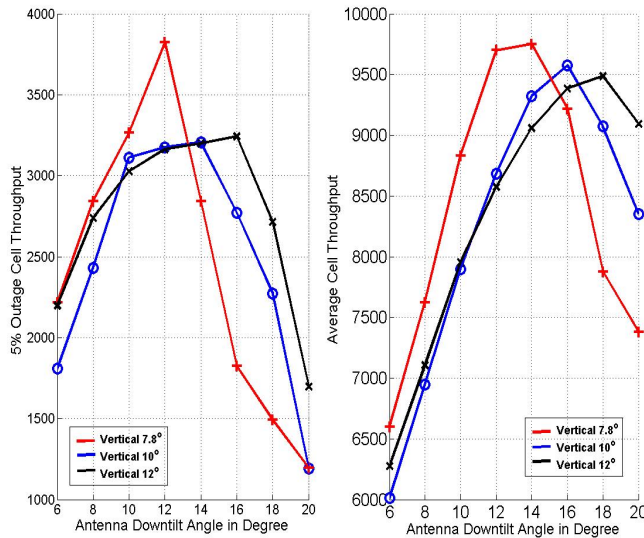

Figure 3.23: Case-1 5%-outage vs. Average Cell Throughput with Vertical Antenna Pattern 7.8^o, 10.0^o and 12.0^o for fixed OLPC parameters $P_0 = -58$ and $\alpha = 0.6$

In Figure 3.23, three vertical antenna patterns with HPBW equal to 7.8^o, 10.0^o and 12.0^o are investigated. As it can be seen, the narrower vertical antenna pattern, i.e. HPBW=7.8^o, provides higher performance at optimal downtilting angle in both 5% outage and average cell throughput. However, it is also very

sensitive to the antenna downtilting angle. If the antenna is downtilted over the optimal angle, the 5% cell-edge UE performance is decreased dramatically. Whereas with wider vertical antenna pattern, the overall performance can be maintained over a certain downtilting angle range. Practically, it can tolerate some extent of downtilting angle bias by installation or tuning defects. In 3GPP, the vertical antenna pattern with HPBW equal to 10° is used for system-level evaluation.

3.6   Conclusions

In this chapter, the mechanical antenna downtilting was studied in the UL LTE. The modeling and influence of mechanical antenna downtilting has been discussed first. A simple antenna downtilting model has been proposed for the practical LTE application. By pointing the first notch of vertical antenna pattern to the boresight cell border, the mechanical downtilted antenna can optimize the cell border user throughput.

The study followed by the system-level evaluations, where the simulations have been performed with network-based mechanical antenna downtilting in the homogeneous UL LTE network, where both Macro Case-1 and Macro Case-3 scenario have been studied. As a sum-up, the performance gain is presented in Table 3.2 compared with the downtilting case of 0°.

Table 3.2: Performance Gain of Mechanical Antenna Downtilting

Parameter	Throughput Gains at Downtilting Angle			
Macro Case-1:	14°		16°	
	5% outage	Aver. Thrpt.	5% outage	Aver. Thrpt.
$\alpha = 0.6, P_0 = -58$	296%	147%	242%	153%
$\alpha = 1.0, P_0 = -106$	239%	111%	196%	121%
Macro Case-3:	2°			
	5% outage		Aver. Thrpt.	
$\alpha = 0.6, P_0 = -64$	13%		4%	

As it can be seen, being an inter-cell interference mitigation technique, the mechanical downtilting works efficiently under the interference-limited Macro Case-1 scenario. Independent of OLPC parameters applied, the optimal antenna downtilting angle for Macro Case-1 is 14° in terms of cell-edge user performance and 16° in terms of average user throughput. Under the noise-limited Macro Case-3 scenario, the application of antenna downtilting is less effective and the optimal antenna downtilting angle is about 2°. It should be mentioned here

that the presented results and conclusions are based on a simplified channel model and valid for the homogeneous network only. For a real deployment the optimal tilting angles are actually smaller depending on the ISD distribution. The results are also based on the 3GPP antenna patterns, which in reality can look much different, hence lead again other optimal tilt angles.

The interaction of antenna downtilting together with the LTE open-loop FPC has also been investigated under the Macro Case-1 scenario. The impact of mechanical antenna tilting can be neglected. The optimization of UL open-loop FPC and antenna tilting can be conducted independently.

The effect of antenna vertical HPBW has also been analyzed under the Macro Case-1 scenario. The results show that the narrower the vertical antenna pattern, the higher performance can be achieved at the optimal downtilting angle. However, it is also very sensitive to the over downtilting of antenna, where both cell-edge user performance and average user throughput are decreased dramatically after the optimal angle. By utilizing wider vertical antenna pattern, the overall network performance can be maintained over a certain downtilting angle range. Practically, it can also tolerate some extent of downtilting bias by installation or tuning defects. In 3GPP application, the vertical antenna pattern with HPBW equal to 10^0 is is used for system-level evaluation purpose.

Uplink CoMP in the Form of Macro-Scopic Combining

Coordinated Multi-Point (CoMP) is an advanced technique for interference mitigation which is proposed in the LTE-A study item as one of the features to further reduce the impact of co-channel inter-cell interference [26]. For the UL LTE application, the CoMP schemes include CoMP reception and coordinated packet scheduling. The CoMP reception is to process signals received from multiple cells which are separated or not (inter- or intra-site, in the description) and the coordinated PS can be seen as an extension of the Inter-Cell Interference Coordination (ICIC) scheme already present in LTE by coordinating different cell sites in terms of the scheduling decision (PRB allocation) in frequency domain.

In this chapter, the potential of CoMP reception in the form of macro diversity combining is analyzed. As shown in the following investigations, with the combination of Interference Cancellation (IC) and Close-Loop fractional Power Control scheme together with macro diversity reception, the overall UL LTE network performance can be further improved.

In Section 4.1, the state of the art of UL CoMP is presented, and the defined UL CoMP scenario for this study is described in Section 4.2. In Section 4.3, the concept of macro diversity reception is briefly discussed, and the principle of utilizing ideal IC is explained in Section 4.4. In Section 4.5, the applied CLPC scheme is described based on the IC-based macro diversity reception. In Section 4.6, the modeling assumptions for this study are depicted, and the performance evaluation results are presented in Section 4.7. Finally, the conclusions for the macro diversity reception study are made in Section 4.8.
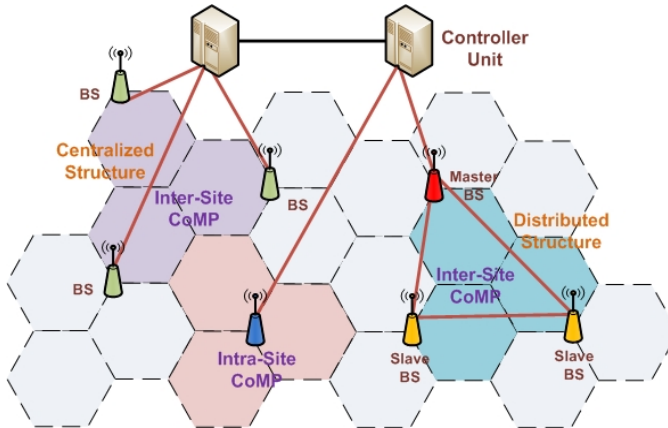
Figure 4.1: CoMP Structure [79]

4.1   Coordinated Multi-Point

Under the interference-limited LTE environment, the main goal for applying UL/DL CoMP techniques is to enhance both the cell-edge UE performance and the average user throughput in an LTE-A system by mitigating the inter-cell interference [26]. Theoretically, the inter-cell interference can be transformed into the useful signal and being completely eliminated.

The basic idea behind CoMP is to make the multiple cells or network nodes co-operate via information exchange with centralized and/or distributed structures [26] as shown in Figure 4.1. With centralized structure, the collaboration eNBs are connected to a controller unit by means of fast backhaul network, e.g. Radio over Fiber (RoF) links. In this way, the central processing of exchanged information can be performed within the controller unit. Alternatively, with the distributed or decentralized structure, the eNBs are inter-connected through microwave or RoF links, i.e. X2-interface in LTE, and a master eNB has the central processing functionality to joint process the exchanged information and coordinate the so-called slave/coordination eNBs. In general, the distributed structure can be applied in the local small area and the centralized structure can be utilized in a wider region which might contain several localized CoMP with distributed manner.

In the practical application, the CoMP cooperation can be applied with either intra-site or inter-site coordination as also shown in Figure 4.1. With the intra-site coordination, the sectorized eNB naturally contains the central processing

unit to control its own cells. Therefore, the latency of information exchange is ideally zero (Practically due to the hardware issues, the latency may be non-zero). Besides, all coordinated sectors belong to the same site could be driven by the same clock. So the synchronization of a certain UE to all the coordinated sectors can be achieved. On the contrary, for the inter-site coordination, the co-operation strategies with information exchange heavily depends on the capacity and latency of the links between the coordinated eNBs, and the synchronization in both time and frequency of all coordinated sectors is a technical challenge in practice [80].

For the UL LTE applications, the CoMP involves the techniques such as CoMP reception and coordinated packet scheduling. The CoMP reception implies reception of UE transmitted signal at multiple geographically separated eNB antennas. Independent of the CoMP cooperation being utilized, it is practically infeasible to fully cooperate network over a large scale. Restriction of the collaboration to a reasonable and small number of cells is required. Therefore, a so-called CoMP cooperation area needs to be defined [81].

In the open literature, there are many research work dedicated to the study of CoMP technology. The initial design concepts of CoMP systems have been reported in [79]. From the theoretical point of view, the common conclusion is that CoMP systems can bring tremendous improvement in the system performance for both cell coverage and cell throughput. The corresponding theoretical results have been presented in [36][37][38] for UL and [39][40][41] for DL. However, considering of the practical aspects, the benefits of CoMP systems come at a high cost of complexity and additional infrastructure. Several papers [82][83][84] and 3GPP contributions [85][86][87][88] have reported the performance evaluation results for CoMP at system level, but most of the studies were focus on the DL CoMP investigations. Depending on the assumptions and the complexity of studied scenarios, the reported CoMP performance gain can be varied significantly . From [84], 52% of average cell throughput gain and 144% of cell-edge user throughput gain have been reported with dual stream CoMP transmission, but no detailed explanations about the CoMP UE selection and scheduling issues. Whereas in [89], detailed CoMP UE selection are employed under the Macro Case-1 scenario, the reported gain for cell throughput and cell-edge throughput is 0% and 15.8% respectively. Based on the 2-D antenna pattern assumption in [90][91], 18% and 30% of gain in terms of 5% outage and average user throughput has been reported for the UL LTE compared to the LTE Rel'8. The field trial results have also been presented in [92] for UL CoMP based on the cellular scenarios of 2 base stations and 2 terminals. The reported 50% practical gain of user throughput is much smaller than the 150% theoretical prediction due to the impact of imperfect channel estimation, limited number of usable modulation and coding schemes, and various RF impairments.

In this study the CoMP reception in the form of macro diversity reception is investigated based on the defined CoMP scenarios and 3-D antenna pattern assumption presented in the previous chapter.

4.2 UL CoMP Study Scenario

In this study, an UL CoMP scheme is assumed where the serving eNB independently performs the RRM, i.e. dynamic PS, for the serving UEs, and it can request coordination from the neighboring eNBs for a specific UE through the X2-interface. An ideal X2 interface is assumed in order to find the upper bound for the performance of UL CoMP, where the link connections, e.g. optical fiber, between the sites have unlimited bandwidth, and no delay is considered.
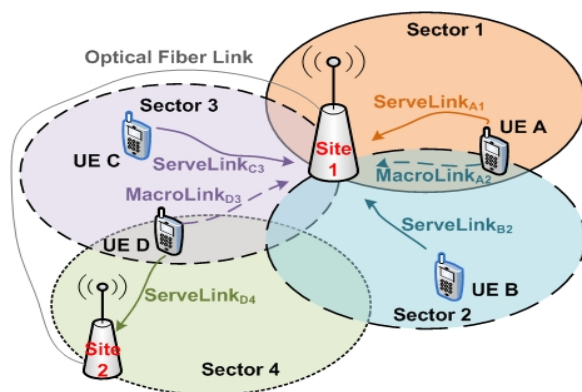

Figure 4.2: CoMP - Macro Diversity Layout

The maximum number of 3 neighboring eNB cooperation is considered, where the macro diversity reception scheme was investigated with either Intra-Site or Inter-Site scenario. For a certain UE, if the serving and coordination cells are limited to having the same site reception, then it is called Intra-Site macro diversity reception. As shown in Figure 4.2, for *UE-A*, the serving link 'A1', where the signal is received in the serving cell, and the macro diversity link 'A2', where the signal is received in the coordination cell, are centrally processed in the same Site-1. In this case no X2-interface is required for information coordination between cells. When the cross site reception is also allowed through the X2-interface coordination, then it is called Inter-Site macro diversity reception, i.e. as shown in Figure 4.2, serving link 'D4' and macro diversity link 'D3' of the *UE-D* signal are separately received in Site-1 and Site-2. By transferring the

necessary reception information from Site 1 to Site 2 through X2-interface, the processing of macro diversity received signals can be performed in the serving Site-2. In this study both cases are studied, and the Intra-Site macro diversity reception is mainly used as a reference to the Inter-Site macro diversity reception.

UL CoMP operation for all the UEs in the network is practically infeasible. In this study the selection of CoMP UEs, i.e. *UE-A* and *UE-D* in Figure 4.2, is based on the RSRP measurement. The RSRP is defined as the linear average over the power contributions of the resource elements that carry DL cell-specific reference signals[1] within the considered measurement frequency bandwidth [16][93]. The measurement reporting is assumed to be UE-assisted and network-decided, where the UE measures the RSRP from the neighboring eNBs and reports the RSRP measurements back to the serving eNB. Based on the measurements, the serving eNB will make the decision on whether a certain UE i should be macro diversity received or not according to the criteria:

$$\mathrm{RSRP}^i_{\mathrm{ServeLink}} - \mathrm{RSRP}^i_{\mathrm{OtherLinks}} \leq \mathrm{X}\,[\mathrm{dB}] \qquad (4.1)$$

where $\mathrm{RSRP}_{\mathrm{ServeLink}}$ is the RSRP measurement taken from the serving eNB, $\mathrm{RSRP}_{\mathrm{OtherLinks}}$ is the RSRP measurement from one of the other surrounding eNBs except the serving eNB and X is called triggering threshold or Combining Window Size (CWS).

If a certain UE fulfills the criteria stated in Equation 4.1, then the UE is defined as 'Macro Diversity UE' with the corresponding eNB.

4.3   Macro Diversity Reception

Diversity is one of the MIMO technology applications. Depending on whether the diversity is implemented in the transmitter or the receiver, it can be determinated as transmitter diversity, i.e. Multiple Input Single Output (MISO) and receiver diversity, i.e. Single Input Multiple Output (SIMO). In this study the receiver diversity reception is considered. The basic idea behind receiver diver-

---

[1]Downlink Reference Signal contains Cell-Specific RS used by the UE for cell search, initial acquisition and DL channel quality measurements, UE-Specific RS used by the UE to estimate the DL channel to decode the eNB DL transmission and MBSFN RS for broadcasting channel. Uplink Reference Signal contains Demodulation RS used by the eNB to estimate the UL channel to decode the UE UL transmission and Sounding RS used by the eNB to estimate the UL channel conditions for each user to decide the best UL scheduling.

sity is that multiple antennas receive different versions of the same signal and the chance of all these copies of signal being in a deep fade is small. Therefore, the reception reliability is enhanced. The combining schemes, such as MRC, Selection Combining (SC) or Equal Gain Combining (EGC), can be utilized to combine the received diversity signals. In this study the MRC scheme is studied in details and the SC scheme is utilized as a reference.

Considering the received signal model with single transmit antenna from UE i as:

$$\mathbf{r}_i = \sqrt{P_{tx,i}}\mathbf{h}_i s_i + \sum_{j=1,j\neq i}^{N_u} \sqrt{P_{tx,j}}\mathbf{h}_j s_j + \mathbf{n} \tag{4.2}$$

$$= \sqrt{P_{tx,i}}\mathbf{h}_i s_i + \boldsymbol{\omega} \tag{4.3}$$

where $\mathbf{r}_i = [r_1 \ r_2 \cdots r_{N_r}]^T$ is the received signal vector from UE i on the N_r coordination cell receive antennas. $\mathbf{h}_i = [h_1 \ h_2 \cdots h_{N_r}]^T$ is the channel vector of UE i on the N_r receive antennas. s_i is the transmitted signal of UE i with transmit power of $P_{tx,i}$. N_u is the number of UEs transmitting on the identical PRB. s_j is the transmitted signal of interference UE j with transmit power of $P_{tx,j}$. $\mathbf{h}_j = [h_1 \ h_2 \cdots h_{N_r}]^T$ is the channel vector associated with the j-th interfering UE. $\mathbf{n} = [n_1 \ n_2 \cdots n_{N_r}]^T$ is the noise vector on the N_r receive antennas and $\boldsymbol{\omega}$ represents the inter-cell interference plus noise vector over the transmission PRBs.

For the MRC, both phase correction and amplitude weighting estimations are required at the receiver. The MRC combiner output signal can be expressed as:

$$\widehat{s}_i = \mathbf{h}_i^H \mathbf{r}_i = \mathbf{h}_i^H \sqrt{P_{tx,i}}\mathbf{h}_i s_i + \mathbf{h}_i^H \boldsymbol{\omega} \tag{4.4}$$

And the SINR of MRC combiner output is:

$$\gamma_{mrc} = \frac{E\left\{\left|\mathbf{h}_i^H \sqrt{P_{tx,i}}\mathbf{h}_i s_i\right|^2\right\}}{E\left\{\left|\mathbf{h}_i^H \boldsymbol{\omega}\right|^2\right\}} = \frac{P_{tx,i}\left|\mathbf{h}_i^H \mathbf{h}_i\right|^2 E\left\{s_i s_i^H\right\}}{E\left\{\left|\mathbf{h}_i^H \boldsymbol{\omega}\boldsymbol{\omega}^H \mathbf{h}_i\right|\right\}} = \frac{P_{tx,i}\left|\mathbf{h}_i^H \mathbf{h}_i\right|^2}{\mathbf{h}_i^H E\left\{\boldsymbol{\omega}\boldsymbol{\omega}^H\right\}\mathbf{h}_i}$$

$$= \frac{P_{tx,i}\left|\mathbf{h}_i^H \mathbf{h}_i\right|^2}{\sigma_\omega^2 \mathbf{h}_i^H \mathbf{U}_{N_r} \mathbf{h}_i} = \frac{P_{tx,i}\left|\mathbf{h}_i^H \mathbf{h}_i\right|^2}{\sigma_\omega^2 \mathbf{h}_i^H \mathbf{h}_i} = \frac{P_{tx,i}\left|\mathbf{h}_i^H \mathbf{h}_i\right|}{\sigma_\omega^2} \tag{4.5}$$

$$= \sum_{a=1}^{N_r} \frac{P_{tx,i}|h_{i,a}|^2}{\sigma_\omega^2} \tag{4.6}$$

$$= \sum_{a=1}^{N_r} \gamma_{i,a} \tag{4.7}$$

where $\mathbf{U}_{N_r}$ denotes an $N_r \times N_r$ identity matrix. The inter-cell interference plus noise power is assumed to be spatially and temporally white with variance σ_ω^2. $h_{i,a}$ is the channel of UE i at a-th receive antenna.

It is intuitive to note that the term $\boldsymbol{h}_i^{\mathrm{H}} \boldsymbol{h}_i = \sum_{a=1}^{N_r} |h_{i,a}|^2$ is actually the sum of the signal channel powers across all the N_r receive antennas and the total MRC output SINR γ_{mrc} is the sum of SINR $\gamma_{i,a}$ at each antenna.

Unlike the MRC scheme, for the SC scheme, the receive antenna with the highest SINR is chosen for further processing. The simple SC scheme only needs a measurement of signal power, whereas the phase correction and amplitude weighting information is not required. The SINR of SC combiner output is:

$$\gamma_{sc} = \max_{a \in [1, \cdots, N_r]} \{\gamma_{i,a}\} \tag{4.8}$$

As seen from Equation 4.8, the SC scheme wastes the signal energy by discarding $(N_r - 1)$ copies of the received signal. This drawback is avoided by the MRC scheme, as shown in Equation 4.7, which exploits all available signal copies by multiplying a complex weight in each signal copy and then sums them up.

According to [43] and presented in Figure 2.1, the user plane protocol stack in LTE includes the protocols MAC, RLC, and PDCP. The MAC layer scheduler decides the transport block size of the MAC Protocol Data Unit (PDU) to be transmitted over the air interface. Based on this decision the RLC protocol provides on request of the MAC layer a RLC PDU of appropriate size to the MAC protocol either by concatenation or segmentation of PDCP PDUs. From the Equation 4.2 and 4.5, for the whole MAC transport block, the received SINR for UE i with MRC can then be expressed as:

$$\gamma_{mrc}^{mac} = \sum_{a=1}^{N_r} \frac{\frac{\mathrm{P}_{tx,i}}{\mathrm{N}_{\mathrm{PRB}}} \sum_{p=1}^{\mathrm{N}_{\mathrm{PRB}}} |h_{i,a,p}|^2}{\sum_{p=1}^{\mathrm{N}_{\mathrm{PRB}}} \left(\sum_{j=1, j \neq i}^{\mathrm{N}_u} \frac{\mathrm{P}_{tx,j}}{\mathrm{N}_{\mathrm{PRB}}} |h_{j,a,p}|^2 + \sigma_n^2 \right)} \tag{4.9}$$

where $\mathrm{N}_{\mathrm{PRB}}$ is the number of assigned PRB and σ_n^2 represents noise power.

With respect to the system-level simulations, the UL macro diversity reception

is also naturally applied to the CSI measurements, which has been discussed in Section 2.2. By applying the CSI macro diversity, better channel knowledge can be acquired for the macro diversity users to perform the LA selection and PS allocation.

4.4   Ideal Interference Cancellation

According to Equation 4.7, for the macro diversity UE, the received SINR with MRC reception can also be expressed as:

$$\gamma_{mrc} = \gamma_{serve} + \sum_{m=1}^{N_{macro}} \gamma_{macro,m} \qquad (4.10)$$

where γ_{serve} is the received SINR at the serving eNB, N_{macro} is the number of macro diversity combining links, and γ_{macro} is the received SINR at the neighboring coordination eNBs.

In general, the macro link of macro diversity UEs experiences strong interference, where the main interference comes from the UE originally served in the coordination cell. As an example shown in Figure 4.3 on the left, *UE-A* and *UE-B* are served by *eNB-1* and *eNB-2* respectively. Both the UEs are assigned on the identical PRBs and transmitted in the same TTI. The *UE-A* is a macro diversity UE who fulfills the criteria shown in Equation 4.1. According to Equation 4.10 and 4.9, the received SINR for macro diversity *UE-A* can then be expressed as:

$$
\begin{aligned}
\gamma_{mrc,A} \quad &= \quad \gamma_{serve,A1} + \gamma_{macro,A2} \\[2em]
&= \quad \gamma_{serve,A1} + \sum_{a=1}^{N_r} \frac{\dfrac{P_{tx,A}}{N_{PRB}} \displaystyle\sum_{p=1}^{N_{PRB}} |h_{A,a,p}|^2}{\displaystyle\sum_{p=1}^{N_{PRB}} \left(\displaystyle\sum_{\substack{j=1 \\ j \neq A \& B}}^{N_u} \frac{P_{tx,j}}{N_{PRB}} |h_{j,a,p}|^2 + \frac{P_{tx,B}}{N_{PRB}} |h_{B,a,p}|^2 + \sigma_n^2 \right)}
\end{aligned}
\qquad (4.11)
$$

where $|h_{B,a,p}|^2$ is the channel from *UE-B* at *p-th* PRB and *a-th* antenna.

The *UE-B*, normally has a good signal quality to its own serving *eNB-2*, which consequently deteriorates the macro link received SINR of *UE-A* by contributing strong interference as shown in Equation 4.11. The received SINR imbalance between the serving and the macro link very much limits the performance of overall macro diversity scheme. However, if the advanced receiver is deployed
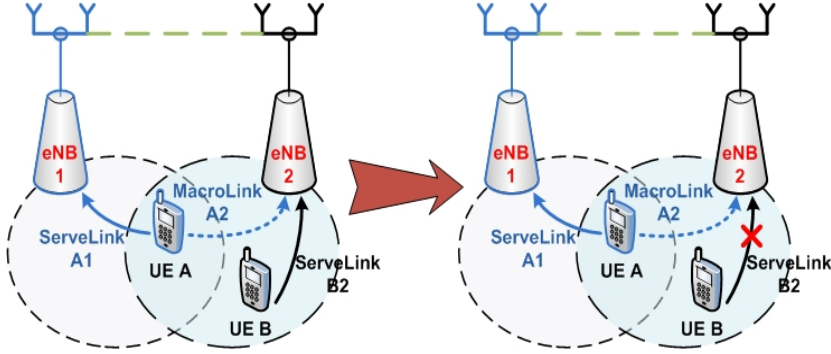
Figure 4.3: CoMP Example Macro Diversity IC

in the eNBs, e.g. SIC receiver, then the correctly received *UE-B* signal in the coordination cell can be subtracted from the total interference in the macro link of *UE-A*, as shown in Figure 4.3 on the right. So the macro link received SINR γ_{macro} can be enhanced, and the total combining gain can be further improved. For the macro diversity *UE-A*, the received ideal SINR under the SIC assumption can be expressed as:

$$
\gamma_{mrc,A}^{IC} = \gamma_{serve,A1} + \sum_{a=1}^{N_r} \frac{\dfrac{p_{tx,A}}{N_{PRB}} \sum_{p=1}^{N_{PRB}} |h_{A,a,p}|^2}{\sum_{p=1}^{N_{PRB}} \left(\sum_{\substack{j=1 \\ j \neq A\&B}}^{N_u} \dfrac{p_{tx,j}}{N_{PRB}} |h_{j,a,p}|^2 + \sigma_n^2 \right)} \tag{4.12}
$$

In this study an ideal Interference Cancellation scheme is assumed, where the UE served by the coordination eNB, e.g. *UE-B*, can always be successfully canceled and the upper bound of macro diversity reception by applying the IC can then be studied.

As shown in the later chapter, the MMSE receiver together with SIC can be utilized in reality instead of ideally removing the full interference. For further references, a more detailed system-level modeling approach for SIC receiver can be found in [94] as discussed in 3GPP.

4.5 IC-based Macro Diversity with Power Control

As discussed in Section 4.4, the performance of macro diversity UEs is enhanced by utilizing the IC-based macro diversity reception. However, the non-macro diversity UEs do not benefit from it at all. By applying the CLPC scheme, together with the IC-based macro diversity reception, the overall network performance can be further improved.

The basic idea behind this scheme is that, generally, the macro diversity UEs generate high inter-cell interference to the other UEs. By lowering their transmit power, less inter-cell interferences will be generated to the network and even the non-macro diversity UEs can also get benefit from it. The negative effect of powering down macro diversity UEs is compensated by the macro diversity reception gain. In the UL LTE, this scheme can be achieved by using standardized CLPC as presented in Section 2.5.

In this study the absolute CLPC command is used, where, as described in Section 2.5.2, the UE applies the transmit power offset based on the latest OLPC command. From the Equation 2.5, the applied power control scheme can be expressed as:

$$P_{tx} = min\left\{P_{max}, P_0 + 10 \cdot \log_{10} N_{PRB} + \alpha \cdot L + f(\Delta_i)\right\} \tag{4.13}$$

where

$$f(\Delta_i) = \begin{cases} -P_{offset}, & \text{if } UE \text{ is a macro diversity UE} \\ 0, & \text{if } UE \text{ is not a macro diversity UE} \end{cases} \tag{4.14}$$

Two strategies were studied for setting the P_{offset} value. For *Scheme-1*, all macro diversity UEs reduce the transmit power by the same amount, e.g. P_{offset} = 1 dB, 2 dB, 3 dB or 4 dB. This *Scheme-1* is used as a baseline reference. It is obvious that this scheme is not the optimal solution since the transmit power for the different macro diversity UEs should not be reduced with the same amount. *Scheme-2* is a further optimization of *Scheme-1*, where the UEs with higher number of macro diversity combining links can be reduced with higher offset value. In this study the UEs with 2 macro diversity link connections are reduced by 2 dB and the UEs with 3 macro diversity link connections are further reduced by 3 dB.

4.6   Simulation Assumptions

The system-level evaluations are performed based on the previous antenna down-tilting study described in Section 3.4. The main simulation assumptions for UL CoMP macro diversity reception study are shown in Table 4.1:

Table 4.1: Simulation Assumptions of UL CoMP Macro Diversity Reception

Parameter	Assumptions
Deployment Scenario	Macro Case-1: ISD=500 m
Number of UEs	30 UEs/cell
P_0 and α value	-58 dBm and 0.6 / -106 dBm and 1.0
Packet Scheduler Metrics	TD-Round Robin, FD-Proportional Fair
BS Antenna Pattern	Horizontal/Vertical HPBW $70^o/10^o$
BS Antenna Downtilting Angle	12°
Receiver Type	MRC
Number of Combining Cells	Maximum 3 cells
	(1 serving cell + 2 coordination cells)
Combining Window Size	3 dB
CoMP Scenario	Intra/Inter-Site

As it can be seen from Table 4.1, the interference-limited Macro Case-1 scenario is the main focus in this study, where the 3GPP standardized, 70° horizontal and 10° vertical, 3-D antenna pattern with 14 dBi antenna gain is utilized. In order to obtain a certain amount of macro diversity UEs for the accurate statistical analysis, 30 UEs are generated per cell with spatially uniform distribution.

The RR metric is assumed in the TDPS and PF metric is assumed in the FDPS. For a certain UE i transmits on PRB p at TTI t, the PF metric is defined as:

$$PF_{i,p,t}^{Metric} = \frac{\widehat{T}_{i,p,t}}{\overline{T}_{i,t}} \tag{4.15}$$

where $\widehat{T}_{i,p,t}$ is the estimated Layer-1 achievable throughput for UE i, on PRB p and at scheduling instant time t. The $\overline{T}_{i,t}$ is the past averaged Layer-1 acknowledge throughput for UE i at scheduling instant time t, which is calculated by using an exponential averaging filter:

$$\overline{T}_{i,t} = (1-\xi)\overline{T}_{i,t-1} + \xi T_{i,t} \tag{4.16}$$

where $T_{i,t}$ is the Layer-1 acknowledged throughput for UE i at scheduling instant time t and ξ is called the filter coefficient.

The locations of macro diversity UEs in the network layout are shown in Figure 4.4. As it can be seen, all UEs are randomly generated in the whole network
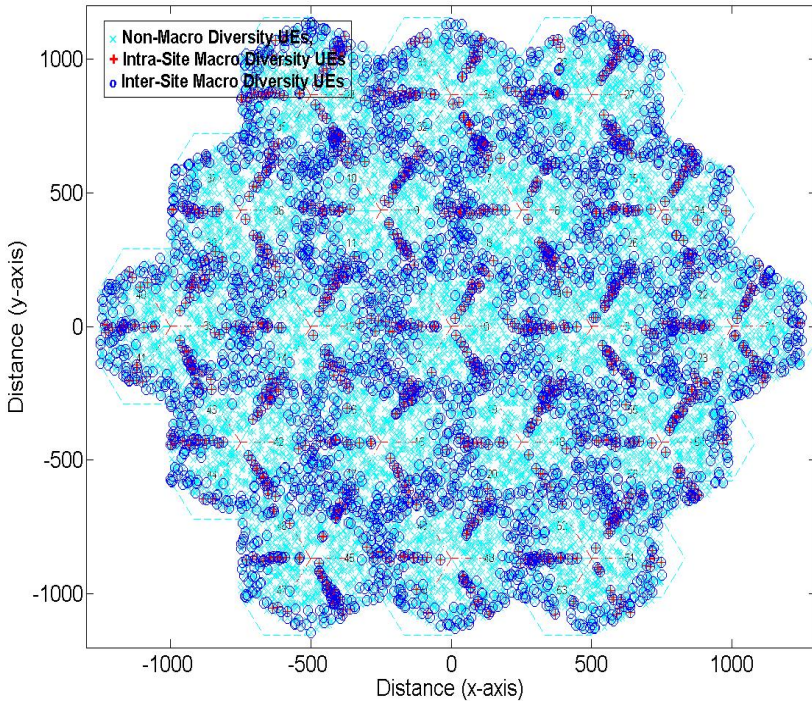
Figure 4.4: Location of Selected Macro Diversity UEs (random realization)

region with balanced load in each cell. The selected macro diversity UEs in the Inter-Site scenario are located in the overlapping area between any 2-3 cells, but the selected macro diversity UEs in the Intra-site scenario are only located in the region between Intra-site cells.

With different antenna downtilting angles, the percentage of macro diversity UEs in both Intra- and Inter- Site scenario is shown in Figure 4.5. As shown in the plot, the amount of macro diversity UEs in the Intra-Site scenario are first decreased from downtilting angle 0° to 6°. At 0° tilt, the wide eNB antenna main-lobe is pointing to the far-away distance which creates a large cell-overlapping area among both Intra-Site and Inter-Site cells. With downtilting of antenna angle from 2° to 6° as discussed in Section 3.3, the wide antenna main-lobe starts touching the ground which reduces the cell-overlapping region. By further mechanically increasing the antenna downtilting angle, as discussed in Section 3.1 and shown in Figure 3.3, the radiation pattern of mechanically downtilted antenna shrinks from the boresight direction and gets wider from the sides, which increases the Intra-Site cell overlapping area and results in
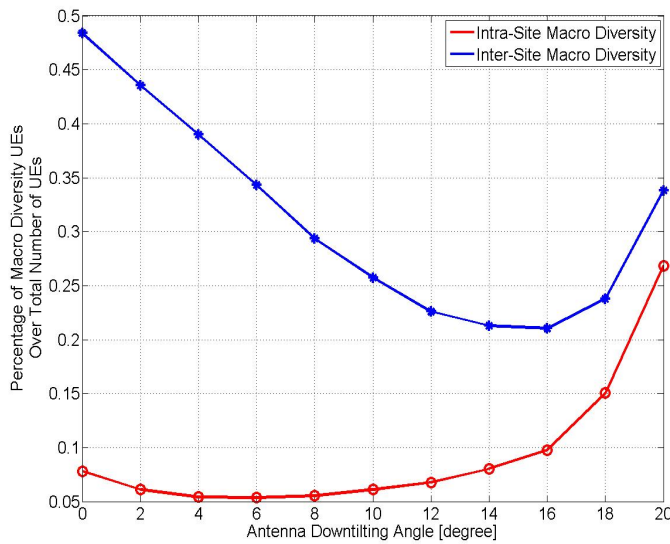
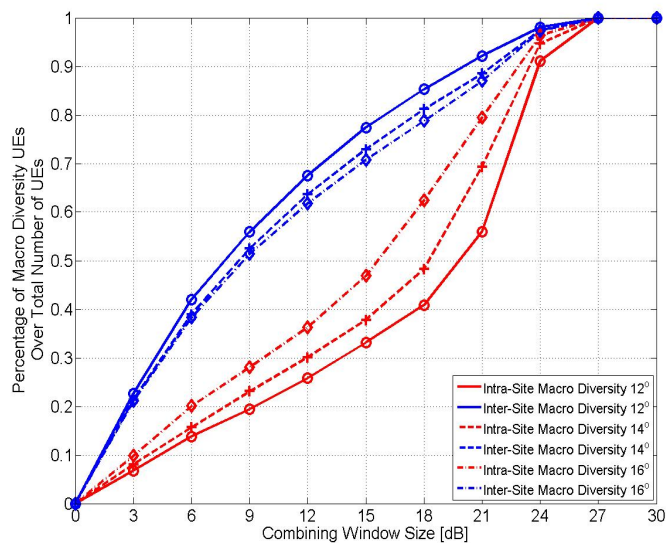Figure 4.5: Percentage of Macro Diversity UEs of varying Downtilting Angle at CWS=3 dB

Figure 4.6: Percentage of Macro Diversity UEs of varying CWS Values with Downtilt Angle $12^o, 14^o, 16^o$

the increasing amount of Intra-Site macro diversity UEs. On the other hand, because of the shrinking of Inter-Site cell-overlapping region, the amount of selected macro diversity UEs in the Inter-Site scenario are reduced with increasing downtilting angles until 16°. By further downtilting, the increasing amount of UEs, located between Intra-Site cells, cause the total amount of macro diversity UEs in the Inter-Site scenario to increase.

The influence of different CWS at downtilting angle of 12°, 14° and 16° is shown in Figure 4.6. At smaller CWS value, the amount of macro diversity UEs for both Intra- and Inter- Site scenario are very close among all three angles. With increased CWS value at higher antenna downtilting angle, the amount of Inter-Site scenario UEs are decreased with increasing Intra-Site scenario UEs.

According to the above analysis, the 12° downtilting angle is applied together with the optimal OLPC parameter $P_0 = -58$ dBm and $\alpha = 0.6$ as discussed in Section 3.5.2. This is done to create larger cell-overlapping area in favor of macro diversity reception. From the practical application point of view, if a UE is located too far away from its coordination eNBs, the received RS signals used for demodulation and channel estimations are too weak. Therefore, the CWS of 3 dB is utilized in this study, where the PL or RSRP differences between serving link and macro links are less than or equal to 3 dB as expressed in Equation 4.1. As shown in Figure 4.6, with CWS equal to 3 dB, there are about 7% macro diversity reception UEs in the Intra-site scenario and 23% macro diversity reception UEs in the Inter-site scenario.

4.7   Performance Evaluation

The investigations of macro diversity reception are carried out for both fractional and full compensation of open-loop FPC, with either $\alpha = 0.6$ or $\alpha = 1.0$ as discussed in Section 2.5.1, where the fractional case of $\alpha = 0.6$ is the main focus. As presented in the following section, the Inter-Site scenario with MRC reception is presented and analyzed in detail. The Intra-Site scenario with MRC and Inter-Site scenario with SC receptions are mainly utilized as a reference guideline.

4.7.1   Evaluation of Macro Diversity with $\alpha = 0.6$

The received SINR distributions for Inter-site MRC UEs are shown in Figure 4.7. The macro link SINR and the total combining SINR are shown respectively

for both with ideal IC and without ideal IC case.

Without the ideal IC applied in the coordination cell, the SINR difference be-
tween serve link and macro link is about 8 dB. This large SINR in-balance
leads to a marginal MRC combining gain. By exploiting the ideal IC in the
coordination cell as also shown in Figure 4.7, the received SINR in the macro
link is improved by nearly 7 dB, which results in about 2.2 dB improvement of
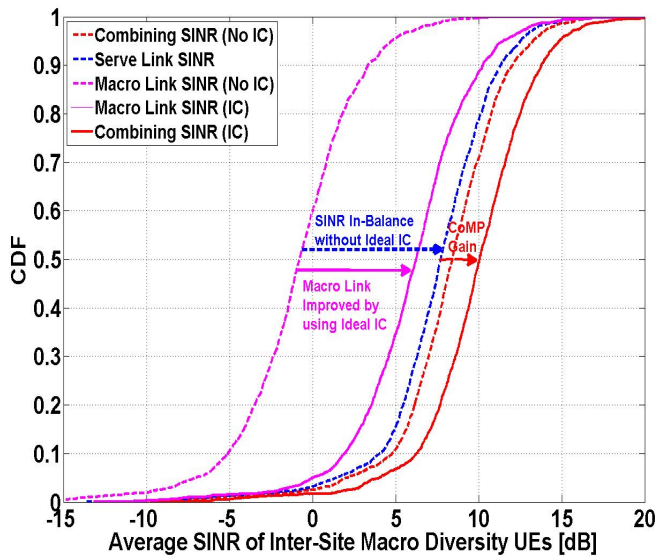total MRC combining gain over the serve link SINR.

Figure 4.7: Average SINR Distribution for Inter-Site MRC
UEs with $\alpha = 0.6$ and $P_0 = -58$ dBm

The reduction of SINR imbalance between serve link and macro link can also be
seen from the link switching frequency of Inter-Site SC UEs shown in Figure 4.8.
This indicator shows how often the strongest SINR is selected from the macro
links. When no ideal IC applied, the strong interference from the coordination
cell lowers the SINR of macro link, which results in nearly no selection switching
from the serving link. In Figure 4.8, 50% of Inter-Site SC UEs experience 5%
or less switching. When the ideal IC is utilized, the balanced serve and macro
links lead to more selection switching or diversity. Still with 50% of Inter-Site
SC UEs, the selection switching to the macro link is improved to about 40%.

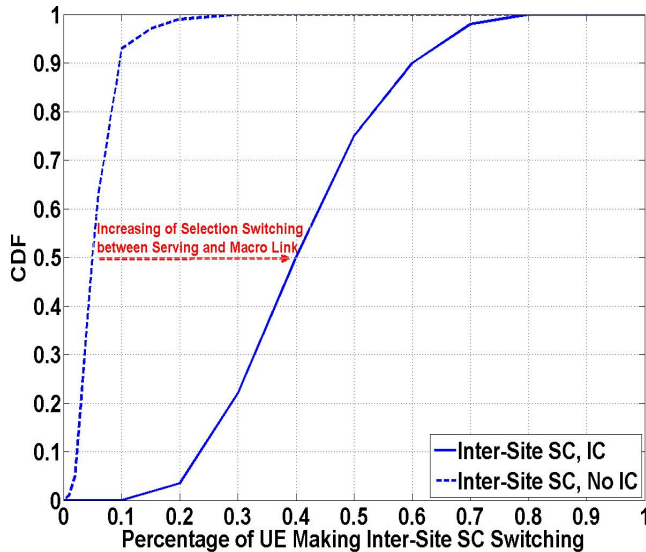The bar plot of 5% outage and average user throughput gains over the no macro

Figure 4.8: Switching Frequency for Inter-Site SC UEs with $\alpha = 0.6$ and $P_0 = -58$ dBm

diversity case[1] are shown in Figure 4.9. With no ideal IC applied[2], the large SINR in-balance results in nearly no gain improvement in the case of Inter-Site SC reception. Because of the small amount of Intra-Site macro diversity UEs with only 7% as shown in Figure 4.6, the overall performance improvement for Intra-Site MRC reception case is quite marginal as well. For the case of Inter-Site MRC reception, the 23% of Inter-Site macro diversity UEs leads to about 8% and 3% gain in terms of 5% outage and avergage user throughput respectively. When the ideal IC is utilized, the overall performance is enhanced for all the three cases compared to the case with no ideal IC. For the best case, the Inter-Site MRC reception provides more benefits for the cell-edge UEs, which gives about 14% gains in terms of 5% outage and 8% gain in terms of average user throughput.

The study of CLPC schemes described in Section 4.5 is performed based on the case of IC-based Inter-Site MRC reception. Figure 4.10 shows the distributions of transmit power for Inter-Site reception UEs. Since no CLPC is applied, the

---

[1]No Macro Diversity Case: which is based on the previous antenna downtilting study with downtilting angle of 12° and depends on the application with either OLPC parameter ($\alpha = 0.6$, $P_0 = -58$ dBm) or ($\alpha = 1.0$, $P_0 = -106$ dBm). The overall throughput gain numbers are presented in Figure 3.17 and Figure 3.18

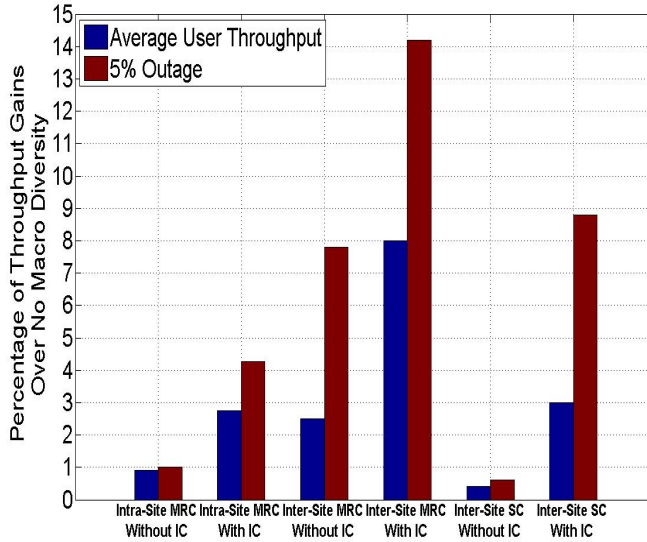[2]No/Without IC Case means when no IC scheme is applied

Figure 4.9: Throughput Gain Plot for No IC vs Ideal IC with $\alpha = 0.6$ and $P_0 = -58$ dBm

CDF curve of no macro diversity case and IC-based Inter-Site reception case overlap and are used as baseline references for the CLPC cases. When the CLPC is exploited, the transmit power reduction of macro diversity UE results in the shifting curves to the left compared to the reference curves. As expected, for CLPC *Scheme-1*, the mean value of the CDF curve is reduced by about 1 dB in each case. For CLPC *Scheme-2*, because the macro diversity UEs are reduced either by 2 or 3 dB as presented in Section 4.5, its CDF curve is lying between the -2 dB and -3 dB curves of *Scheme-1*.

The CDF curves of the average SINR for Inter-Site MRC UEs are shown in Figure 4.11. To compare with the reference case of IC-based Inter-Site MRC when no CLPC is applied, it is no surprise that the received SINR values are also decreased for the CLPC cases because of transmit power reduction.

The plot of throughput gains relative to the no macro diversity case is shown in Figure 4.12. To compare with the IC-based Inter-Site MRC without CLPC applied, which was the the best scheme as shown in Figure 4.9, by using CLPC *Scheme-1*, both 5% outage and average user throughput are enhanced by reducing the transmit power of macro diversity UEs. At the optimal case of powering down 2dB, the 5% outage and average user throughput can be enhanced by 24%
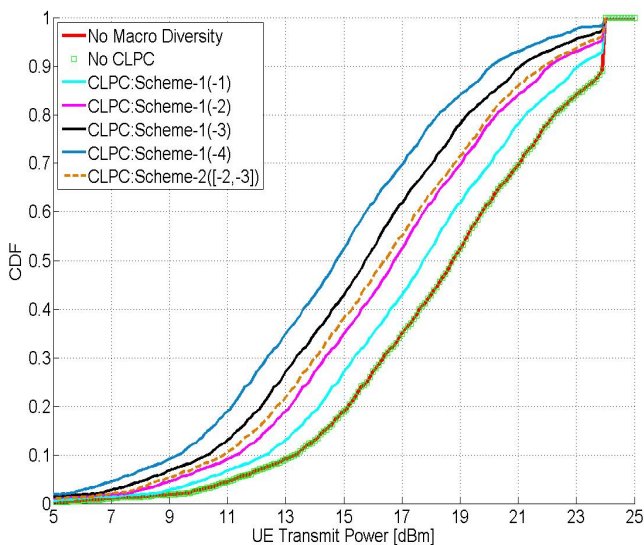
Figure 4.10: Transmit Power Distribution for Ideal IC-base Inter-Site MRC UE with CLPC ($\alpha = 0.6$ and $P_0 = -58$ dBm)
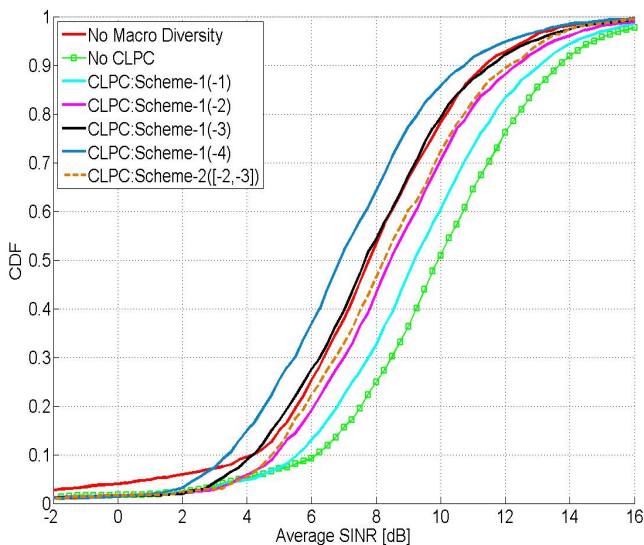

Figure 4.11: Average SINR Distribution for Ideal IC-base Inter-Site MRC UE with CLPC ($\alpha = 0.6$ and $P_0 = -58$ dBm)
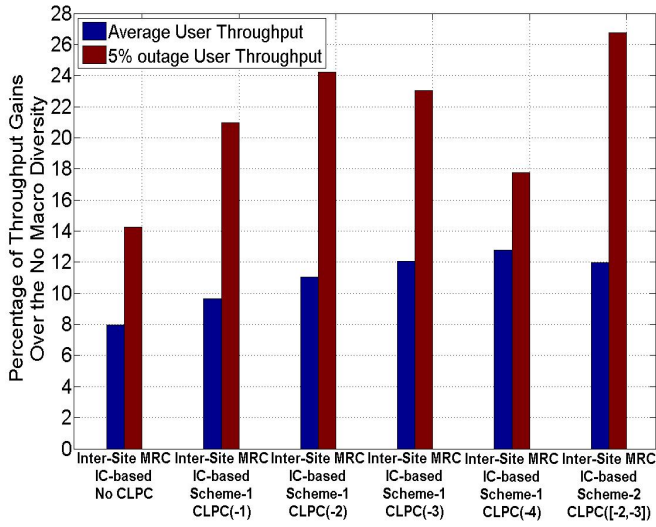
Figure 4.12: Throughput Gain Plot with CLPC for $\alpha = 0.6$ and $P_0 = -58$ dBm
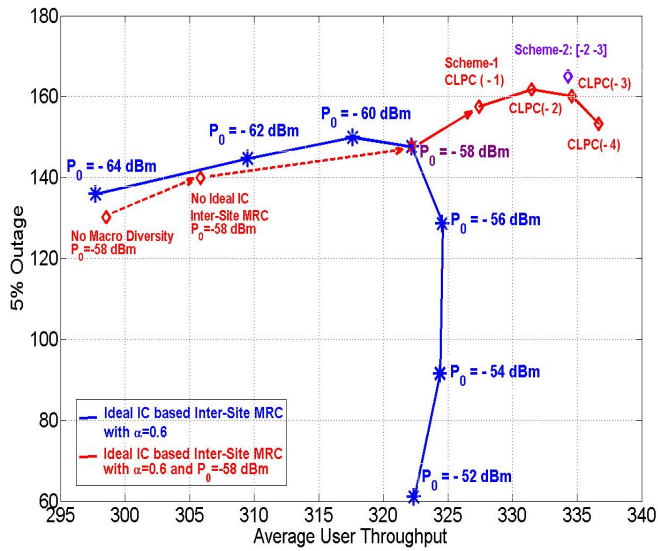

Figure 4.13: Comparison of different P_0 values with CLPC Schemes for $\alpha = 0.6$

and 11% respectively. Further decrease of the transmit power, i.e. the transmit power reduction of 4 dB, the average user throughput performance can still be further improved, which means the other non-macro diversity UEs can still benefit from the CLPC. But the 5% outage user throughput is penalized by decrease of the performance for some of the macro diversity users. By applying the *Scheme-2*, the variety of the transmit power brings additional gains for both 5% outage and average user throughput over the *Scheme-1*. To compare with the no macro diversity case, there are about 27% and 12% gains for the 5% outage and average user throughput respectively.

Since the CLPC scheme applied was based on the OLPC parameters, the optimum P_0 value was investigated with $\alpha = 0.6$ for the IC-based Inter-Site MRC reception as shown in Figure 4.13. The blue curve in Figure 4.13 presents the performance of IC-based Inter-Site MRC with varying of P_0 values and the red curve shows the performance of IC-based Inter-Site MRC with $P_0 = -58$ at different macro diversity schemes. According to the previous antenna downtilting study, the $P_0 = -58$ dBm was the optimal value for $\alpha = 0.6$. As it can be seen from the blue curve in Figure 4.13, for the macro diversity reception, the $P_0 = -58$ dBm still gives the optimal performance compared with other P_0 values in terms of both 5% outage and average user throughput. Utilizing the CLPC schemes on the top of $P_0 = -58$ provides even higher gains as shown in the trend of the red curve.

4.7.2   Evaluation of Macro Diversity with $\alpha = 1.0$

Compared with the OLPC parameter $\alpha = 0.6$, by utilizing $\alpha = 1.0$, UEs have less transmit power and identical received power spectral density in the eNB. As shown in Figure 4.14 of the two no macro diversity cases, $\alpha = 1.0$ is more favorable for the cell-edge UE performance.

In this section, the average network performance of CoMP macro diversity reception with FPC parameter $\alpha = 1.0$ are presented with $P_0 = -106$, which is the optimal parameter setting as discussed in Section 3.5.2.

In Figure 4.14(a), the CDF curve of received SINR for Inter-Site MRC UEs are shown. As expected, compared to the baseline of no macro diversity with $\alpha = 1.0$ and $P_0 = -106$ dBm, the ideal IC-based Inter-Site MRC reception improves the performance of macro diversity UE, and there is still much higher gain when the ideal IC scheme is applied in the coordination cell.

In Figure 4.14(b), the CDF curves of UE throughput are shown. It can be seen that, with the joint effect of using $\alpha = 1.0$ and macro diversity reception, the

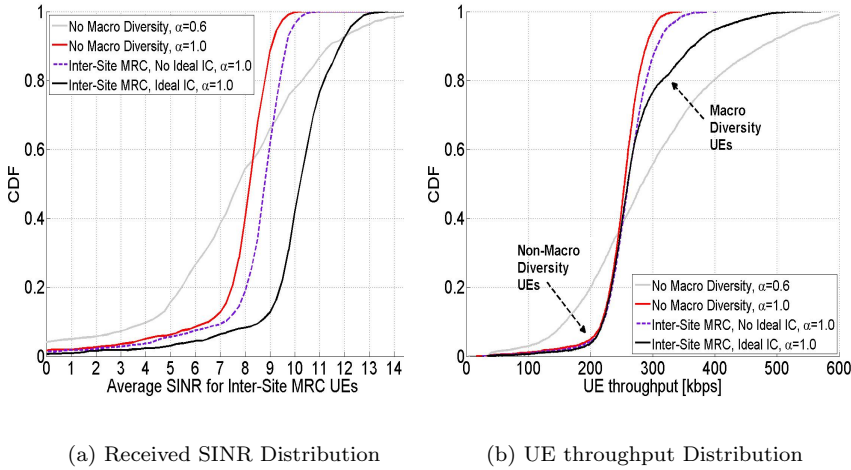(a) Received SINR Distribution   (b) UE throughput Distribution

Figure 4.14: Average SINR & UE Throughput Distribution without CLPC with $\alpha = 1.0$ and $P_0 = -106$ dBm

macro diversity UE statistics are actually moving to the top part of the CDF curve, i.e. around 95% region, whereas the non-macro diversity UEs are down to the tail of the CDF curve. So the 5% outage of average user throughput is now representing the non-macro diversity UE performance.

The plot of throughput gains relative to the baseline of no macro diversity with $\alpha = 1.0$ and $P_0 = -106$ dBm are shown in Figure 4.15 for all three combining reception cases. Similar to $\alpha = 0.6$, the cancelled coordination cell interference can always help to improve both 5% outage and average user throughput. However, the enhancement of 5% outage user throughout is very marginal. With the best case of ideal IC-based Inter-Site MRC reception, there is only 3% gain in terms of 5% outage, where it was 14% gain when $\alpha = 0.6$ is applied as shown in Figure 4.9. This is simply because the cell-center UE does not enjoy much of the benefits from the macro diversity receptions. However, for the cell-edge UE, its benefit from the macro diversity reception brings about 9.5% gain in terms of average user throughput.

In Figure 4.16, the CDF of UE throughput are shown to present the performance gain by using CLPC *Scheme-1*. As it can be seen the throughput of macro diversity UEs is reduced with the increasing of power reduction. However, the performance of cell-center UEs around the 5% outage region is actually further enhanced and maximized with power reduction of 3 dB.
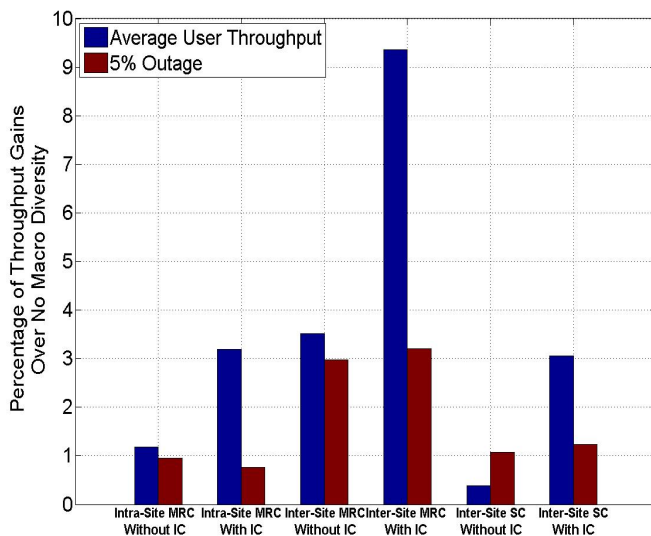
Figure 4.15: Throughput Gain Plot for No IC vs IC with $\alpha = 1.0$ and $P_0 = -106$ dBm

The plot of CLPC throughput gains are shown in Figure 4.17. For the *Scheme-1*, in general, the same trend of gains can be seen as described in $\alpha = 0.6$. Except that the maximum gains are now optimized at power reduction of 3 dB, where it was 2 dB for the case of $\alpha = 0.6$. This is due to the fact that, by applying the cell-edge UE favorable parameter $\alpha = 1.0$, the performance of cell-edge macro diversity UEs is improved, where in return, by applying the CLPC scheme on the top, they can reduce even more power in favor of other UEs' transmission. So all in all at -3 dB of *Scheme-1*, there are further improvements of 18% and 5% gains in terms of 5% outage and average user throughput respectively. The large 5% outage gain number also proves that, for the application of $\alpha = 1.0$, it is very important to have the CLPC schemes applied together with IC-based macro diversity receptions in order to have the overall enhancement of network performance. The utilization of *Scheme-2* has also been investigated where it shows the same performance as the optimum case of *Scheme-1*.
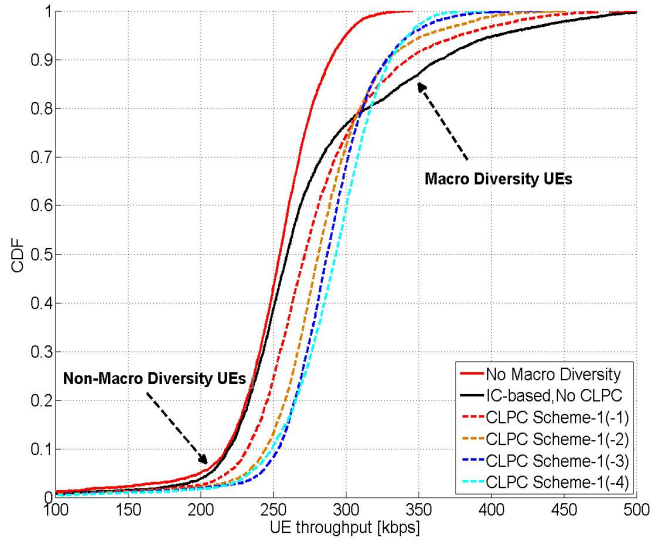
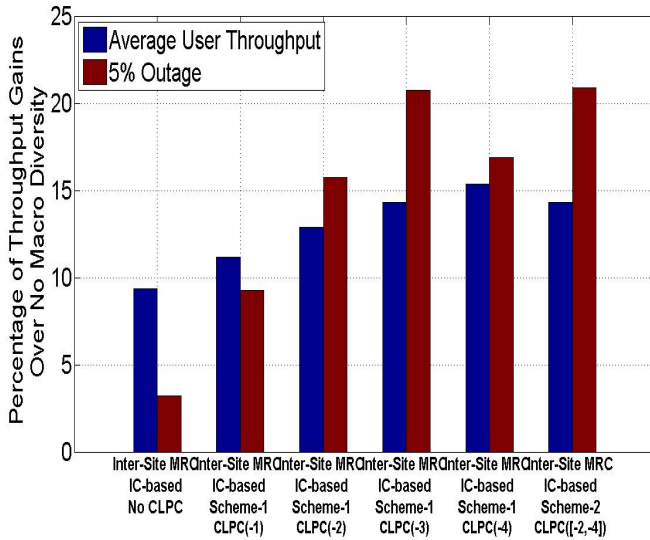Figure 4.16: Average User Throughput Distribution with CLPC for $\alpha = 1.0$ and $P_0 = -106$ dBm

Figure 4.17: Throughput Gain Plot for No CLPC vs CLPC with $\alpha = 1.0$ and $P_0 = -106$ dBm

4.7.3   Interaction of Antenna Tilting and UL CoMP

The interactions of antenna downtilting and macro diversity reception are analyzed in this section. In Figure 4.18, the throughput gains of Intra- and Inter-Site MRC receptions are shown with varying downtilting angle from 10° to 16°. The no macro diversity case, with 12° downtilting and $\alpha = 0.6$, is used as a baseline reference to compare with (0% gain).
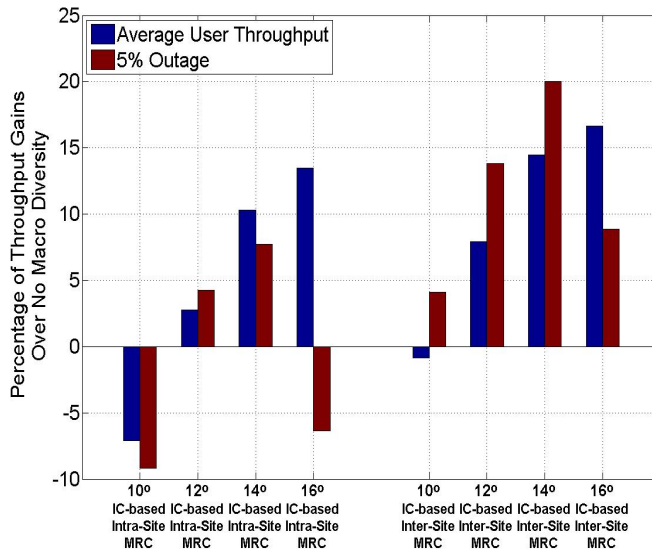

Figure 4.18: Throughput Gain Compare for different Antenna Downtilting Angles with $\alpha = 0.6$ and $P_0 = -58$ dBm

As it can be seen, for the case of Intra-Site MRC reception, the 14° antenna downtilting can provide even better throughput gains than 12° case. It is because the increased number of selected Intra-Site macro diversity UEs as shown in Figure 4.5 and the enhanced performance by downtilting antenna angle as shown in Figure 3.16. Generally, there is about 5% gain for both 5% outage and average user throughput over the 12° case. By further downtilting to 16°, the average user throughput can be further enhanced by the combined effect of increased number of Intra-Site macro diversity UEs and antenna dowtilting gain. However, the increased number of MRC UEs are mainly located around a high SINR region. Because of losing cell coverage at 16°, the low SINR UEs can get no benefit from the Intra-Site MRC reception, which results in the decreased performance of 5% outage at 16°. Besides, also due to the loss of antenna downtilting gain at 10° as shown in Figure 3.16, 10° case shows a negative gain in both 5% outage and average user throughput to compare with the 12° reference

case.

For the case of Inter-Site MRC reception, the 14° antenna downtilting can still provide about 6% more gains than the 12° in both 5% outage and average user throughput, because the selected macro diversity UEs in the Inter-Site scenario contain the low SINR UEs, who are located at the borsight cell-border area. It is very interesting to see that by taking the benefit of Inter-Site MRC reception, even for downtilting angle at 16°, the 5% outage UEs can still achieve about 9% improvement.
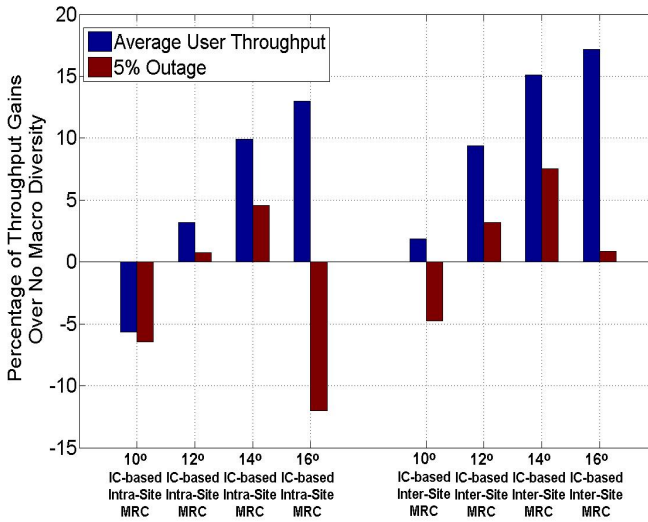

Figure 4.19: Throughput Gain Compared for different Antenna Downtilting Angles with $\alpha = 1.0$ and $P_0 = -106$ dBm

In Figure 4.19, the same investigation is shown for the case of $\alpha = 1.0$ and $P_0 = -106$ dBm, where the same trend can be seen as the previous case with $\alpha = 0.6$ and $P_0 = -58$ dBm. For both Intra-Site and Inter-Site MRC schemes, the downtilting angle of 14° can provide further enhancement in both 5% outage and average user throughput compared to the 12° downtilting.

4.7.4   Non-Ideal Cell Selection

In the previous analysis the studies were based on the ideal cell selection, where the UEs are always connected to the highest path gain sector as its serving cell. However, in reality, the UE selected serving cell might not be the strongest link

because of measurement errors. This imperfection from serving cell selection influences the UE performance. So in this section the non-ideal cell selection scenario is being considered, and the potential gain by using CoMP macro diversity reception is evaluated.
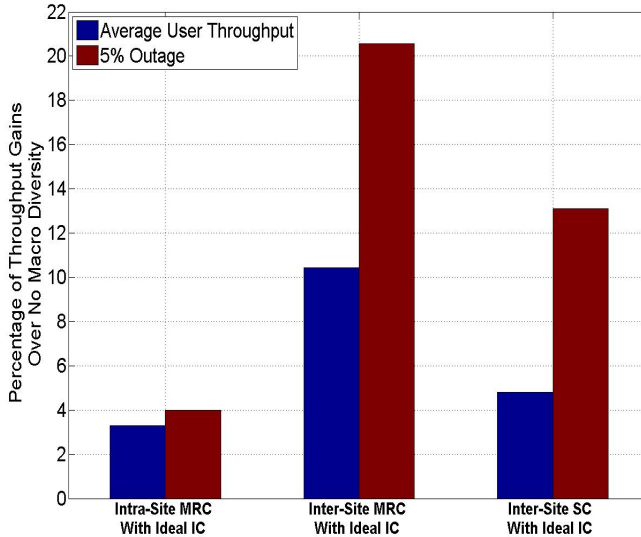

Figure 4.20: Throughput Gains Of Non-Ideal Cell Selection with $\alpha = 0.6$ and $P_0 = -58$ dBm

In this study the non-ideal cell selection is modeled as the UE randomly connects to one of sectors from the so-called virtual active set size (ASS) [95], where the maximum number of sectors in the virtual ASS is 3.0 as default [95]. The window margin is used to determine the sectors in the virtual ASS, where the default setting is selected as 3.0 dB. By using this setting, as studied in [96], about 20% of the UEs take the non-strongest link as their serving link within the virtual ASS.

In Figure 4.20, the bar plot throughput gains are shown for all the combining reception cases with ideal IC applied. For the Intra-Site MRC, not much gain is observed because of limited number of Intra-Site macro diversity UEs. For the Inter-Site scenario with MRC, the impact of non-ideal cell selection deteriorates the performance of reference case. No matter which combining scheme is utilized, there are much higher gains in both 5% outage and average user throughput to compare with the gain numbers shown in Figure 4.9 with ideal cell selection.

4.8 Conclusions

In this chapter, the CoMP in the form of macro diversity reception has been studied in the UL LTE, where both OLPC parameter with $\alpha = 0.6$ and $\alpha = 1.0$ are evaluated. The study is concentrated on the analysis of Inter-Site scenario with MRC reception. The Intra-Site MRC and Inter-Site SC are utilized as references. The baseline scenario is no macro diversity case with 12° downtilting as investigated in the earlier chapter. The main conclusions from the study is summarized in Figure 4.21 by taking Inter-Site MRC reception with $\alpha = 0.6$ as an example.
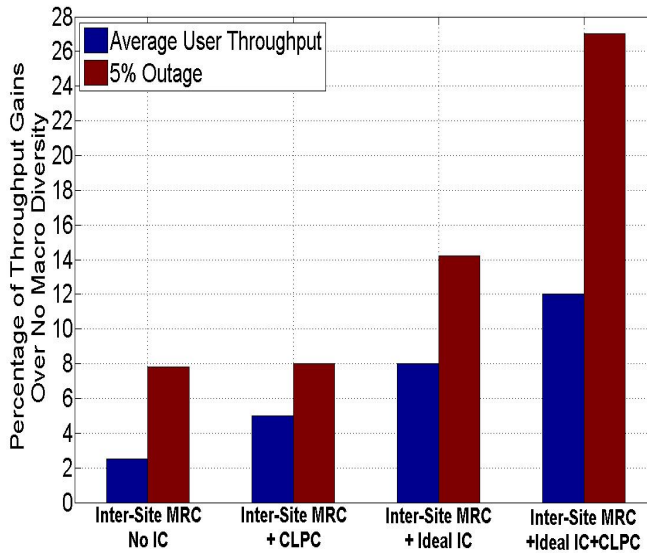
Figure 4.21: Conclusion Comparison at 12° downtilting with $\alpha = 0.6$ and Ideal-Cell Selection

As it can be seen, with standing alone macro diversity reception, the improvement of both 5% outage and average user throughput is very marginal. To exploit the CLPC scheme alone, the enhancement is limited as well without the support of ideal IC in the coordination cell. By cancelling the strongest interference in the macro diversity link, the performance of both 5% outage and average user throughput can be largely enhanced, and by applying the CLPC scheme on top of IC-based MRC reception, the outage gain number can nearly be doubled together with further improvement of average user throughput. So the combination of macro diversity reception together with IC and CLPC scheme is very important in order to maximize the overall network enhancement.

When evaluating the case of $\alpha = 1.0$, the 5% outage UEs represent the cell-center UE performance where no macro diversity applied. The use of ideal IC-based Inter-Site MRC reception slightly improve the average user throughput, the outage UEs do not enjoy much of the benefit from the combining gain. However, by applying the CLPC schemes to reduce the power of macro diversity UEs, the outage throughput UEs are largely improved since less interference is received from macro diversity UEs. And the effect of powering down the macro diversity UEs is compensated by macro diversity reception gain.

The interaction of antenna downtilting angle together with macro diversity receptions has also been studied. At downtilting angle of 14°, both Intra-Site MRC and Inter-Site MRC schemes provide better performance than at 12°. The study with non-ideal cell selection scenario also demonstrated that, in the practical application, macro diversity receptions can provide even higher gain than the simulated ideal cell selection assumption.

Of course it has to be realized that the study results presented in this chapter were based on the MRC receiver with ideal IC. By doing so, the upper bound performance of CoMP macro diversity reception can be studied. By applying the realistic MMSE/SIC receiver as presented in the next chapter, the performance gain numbers will be decreased correspondingly.

Furthermore, compared with the theoretical CoMP investigations shown in the earlier literature, the achievable CoMP gain in this study is generally lower than the theoretical limits because of limited number of coordination eNBs and selected number of macro diversity UEs. In the realistic network, the overall CoMP performance may be even reduced due to the practical issues such as channel estimation errors, synchronization and latency challenges.

CHAPTER 5

Uplink CoMP Joint Reception

In the UL LTE, CoMP reception can also be jointly applied between the paired UEs. Comparing with CoMP macro diversity with MRC reception as presented in Chapter 4, higher performances in terms of both 5% outage and average user throughput are expected for CoMP joint reception to better exploration of the channel spatial signature. On the other hand, the CoMP joint reception requires a large amount of information exchange between eNBs. Especially for the Inter-Site scenario, it involves the coordination of multiple network sites through backhaul transport, and a large amount of information exchange will result in additional burdens and requirements on the network backhaul design.

In this chapter, the performance of CoMP joint reception is investigated in detail compared with the CoMP macro diversity with MRC reception. The requirements of LTE network backhaul are analyzed for both cases based on the realistic MMSE/SIC receiver. The independent PS performed in each individual cell is utilized in this study, whereas the performance of multi-cell coordinated PS is presented in the later chapter.

In Section 5.1, the study scenario of CoMP joint reception is described, and the requirement on LTE X2-interface for UL CoMP applications is analyzed in Section 5.2. In Section 5.3, the UL CoMP with MMSE/SIC receiver is presented for joint reception. The modeling of RS for CoMP joint reception is described in Section 5.4. In Section 5.5, the modeling assumptions for this study are depicted, and the performance evaluation results are presented in Section 5.6. Finally, the conclusions for the CoMP joint reception study are made in Section 5.7.

5.1   CoMP Joint Reception

5.1.1   Single-Cell Multi-User MIMO in UL LTE

In LTE Rel'8, Single-User MIMO (SU-MIMO) cannot be supported in the UL but the UL can support single-cell Multi-User MIMO (MU-MIMO) transparently. With only one UE transmit antenna and multiple eNB receive antennas, 3GPP has agreed to offer some rudimentary support for spatial multiplexing of different UEs in the same cell [43]. Rel'8 standard adopts 2-by-2 (2x2) single-cell MU-MIMO in the LTE uplink, i.e. each group contains two UEs with single transmit antenna and the eNB has two receive antennas. It may be noted that the support of multiple transmit antennas at the UE is being considered for LTE-A.
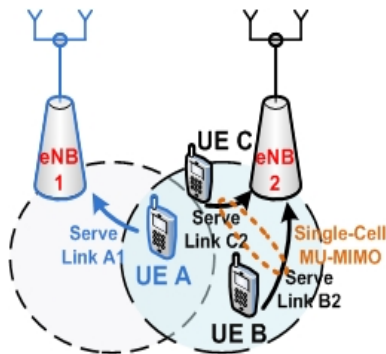

Figure 5.1: Single-Cell MU-MIMO (UE-B and UE-C are single-cell spatial multiplexing users at eNB-2)

The multi-user technique is known from the CDMA system. In a CDMA system, each user assigns a unique spreading code to encode the transmitted signal and allows multiple users to share the same frequency band and the same time slot. At the receiver side, the multi-user data are separated on the basis of their signature waveforms (which is the spreading code convolved with the channel impulse response). Ideally the user signature waveforms are mutually orthogonal so as to avoid MAI among different users. Practically the non-orthogonality due to the near-far effect and MAI can be suppressed by using the advanced signal processing with multiple antenna array at the eNB receiver [97].

To exploit the single-cell multi-user technique in the UL LTE, the packet scheduler allow multiple UEs to simultaneously transmit independent data in a cell on the same assigned physical resource blocks and the users' data can be separated

in the space domain at the eNB with multiple antenna array. The UE-specific spatial signature[1] generated by the independent multipath channel over the transmitted signal acts like the signature waveforms in the CDMA system. The packet scheduler can allocate the spatial multiplexing UEs with the best and most orthogonal spatial channels in order to exploit the multi-user spatial diversity[2] [98]. The interference seen by the spatial multiplexing UE comes from two parts: the intra-cell interference due to the co-scheduled UE involved in the UL MU-MIMO and the inter-cell interference due to co-channel UEs in other cells. By utilizing the Multi-User Detection (MUD) with multiple antenna at eNB, the intra-cell interference between these two UEs can be significantly reduced [16].

Many MUD algorithms have been studied from both theoretical and practical point of view with the CDMA-based system and OFDM-based SU-MIMO transmission [99]. In general, the optimum multi-user detectors require a high computational complexity which is not feasible for the practical implementation. Therefore, many sub-optimum MUD algorithms have been investigated with low complexity. Basically it can be divided into linear detectors, e.g. decorrelator [100] or MMSE detector [101], and non-linear detector, e.g. decision feedback detector [102][103], multi-stage detector [104] or interference cancellation detector [105]. As presented in [106][107], those MUD algorithms have been further extended and utilized in the single-cell MU-MIMO transmission.

5.1.2   Extension of Single-Cell Multi-User MIMO

In some of the literature [82][108], CoMP is also denoted as Multi-Cell / Network / Cooperative MIMO. In this study, UL CoMP can be considered as a multi-cell MU-MIMO solution which is the extension of single-cell MU-MIMO scenario.

In Chapter 4, UL CoMP in the form of macro diversity reception has been studied. As shown in Figure 5.2(a), *UE-A* and *UE-B* are co-channel users and served in the different cell, *eNB-1* and *eNB-2*. In order to reduce the link imbalance to improve the overall macro combining gain as discussed in Section 4.4, in the coordination cell *eNB-2*, a 2x2 multi-cell MU-MIMO can be performed between the serve link of *UE-B* and the macro link of *UE-A*. In Chapter 4, the upper bound of CoMP macro diversity reception has been investigated. The mutual interference between the two cross-cell multiplexing UEs has been ideally (full) removed. Practically the cross user interference can be suppressed with multi-user detection receiver as exploited in the single-cell MU-MIMO. As presented in [109], the linear MMSE detector and non-linear SIC receiver

---

[1]Spatial signature is the response vector of an antenna array from a certain UE.
[2]Spatial diversity is the difference of spatial signatures of UEs.

has fairly low complexity and near-optimum performance to compare with the Maximum-Likelihood (ML) receiver, which requires very high complexity but very optimal performance. In the following section, the CoMP macro diversity reception is studied with the linear MMSE detector or non-linear MMSE-SIC receiver, and utilized as a reference.
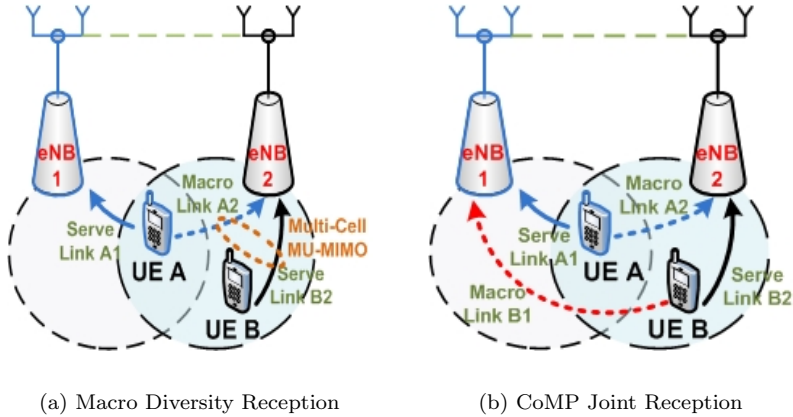

(a) Macro Diversity Reception   (b) CoMP Joint Reception

Figure 5.2: Structure of CoMP Joint Reception

By further extending the CoMP macro diversity scenario through the multi-eNB coordination,, all the received signals can be exploited as desired signals rather than treated as interference. As shown in Figure 5.2(b), with the macro link signal of *UE-B* also considered in *eNB-1*, a 2x4 multi-cell MU-MIMO can be formed. Based on this scenario, the CoMP technology in the form of joint reception is investigated in this chapter. As known from the earlier literature [110], with multiple receiving antennas at eNB, the received signal strength can be enhanced by applying the advanced baseband signal processing and the impact of co-channel interferences can be mitigated. It is also known that the performance gain of multi-antenna signal processing is proportional to the number of antennas. With higher number of antennas, the diversity of different branches can be utilized to mitigate the serious channel fading and improve the reliability of system performance. By cooperating multiply eNBs in the UL direction as shown in Figure 5.2, a serving eNB can virtually increase its number of receiving antennas. The received information from the coordination eNB antennas can be exchanged through the LTE X2-interface and utilized in the serving eNB to perform the joint signal processing of cross-cell multi-user detection. The application and performance comparison with the CoMP macro diversity reception is the key interest in this study.

Similar to the function of PS in the single-cell MU-MIMO, the multi-cell CPS can also be used to allocate the cross-cell spatial multiplexing UEs with the best and most orthogonal spatial channels in order to fully exploit the multi-cell multi-user spatial diversity. In this chapter, the CoMP receiver with joint reception is the main focus. No specific multi-cell CPS is applied. The two joint detection UEs are allocated respectively by their own serving cell PS and can be considered as paired by a random-fashion PS algorithm between the coordination cells. In Chapter 6, the performance of CoMP joint reception will be further investigated when the algorithm of multi-cell CPS is exploited.

5.2   LTE X2-Interface for CoMP Applications

In order to support different CoMP applications, the X2-interface in the LTE network as presented in Figure 2.1 needs to fulfill a certain bandwidth and latency requirements. In this section, the theoretical capacity requirement of X2-interface is estimated.

In Figure 5.3, the eNB protocol stack for CoMP reception in the case of both macro diversity and joint schemes are shown. For the macro diversity reception as shown in Figure 5.3(a), in the PHY layer of coordination *eNB-2*, it performs the channel estimation for both signals from *UE-A* and *UE-B*, and is followed by the multi-user detection, i.e. MMSE or MMSE-SIC, between the two UEs. For the macro diversity combining of *UE-A*, the MRC can be applied in the Chase Combining fashion, where the packets are combined at bit level before decoding by direct addition of the demodulation soft bits[1]. By transferring the quantized soft bits to the serving *eNB-1* through X2-interface, the serving *eNB-1* combines the soft bits with its own demodulated soft bits received from *UE-A* and proceeds with the final decoding and Cyclic Redundancy Check (CRC) afterward.

Based on the physical resource structure in UL LTE as specified in [43], one PRB consists of $N_{subcarrier} = 12$ OFDM sub-carriers and $N_{symbol} = 14$ OFDM symbols, where 2 OFDM symbols are Reference Symbols used for demodulation. Assume the signal demodulation is performed at the coordination *eNB-2*, the RS information does not have to be sent to the serving *eNB-1*. Assume the Quadrature Phase Shift Keying (QPSK) is used, the demodulation soft bits are quantized with resolution of $N_{resolution} = 6$ bits over the X2-interface transmission, for the MRC application, the capacity requirement for X2-interface per

---

[1]Demodulation soft bit is equivalent to values of Log Likelihood Ratio (LLR) given as: $LLR(b) = \log \frac{Pr\{b=1|r\}}{Pr\{b=0|r\}}$. Summation of LLR values at bit levels is mathematically equivalent to perform MRC at symbol level before calculating the LLR [111].
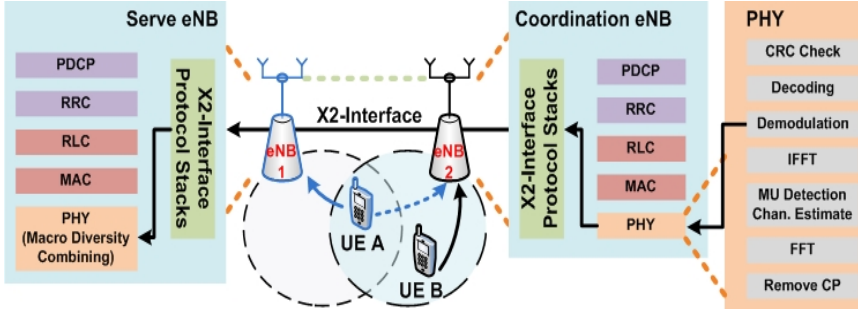
(a) Macro Diversity Reception
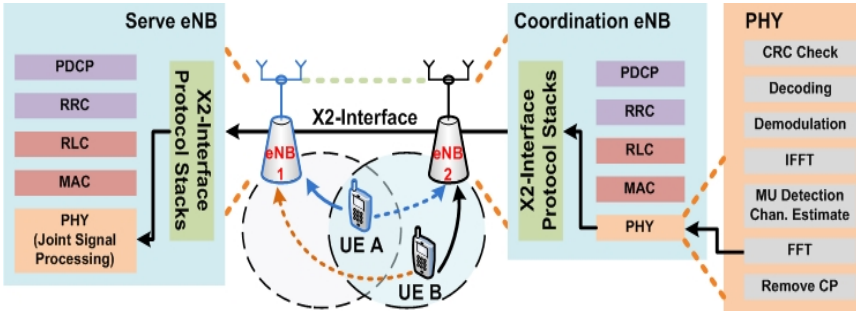
(b) Joint Reception

Figure 5.3: Macro Diversity Reception vs. Joint Reception Backhaul Stacks

PRB per TTI can simply be estimated as:

$$N_{subcarrier} \times N_{symbol} \times N_{resolution} \tag{5.1}$$
$$= 12 \text{ subcarriers} \times (14 - 2) \text{ symbols} \times 6 \text{ bits} \tag{5.2}$$
$$= 0.864 \text{ Mbit per PRB (180 kHz) per TTI (1 ms)} \tag{5.3}$$

Assume a practical scenario, with CoMP application of 16 PRBs or 3 MHz, the capacity requirement for X2-interface to facilitate MRC reception is about $0.864 \times 16 \approx 14$ Mbit per TTI. By considering the maximum scalable bandwidth 20 MHz specified in Release 8 [43] with 100 PRBs, the maximum capacity requirement for X2-interface with MRC reception is about $0.864 \times 100 \approx 86.4$ Mbit per TTI.

Whereas for the joint CoMP reception as shown in Figure 5.3(b), in order to

perform the 2x4 multi-cell multi-user signal processing in the PHY of serving *eNB-1*, the In-phase and Quadrature (I&Q) samples[1] of received *UE-A* and *UE-B* signals at each antenna have to be transferred from the coordination *eNB-2* via the X2-interface, because the joint signal processing in the serving *eNB-1* requires the channel information from the coordination *eNB-2*. The RS symbols also need to be transferred through the X2-interface.

By assuming the I&Q samples quantized with 8 bits each ($N_{i\&q} = 2$) for QPSK transmission through X2-interface, with $N_t = 1$ transmit antenna and $N_r = 2$ receiving antenna, the capacity requirement for X2-interface with joint CoMP reception per PRB per TTI can simply be estimated as:

$$N_{subcarrier} \times N_{symbol} \times N_{resolution} \times N_{i\&q} \times N_t \times N_r \qquad (5.4)$$

$$= 12 \text{ subcarriers} \times 14 \text{ symbols} \times 8 \text{ bits} \times 2 \text{ iq} \times 2 \text{ rx} \qquad (5.5)$$

$$= 5.38 \text{ Mbit per PRB (180 kHz) per TTI (1 ms)} \qquad (5.6)$$

Still by assuming the practical CoMP application with 16 PRBs or 3 MHz, the capacity requirement for X2-interface to support joint reception is about $5.38 \times 16 \approx 86.08$ Mbit per TTI. By considering the maximum scalable bandwidth 20 MHz in Release 8 with 100 PRBs, the maximum capacity requirement for X2-interface with joint reception is about $5.38 \times 100 \approx 0.54$ Gbit per TTI. To compare with the X2-interface capacity requirement for CoMP MRC macro diversity application presented in Equation 5.1, the backhaul requirement for the CoMP joint reception is about 6 times higher.

It can be foreseen that the HARQ operations has also impact on the CoMP application. Based on the LTE Release 8 specifications, the Round-Trip Time (RTT) for synchronous HARQ application is about 8 Millisecond (ms) as discussed in Section 2.3. So it is expected that, in general, the X2-interface transmission time and processing delay in the eNB should not contribute significantly to the total delay budget for the CoMP application. Otherwise, the longer delay could cause data stalling in the HARQ process. According to the present assumptions in the LTE Release 8, the transmission time of X2-interface, from serving *eNB-1* to coordination *eNB-2*, should be less than 1 ms, and the estimation for X2-interface related eNB processing delay should also be less than 1 ms. Otherwise, the changes for the HARQ RTT are required in the LTE-A network for the CoMP applications.

---

[1]An I&Q sample is the complex representation of a constellation point for a given sub-carrier, which is received on a given antenna. It is the output of Fast Fourier Transform (FFT) at the Orthogonal Frequency Division Multiplexing (OFDM) receiver chain and basically contains the amplitude and phase information where a particular sub-carrier has been modulated.

5.3 System Modeling of MMSE/MMSE-SIC Receiver for CoMP Joint Reception

In recent years, substantial amount of research has been conducted to the task of MUD. With multiple antenna exploited at the CoMP receiver end, the separation of different users can be performed based on their unique spatial signature by assuming the knowledge of the channel parameter [21][110].

MMSE detector is one of the well-known linear multi-user detectors. It can balance the signal decoupling and noise enhancement [112]. In [113], it has been shown that at low Signal-to-Noise Ratio (SNR) the MMSE detector converges to the conventional (single-user) receiver and at high SNR it converges to the decorrelator detector. MMSE multi-user detector has been studied and utilized in the CDMA-based system [114], OFDM-based SU-MIMO [115] and MU-MIMO [116][117] system. In this study, we will exploit the MMSE-based multi-user detector to the UL CoMP applications. The basic MMSE receiver are first presented in Section 5.3.1 and the advanced MMSE-SIC are described in later Section 5.3.2.

5.3.1 Linear MMSE Detector

Considering a general scenario of CoMP joint reception, N_u joint transmission UEs have single transmit antenna each and coordinated eNBs contain N_r receive antennas. Assuming that the channel is static over the duration of a PRB, as shown in Figure 5.3 of the physical layer block diagram, the received signal after Cyclic Prefix (CP) removal and FFT can then be expressed as:

$$\mathbf{r}_{N_r \times 1} = H_{N_r \times N_u} \sqrt{P_{tx, N_u \times N_u}} \mathbf{s}_{N_u \times 1} + \boldsymbol{\omega}_{N_r \times 1} \tag{5.7}$$

where $\mathbf{r}_{N_r \times 1}$ is the received signal vector with dimension $N_r \times 1$, $\mathbf{s}_{N_u \times 1}$ is the transmit signal vector of joint reception UEs with dimension $N_u \times 1$, $P_{N_u \times N_u}$ is the $N_u \times N_u$ diagonal matrix of UE transmit power, $\boldsymbol{\omega}_{N_r \times 1}$ is the $N_r \times 1$ inter-cell interference plus noise vector assumed with Gaussian distribution and variance σ_ω^2. The channel matrix H represents the links between joint transmission UEs

and receive antennas, and it can be expressed as:

$$H_{N_r \times N_u} = \begin{pmatrix} h_{11} & h_{12} & \cdots & h_{1N_u} \\ h_{21} & h_{22} & \cdots & h_{2N_u} \\ h_{31} & h_{32} & \cdots & h_{3N_u} \\ h_{41} & h_{42} & \cdots & h_{4N_u} \\ \vdots & \vdots & \ddots & \vdots \\ h_{N_r1} & h_{N_r2} & \cdots & h_{N_rN_u} \end{pmatrix} \tag{5.8}$$

where h_{ji} denotes the complex channel gain from the transmit antenna of UE i to the coordinated eNB receive antenna j.

After the FFT block as shown in Figure 5.3, the received signal $\mathbf{r}_{N_r \times 1}$ is fed into the MUD block, which performs the separation of joint reception UEs. For the MMSE detector, the knowledge of channel transfer function is required and practically can be estimated from the RS inserted in predefined sub-carrier positions at each UE's transmit antenna. In this study perfect channel knowledge is assumed to be known at the CoMP receiver end. The weight of MMSE detector W can be expressed as [118]:

$$W_{N_u \times N_r} = H_{N_r \times N_u}^H \left(H_{N_r \times N_u} H_{N_r \times N_u}^H + \sigma_\omega^2 I_{N_r} \right)^{-1} \tag{5.9}$$

where $(\bullet)^H$ denotes the Hermitian transpose operator and I_{N_r} is the $N_r \times N_r$ identity matrix. The $N_u \times N_r$ weight matrix W can be depicted as:

$$W_{N_u \times N_r} = \begin{pmatrix} w_{11} & w_{12} & w_{13} & w_{14} & \cdots & w_{1N_r} \\ w_{21} & w_{22} & w_{23} & w_{24} & \cdots & w_{2N_r} \\ \vdots & \vdots & \vdots & \vdots & \ddots & \vdots \\ w_{N_u1} & w_{N_u2} & w_{N_u3} & w_{N_u4} & \cdots & w_{N_uN_r} \end{pmatrix} \tag{5.10}$$

where w represents the weight coefficient.

Combining the Equation 5.7 and Equation 5.10, the estimate of transmit signal vector, $\widehat{\mathbf{s}}$, can then be expressed as:

$$\widehat{\mathbf{s}} = W_{N_u \times N_r} \mathbf{r}_{N_r \times 1} \tag{5.11}$$

$$= W_{N_u \times N_r} H_{N_r \times N_u} \sqrt{P_{tx,N_u \times N_u}} \boldsymbol{s}_{N_u \times 1} + W_{N_u \times N_r} \boldsymbol{\omega}_{N_r \times 1} \tag{5.12}$$

Take the joint reception scenario in Figure 5.2(b) as an example, with two joint reception UEs $N_u = 2$ and two coordinated eNBs $N_r = 4$ (2 antenna per eNB), the estimate of transmit signal of *UE-A*, $\widehat{s_A}$, can then be expressed as:

$$
\begin{aligned}
\widehat{s_A} &= \mathbf{w}^T_{A,1\times N_r}\mathbf{r}_{N_r\times 1} \qquad\qquad\qquad\qquad\qquad\qquad (5.13)\\
&= \mathbf{w}^T_{A,1\times N_r}\mathbf{h}_{A,N_r\times 1}\sqrt{\mathrm{P_{tx,A}}}s_A + \mathbf{w}^T_{A,1\times N_r}\mathbf{h}_{B,N_r\times 1}\sqrt{\mathrm{P_{tx,B}}}s_B\\
&\quad + \mathbf{w}^T_{A,1\times N_r}\boldsymbol{\omega}_{N_r\times 1} \qquad\qquad\qquad\qquad\qquad\quad (5.14)
\end{aligned}
$$

where $\mathbf{w}^T_{A,1\times N_r} = [\mathrm{w}_{A1}\ \mathrm{w}_{A2}\ \mathrm{z}_{A3}\ \mathrm{w}_{A4}]$ is the Ath row of $\mathrm{W}_{N_u\times N_r}$ as presented in Equation 5.10 and $\mathbf{h}_{A,N_r\times 1} = [\mathrm{h}_{1A}\ \mathrm{h}_{2A}\ \mathrm{h}_{3A}\ \mathrm{h}_{4A}]^T$ is the Ath column of $\mathrm{H}_{N_r\times N_u}$ as presented in Equation 5.8. $(\bullet)^{\mathrm{T}}$ denotes the Transpose operator.

According to Equation 5.14, the received signal power of *UE-A* can be represented by $\mathrm{P_{tx,A}}\left|\mathbf{w}^T_{A,1\times N_r}\mathbf{h}_{A,N_r\times 1}\right|^2$. The received mutual interference power from the joint pairing *UE-B* can be expressed by $\mathrm{P_{tx,B}}\left|\mathbf{w}^T_{A,1\times N_r}\mathbf{h}_{B,N_r\times 1}\right|^2$. And the received inter-cell interference from the $UE \neq A\&B$ plus noise power can be denoted by $E\left[\mathbf{w}^T_{A,1\times N_r}\boldsymbol{\omega}_{N_r\times 1}\boldsymbol{\omega}^{\mathrm{H}}_{N_r\times 1}\left(\mathbf{w}^T_{A,1\times N_r}\right)^{\mathrm{H}}\right] = \mathbf{w}^T_{A,1\times N_r}\sigma^2_\omega\left(\mathbf{w}^T_{A,1\times N_r}\right)^{\mathrm{H}}$ and it is assumed to be white Gaussian distributed. $E\left[\bullet\right]$ represented the expected value.

Considering on one PRB, the *UE-A* MMSE output SINR, $\gamma_{mmse,A}$, can be represented as:

$$
\gamma_{mmse,A} = \frac{\mathrm{P_{tx,A}}\left|\mathbf{w}^T_{A,1\times N_r}\mathbf{h}_{A,N_r\times 1}\right|^2}{\mathrm{P_{tx,B}}\left|\mathbf{w}^T_{A,1\times N_r}\mathbf{h}_{B,N_r\times 1}\right|^2 + \mathbf{w}^T_{A,1\times N_r}\sigma^2_\omega\left(\mathbf{w}^T_{A,1\times N_r}\right)^{\mathrm{H}}} \qquad (5.15)
$$

With $\mathrm{N_{PRB}}$ assigned PRBs for the whole MAC transport block, the MMSE output SINR of *UE-A*, $\gamma^{mac}_{mmse,A}$, can then be represented as:

$$
\gamma^{mac}_{mmse,A} = \frac{\frac{\mathrm{P_{tx,A}}}{\mathrm{N_{PRB}}}\sum\limits_{p=1}^{\mathrm{N_{PRB}}}\left|\mathbf{w}^T_{A,p,1\times N_r}\mathbf{h}_{A,p,N_r\times 1}\right|^2}{\sum\limits_{p=1}^{\mathrm{N_{PRB}}}\left(\frac{\mathrm{P_{tx,B}}}{\mathrm{N_{PRB}}}\left|\mathbf{w}^T_{A,p,1\times N_r}\mathbf{h}_{B,p,N_r\times 1}\right|^2 + \mathbf{w}^T_{A,p,1\times N_r}\sigma^2_\omega\left(\mathbf{w}^T_{A,p,1\times N_r}\right)^{\mathrm{H}}\right)}
$$

$$(5.16)$$

5.3.2 Non-Linear MMSE-SIC Detector

For the linear MMSE detector, it assumes that linear combiner output associated to different users are corrupted only by Additive White Gaussian Noise (AWGN). In fact the linear combiner output signals also contain residual interference, which is not Gaussian distributed [119]. Therefore, further performance improvement of MUD can be made by using non-linear detector.

SIC is a popular non-linear MUD technique which has been widely investigated [120]. It serially cancels the interfering user signals from the outputs of linear detector in order of decreasing power. Compared with the Parallel Interference Cancellation (PIC)[1], SIC performs better for systems without power control. By removing the strong interference user signals in an iterative SIC manner, the weak user signals can be recovered and will see a tremendous signal gain from the interference reduction [120]. In this UL CoMP study, no power control is applied to the UEs across the coordinated multiple cells. Therefore, SIC is the better scheme to be used. As presented in the following section, the MMSE-SIC detector is investigated with the CoMP joint reception.

MMSE-SIC detector is an iterative process of MMSE detector. It progressively reduces the mutual interference of joint reception UEs by including the estimate of transmitted data sequences from the previous users/iterations in the detection process. As presented in [118] and shown in Figure 5.4, Turbo decoder can be utilized jointly with the MUD detector in an iterative-loop. The output of Turbo decoder provides an estimate of coded bit in the form of log-likelihood ratios, which are then interleaved and soft-modulated in order to obtain an estimate of the transmitted symbols. The soft estimates are then fed back to an interference canceller. Starting with subtracting off the strongest joint reception user signal from the rest of joint reception user signals in a successive fashion, the mutual interference contributions are progressively removed and the reliability of data estimates for each joint reception user is iteratively enhanced.

Considering the same system model as defined in Section 5.3.1, the output of interference canceller block for the UE i on the PRB p at l-th iteration can be written as:

$$\mathbf{r}^l_{i,p,\mathrm{N_r}\times 1} = \mathbf{r}_{p,\mathrm{N_r}\times 1} - \mathrm{H}_{Z-\{i\},p,\mathrm{N_r}\times 1}\sqrt{\mathrm{P}_{\mathrm{tx},Z-\{i\}}}\widehat{\mathbf{c}}^m_{Z-\{i\},p,\mathrm{N_r}\times 1} \tag{5.17}$$

where $Z = \{1,2\}$ is the set of joint reception UE index, $\mathrm{H}_{Z-\{i\}}$ represents

---

[1]PIC is a non-linear MUD technique. It parallely cancels the interfering user signals from the output of linear detector and performs better for systems with power control, which ensures equal receive power of all users and all signals can be detected simultaneously [120].
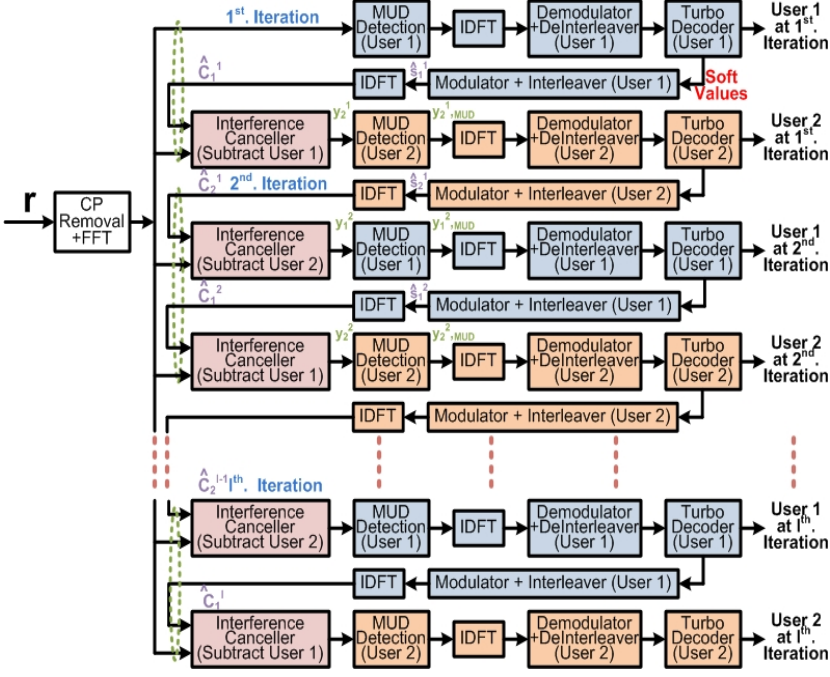
Figure 5.4: MMSE-SIC Structure

the column of H where the $(Z - \{i\})$-th joint reception UE has been mapped. $P_{tx,Z-\{i\}}$ is the transmit power of $(Z - \{i\})$-th joint reception UE. $\widehat{\mathbf{c}}_{Z-\{i\}}^{m}$ is the soft estimate symbols of the $(Z - \{i\})$-th joint reception UE, which obtained from the iteration $m = l$ if $(Z - \{i\})$-th joint reception UE has the highest SINR or from the previous iteration $m = l - 1$ if $(Z - \{i\})$-th joint reception UE has not the highest SINR.

After the interference cancellation, the residual error should be taken into consideration in the MUD block as shown in Figure 5.4. The output of MUD block for the UE i on the PRB p at l-th iteration can then be represented as:

$$\mathbf{r}_{i,p,MUD}^{l} = \mathbf{H}_{i,p,\mathrm{N_r} \times 1}^{H} \left[\mathbf{H}_{p,\mathrm{N_r} \times \mathrm{N_u}} \mathbf{Q}_{\mathrm{N_u} \times \mathrm{N_u}}^{l} \mathbf{H}_{p,\mathrm{N_r} \times \mathrm{N_u}}^{H} + \sigma_{\omega}^{2} \mathbf{I}_{N_r} \right] \mathbf{r}_{i,p,\mathrm{N_r} \times 1}^{l} \tag{5.18}$$

where $Q^{l} = \mathrm{diag}\,[q_1, \cdots, q_{N_u}]$ is the $N_u \times N_u$ diagonal matrix of the residual interference powers conditionally to the interference cancellation process, whose

k-th element can be denoted as:

$$q_k = \begin{cases} 1, & \text{if } k = i \\ 1 - \widehat{\sigma}^2_{Z-\{i\},l} & \text{if } k \neq i, \text{ UE } k \text{ has not the highest SINR} \\ 1 - \widehat{\sigma}^2_{Z-\{i\},l-1}, & \text{if } k \neq i, \text{ UE } k \text{ has the highest SINR} \end{cases} \quad (5.19)$$

where $\widehat{\sigma}^2_{Z-\{i\},l-1}/\widehat{\sigma}^2_{Z-\{i\},l}$ is the variance of soft modulated symbols obtained after decoding of $(Z-\{i\})$-th joint reception UE at $(l-1)$-th/l-th iteration.

It should be noted that, when no priori information is available at the start of SIC iteration, $\widehat{\sigma}^2 = 0$ and the covariance matrix Q is an identity matrix. The Equation 5.18 acts as a linear MMSE detector. Once the priori information is available, the covariance matrix Q is updated at each iteration with the new symbol variance σ_{new}, which will be used for the next UE or iteration prediction.

The output SINR of MUD block for UE i on the PRB p at l-th iteration can be expressed as [94]:

$$\gamma^l_{sic,i,p} = \frac{P_{tx,i}\eta^l_{i,p}}{1 - \eta^l_{i,p}} \quad (5.20)$$

The factor $\eta^l_{i,p}$ represents the equivalent channel gain for UE i on the PRB p at l-th iteration and can be expressed as:

$$\eta^l_{i,p} = H^H_{i,p,N_r \times 1}(H_{p,N_r \times N_u}Q^l_{,N_u \times N_u}H^H_{p,N_r \times N_u} + \sigma^2_\omega I_{N_r})^{-1}H_{i,p,N_r \times 1} \quad (5.21)$$

In this study, the symbol variance and instantaneous BLER are predicted at system-level simulator without performing detailed link-level processing steps. A fast prediction method based on Gaussian Approximation (GA) is proposed in [94] for the iterative MMSE-SIC multiuser MIMO joint decoding. This method exploited a compressed SINR scalar value, which is given by:

$$\gamma^l_{sic,i,compress} = M_i^{-1}\left(\frac{1}{N_{PRB}}\sum_{p=1}^{N_{PRB}} M_i\gamma^l_{sic,i,p}\right) \quad (5.22)$$

where M_i is defined in [94] which is the Average Mutual Information (AMI) associated to the constellation of user i in a Gaussian case.

As shown in [121], under GA, the compressed SINR is assimilated to the SNR of a Gaussian transmission model. Therefore the compressed SINR can be used to find an estimate of the symbol variance and BLER for the relevant MCS by using the basic AWGN link-level-performance curves. It has shown in [122] that this prediction model is able to provide a reliable estimate of decoder performance. The reference AWGN curves used in this study are shown in Figure 5.5. When the SINR is high the estimate becomes more and more accurate, and therefore $\widehat{\sigma^2}$ approaches 1. In that case, the mutual interference can be completely removed from the weak UE signal. The term in the diagonal of the Q matrix, $1 - \widehat{\sigma^2}$ is then equal to 0 and this means that the residual error concerning the estimate of the strong UE is not taken into account anymore in the MUD detector, since the contribution of the strong UE has been completely removed.
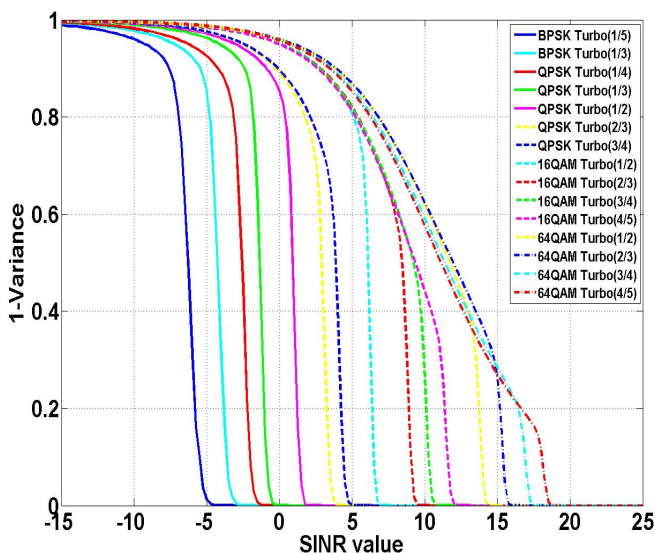

Figure 5.5: Compressed SINR to Symbol Variance Mapping with 6 PRBs, 2 antennas, 10 MHz bandwidth at 2 GHz carrier frequency [117]

In Table 5.1, the prediction and updating procedure of symbol variance for the MMSE-SIC detector are shown. For the number of N_l SIC iterations and N_u joint reception UEs, the joint reception UEs are first detected when no a priori information is available. This detection is corresponding to the linear MMSE detector with a identity symbol covariance matrix Q. Afterward, the joint reception users are ordered according to the SINR values. The SIC iteration start from the highest SINR users. By computing the instantaneous SINR

Table 5.1: Link-to-System Performance Mapping of Symbol Variance for MMSE-SIC Detector

Prediction and Updating Procedure:

Initialize the symbol covariance matrix Q_i^l to identity matrix (corresponding to no a priori information)
for $l = 1$ **to** $l = N_l$
   Order the UEs in descend based on the SINR value
   for $i = 1$ **to** $i = N_u$
     Step-1: Compute the instantaneous SINR $\gamma_{sic,i,p}^l$ according to Equation 5.20
     Step-2: Compress the SINRs of $\gamma_{sic,i,p}^l$ into $\gamma_{sic,i,compress}^l$ using Equation 5.22
     Step-3: Based on the compressed SINR value, read the symbol variance σ_{new} from Figure 5.5 associated to the UE's MCS
     Step-4: Update the symbol covariance matrix Q_i^l with new symbol variance $\sigma_{new} = Q_{i+1}^l$ used for the next user prediction
   end for
   Update the symbol covariance matrix $Q_{i=1}^{l+1} = Q_{i+1}^l$ for the next iteration prediction
end for

of all the streams for a single user, the compressed SINR is used to find the symbol variance from the AWGN curve shown in Figure 5.5. By updating the corresponding symbol variance in the covariance matrix, the updated covariance matrix is used for the detection filter computation to the next user/iteration.

5.4 LTE RS Modeling for CoMP Applications

In the UL LTE as specified in Rel'8, there are two RSs, which are called De-Modulation Reference Signal (DMRS) and SRS [22]. DMRS is used for channel estimation which is needed for coherent detection and demodulation, and SRS is used to provide information on UL channel quality. For the Physical Uplink Shared Channel (PUSCH), DMRS has the same bandwidth as the UL data transmission and occupies the 4-th SC-FDMA symbol for each UL slot. Whereas SRS has larger/potentially much larger transmission bandwidth and is less often transmitted than the DMRS [15].

The DMRS transmissions are orthogonal among the Intra-cell UEs in Rel'8 LTE. Interference can be mitigated because the UEs are transmitted on the

assigned PRBs within a cell [15]. However, for the CoMP application as shown in Figure 5.2, CoMP UE pairs will be simultaneously transmitting with the same PRBs across cells and estimated at separated CoMP eNBs. In order to avoid the high interference between the DMRS among CoMP UEs, the support of multi-cell orthogonal DMRS transmissions is required in the LTE-A. For the SRS transmission, there is a possibility to sound from multiple intra-cell UEs within the same frequency band by using orthogonal code in LTE Rel'8 [22]. But for the CoMP application, it is also required to extend the simultaneous orthogonal sounding for the cross-cell UEs within the same frequency band.

In this study the DMRS is not modeled explicitly by assuming the perfect channel knowledge estimated at the CoMP eNBs. So the full channel knowledge of joint detection users is assumed for the CoMP MUD detection as described in Section 5.3. The orthogonal SRSs are assumed for the UEs not only within a cell but also between the cross cell joint reception UEs. Therefore, the mutual interference of joint reception UEs is ideally removed in the weight calculation shown Equation 5.9 because of orthogonality. In practice, the multiple orthogonal SRS can be generated by using either cyclic shift of a RS sequence or different RS sequences [22].

5.5   Simulation Assumptions

The main simulation assumptions for UL CoMP joint reception study are shown in Table 5.2:

As it can be seen from Table 5.2, the interference-limited Macro Case-1 scenario is still the main focus in this study. Based on the previous antenna tilting study, the 3-D antenna pattern with 70° horizontal and 10° vertical patterns is considered. The eNB antenna is downtilted at the optimal angle of 14° as investigated in Section 3.5.1, and it also achieves the optimum performance for the CoMP macro diversity study as presented in Section 4.7.3. In order to obtain a certain amount of CoMP UEs for the accurate statistical analysis, 30 UEs per cell are generated.

The maximum number of CoMP cells is limited to 2 cells (1 serving cell + 1 coordination cell) in this study. Therefore, with 2 antennas per cell, there are in total 4 receive antenna at the CoMP eNB side. The CoMP UEs are selected based on the RSRP measurement as described in Section 4.2 and the selection criteria is defined in Equation 4.1. The selection window size of 3 dB is considered, which is also a practical value used in the WCDMA soft handover scheme [123].

Table 5.2: Simulation Assumptions of UL CoMP Joint Reception

Parameter	Assumptions
Deployment Scenario	Macro Case-1: ISD=500 m
Number of UEs	30 UEs/cell
OLPC P_0 and α value	-58 dBm and 0.6/-106 dBm and 1.0
CLPC P_{offset}	-1,-2,-3 or -4 dB
BS Antenna Pattern	Horizontal HPBW 70°
	Vertical HPBW 10°
BS Antenna Downtilting Angle	14°
Receiver Type	MMSE/MMSE-SIC
Number of Joint Detection Cells	Maximum 2 cells
	(1 serving cell + 1 coordination cell)
PS Algorithm	Proportional Fair
Coordinated PS Algorithm	Random Pairing
CoMP UE Selection	RSRP-based, 3 dB window size
CoMP Scenario	Intra-Site, Inter-Site, Case-1, Case-3

No specific CPS algorithm is applied in this study, which means all UEs are allocated respectively by their own serving cell packet scheduler and the selected CoMP UEs are then paired with the corresponding co-channel UE scheduled in the coordination cell to perform the CoMP joint detection. The two joint detection UEs can also be considered as paired by a random-fashion PS algorithm. In each serving cell the default PF scheduling algorithm is used as described in Section 4.6.

Both open-loop FPC parameter with $\alpha = 0.6$ and $\alpha = 1.0$ are investigated in this study for the CoMP joint reception, where the case of $\alpha = 0.6$ is the main focus and presented in detail. A simple CLPC scheme is considered in this study by applying the P_{offset} to the joint reception UEs. The P_{offset} is equal to -1,-2,-3 or -4 dB in each study case.

The case of no CoMP with 14° antenna downtilting is utilized as the baseline in this study. Instead of the ideal IC with MRC reception investigated in the previous study, as shown in Figure 5.6, the realistic MMSE/MMSE-SIC detection of MRC macro diversity is used as a reference to MMSE/MMSE-SIC CoMP joint reception study.

This study is carried out in both Intra-Site and Inter-Site scenarios as described in Section 4.6. The Intra-Site scenario limits the UL CoMP reception within the same site cells and the Inter-Site scenario allows the UL CoMP reception between any neighboring cells, which is also called unlimited Inter-Site scenario in this study. So naturally, the Intra-Site scenario is included as part of the

(a) MMSE Macro MRC

(b) MMSE-SIC Macro
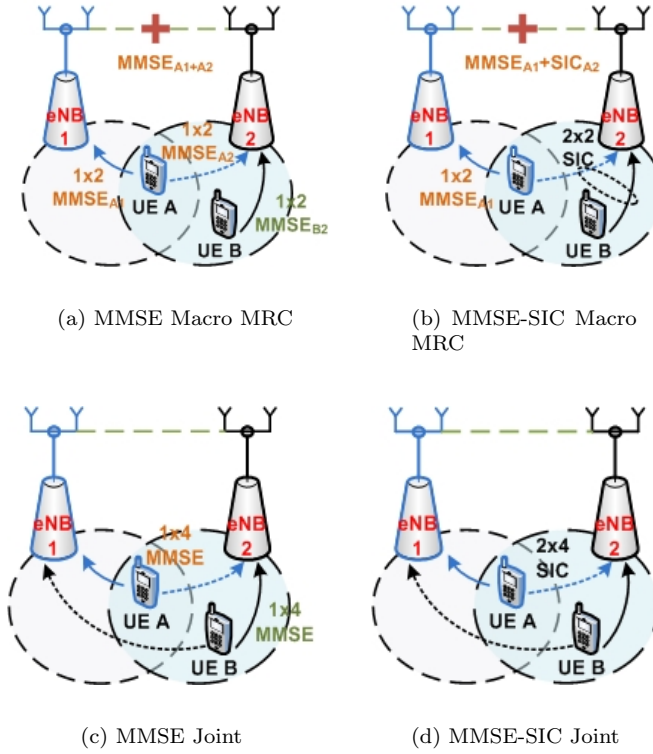MRC

(c) MMSE Joint

(d) MMSE-SIC Joint

Figure 5.6: MMSE/MMSE-SIC MRC Macro Diversity versus MMSE/MMSE-SIC CoMP Joint Reception

unlimited Inter-Site scenario. The number of selected CoMP UEs with 3 dB window size are shown in Figure 4.6 for both Intra-Site and unlimited Inter-Site scenario. As it can be seen, there are about 8% of CoMP UEs[1] for the Intra-Site scenario and 22% of CoMP UEs for the unlimited Inter-Site scenario.

In order to further analyze the CoMP joint reception in the unlimited Inter-Site scenario, the unlimited Inter-Site scenario is decomposed into three limited cases as shown in Figure 5.7. The Figure 5.7 only highlights a set of coordination cells for illustration purpose, and the full picture of the CoMP network layout can be seen in Figure B.1. The decomposed unlimited Inter-Site scenarios are restricted to 3 neighboring cell coordinations, where the Case-1 scenario is identical to the

---

[1]CoMP UE: is defined as the UE located at the CoMP cooperation area, which was called macro diversity UE in the previous macro diversity study in Chapter 4.
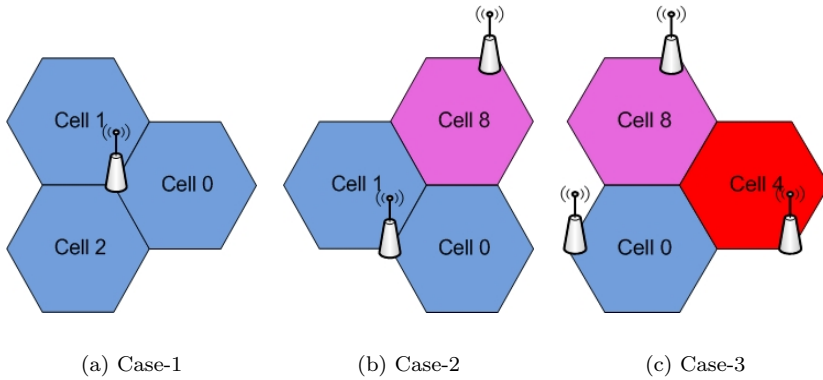
(a) Case-1   (b) Case-2   (c) Case-3

Figure 5.7: Three Limited Cases of Unlimited Inter-Site Scenario

Intra-Site scenario, the Case-2 scenario is the Inter-Site coordination with 2-Site, and the Case-3 scenario is the 3-site Inter-Site coordination. It is worth pointing out that these 3 cases are the general description of network coordination. Any 3 neighboring cell CoMP coordinations are covered by those 3 cases, i.e. the coordination of cells 1, 9 and 11 as shown in Figure B.1 is actually corresponding to the Case-2 scenario with 2 cells belonging to the same site and the third cell from the neighboring site.

The number of selected CoMP UEs for the limited Inter-Site scenarios are shown in Table 5.3 compared with the Intra-Site and unlimited Inter-Site scenario. As expected, the Case-1 scenario is identical to the Intra-Site case with 8% CoMP UEs. The Case-2 and Case-3 scenario have about 10% and 8% CoMP UEs respectively.

Table 5.3: Number of Selected CoMP UEs

Scenario	Percentage of CoMP UEs in total UEs
Intra-Site	8%
Unlimited Inter-Site	22%
Case-1 (Limited Inter-Site)	8%
Case-2 (Limited Inter-Site)	10%
Case-3 (Limited Inter-Site)	8%

The path gain distributions of CoMP UEs in the three limited Inter-Site scenarios are shown in Figure 5.8(a). As it can be seen, the CoMP UEs in the Case-1 scenario have the highest path gain distribution, because the selected

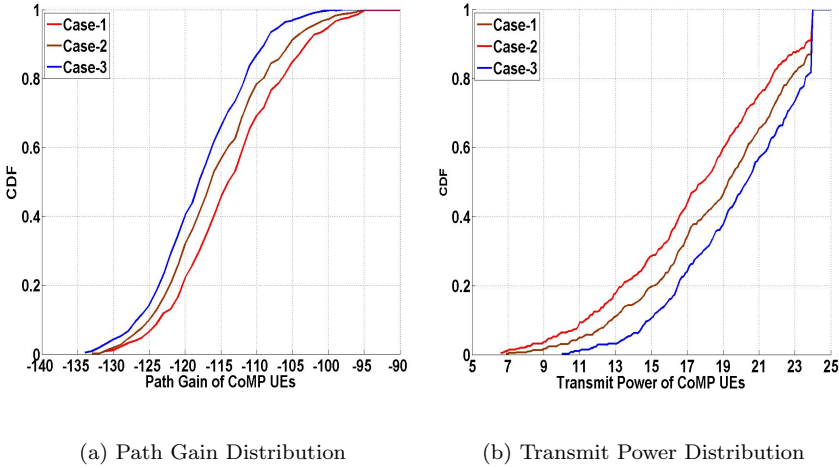(a) Path Gain Distribution   (b) Transmit Power Distribution

Figure 5.8: Comparison of Limited Inter-Site Scenarios of CoMP UEs

CoMP UEs are located at the close-by Intra-Site cell overlapping area as shown in Figure 5.9(a) and have a good signal quality to the eNB. For the Case-3 scenario, the CoMP UEs have the lowest path gain distribution, because the selected CoMP UEs are mainly located at the far-away cell-border region, as shown in Figure5.9(b), with a high signal attenuation. As shown in Figure 5.6, the CoMP UEs in the Case-2 scenario contain both Intra-Site and cross-site coordination, which results in the path gain distribution of CoMP UEs between Case-1 and Case-3 scenarios as shown in Figure 5.8(a).

In Figure 5.8(b), the transmit power distribution of CoMP UEs is shown. Based on the open-loop FPC as presented in Section 2.5.1 and as expected, the Case-3 scenario with low path gain CoMP UEs have the highest transmit power distribution, and about 20% of CoMP UEs operated at maximum power. The Case-1 scenario with high path gain CoMP UEs has the lowest transmit power distribution which has about 10% of CoMP UEs transmitted at saturated power. The curve of mixed Case-2 scenario is between Case-1 and Case-3 scenarios.

For the rest of the study, the Case-1 and Case-3 are going to be investigated and presented in detail.
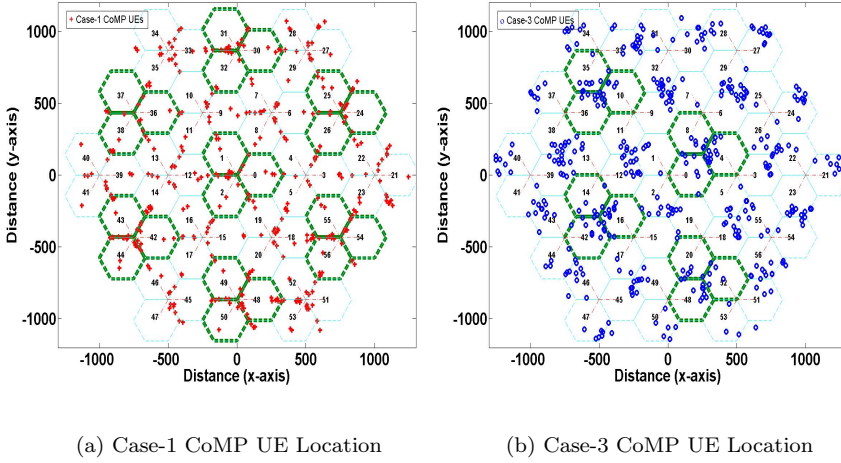
(a) Case-1 CoMP UE Location (b) Case-3 CoMP UE Location

Figure 5.9: Location of CoMP UEs in Limited Case-1 and Case-3 Scenarios

5.6 Performance Evaluation

With open-loop FPC parameter $\alpha = 0.6$ and $P_0 = -58$ dBm, the performance comparison of CoMP joint reception with CoMP macro diversity reception is first presented under the Intra-Site and unlimited Inter-Site scenarios. The detailed investigation of joint reception are performed afterwards for the Case-1 and Case-3 scenarios.

5.6.1 Comparison of CoMP Joint and Macro Diversity Reception

The comparison of CoMP joint and macro diversity reception are conducted in both Intra-Site and unlimited Inter-Site scenarios with open-loop FPC of $\alpha = 0.6$ and $P_0 = -58$ dBm, where the macro diversity with MRC scheme is used as reference.

In Figure 5.10, the SINR distribution of CoMP UEs per TTI are shown for the case of MMSE-SIC receiver. As expected, with better diversity of wireless channels and higher array gain by 4 CoMP eNB antennas as shown in Figure 5.6, the CoMP joint reception has higher SINR per TTI than the macro diversity

MRC reception in both Intra-Site and unlimited Inter-Site scenarios. The unlimited Inter-Site scenario also contains the high path loss CoMP UEs located at boresight cell-overlapping regions as shown in Figure 4.4. So the overall CDF distribution of SINR per TTI is lower in the unlimited Inter-Site scenario compared with the Intra-Site scenario for both CoMP joint and macro diversity MRC receptions.
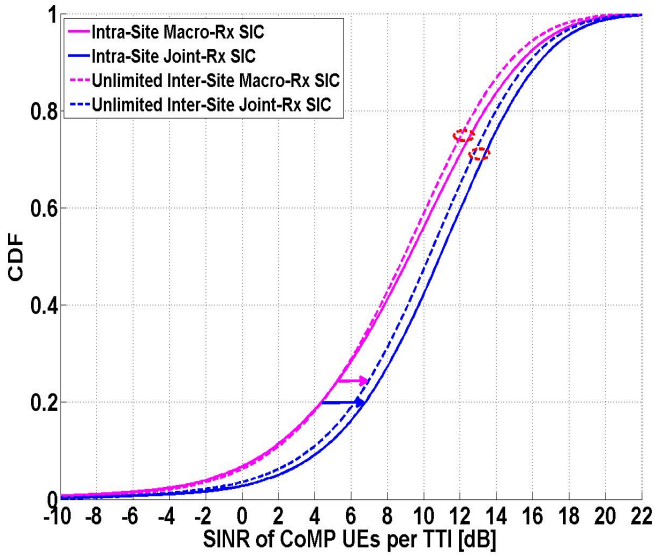

Figure 5.10: SINR per TTI for CoMP UEs in Intra-Site and Unlimited Inter-Site Scenarios with $\alpha = 0.6$ and $P_0 = -58$ dBm

In Figure 5.11, the average SINR distribution of unlimited Inter-Site CoMP UEs with CoMP joint reception are shown. The Non-CoMP case is utilized as a reference, because the Intra-Site scenario is included as part of the unlimited Inter-Site scenario, and there are only about 8% of CoMP UEs in the Intra-Site scenario stated in Table 5.3. As expected, the average SINR distribution of unlimited Inter-Site scenario shows better performance than the Intra-Site scenario, and at high average SINR region the MMSE-SIC receiver outperforms the MMSE receiver in both scenarios.

The throughput gain plot over the baseline, no CoMP case, is shown in Figure 5.12. The CoMP MRC macro diversity reception with MMSE and MMSE-SIC receivers are utilized as a reference. To compare with the previous MRC receiver with ideal IC cases as shown in Figure 4.9, the throughput gain of CoMP MRC macro diversity reception for the realistic MMSE and MMSE-SIC receivers is
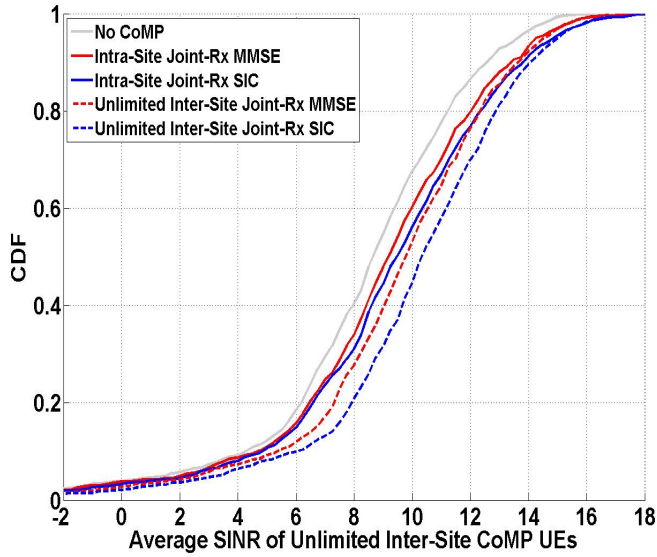
Figure 5.11: Average SINR of unlimited Inter-Site CoMP UEs in Intra-Site and Unlimited Inter-Site Scenarios with $\alpha = 0.6$ and $P_0 = -58$ dBm
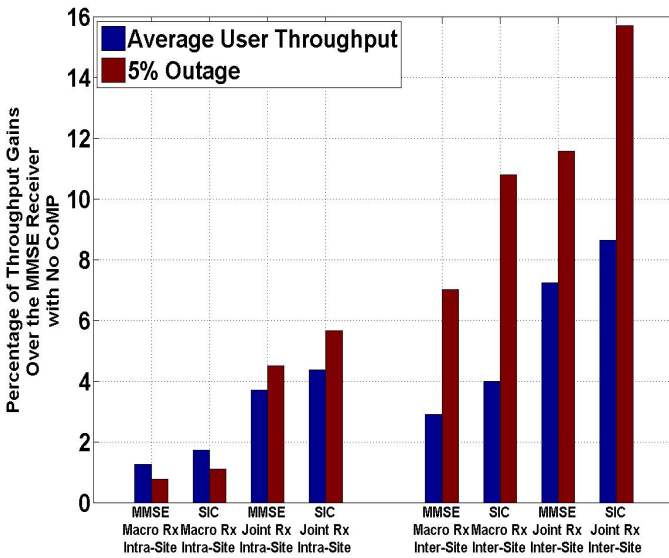

Figure 5.12: Intra-Site and Unlimited Inter-Site Scenarios with $\alpha = 0.6$ and $P_0 = -58$ dBm

expected to be lower because of partial interference removal.

As it can be seen in Figure 5.12, considering the CoMP joint reception with both MMSE and MMSE-SIC receivers, it has better performance than the corresponding CoMP macro diversity reception in both 5% outage and average UE throughput. For the best case with MMSE-SIC receiver, there is about 6% outage gain and 4% average UE throughput gain in the Intra-Site scenario and about 16% outage gain and 8% average UE throughput gain in the unlimited Inter-Site scenario.

The small improvement in the Intra-Site scenario is very limited by the number of CoMP UEs and the weak coordination link of the joint reception pair, i.e. the link B1 as shown in Figure 5.2(b). The improvement of the weak coordination link of the joint reception pair can be made by using multi-cell coordinated packet scheduling presented in Chapter 6.

In order to further investigate the performance of CoMP joint reception in the unlimited Inter-Site scenario, the limited Inter-Site scenarios with Case-1 and Case-3 are presented in detail in the following section.

5.6.2 CoMP Joint Reception in Limited Inter-Site Scenarios

Based on the description of Case-1 and Case-3 presented in Section 5.5, in Figure 5.13, the average SINR distribution of CoMP UEs is shown in the limited Case-1 and Case-3 scenarios. The selected CoMP UEs are different in the Case-1 and Case-3, two baseline curves for Non-CoMP case are plotted. The selected CoMP UEs in the Case-1 scenario have higher path gain distribution than the Case-3 scenario as shown in Figure 5.8(a). As expected, the averaged SINR distribution of selected CoMP UEs in the Case-1 scenario also have about 2 dB higher than the Case-3 scenario.

The throughput gain plot over the baseline, no CoMP case, is shown in Figure 5.14. In the Case-1 scenario, the throughput gain plot is exactly identical to the Intra-Site scenario as shown in Figure 5.12. To compare with the Case-3 scenario, which also contains about 8% of CoMP UEs as presented in Table 5.3, it shows 5% higher outage gain in the Case-3 scenario than in Case-1. The reason is that, the Case-3 scenario has about 26% of 5%-outage UEs locate at the CoMP area and selected as the CoMP UEs as shown in Table 5.4, whereas the Case-1 scenario has only about 11% of 5% outage UEs within the CoMP area. The CoMP reception improves the performance of CoMP UEs and consequently results in higher 5% outage gain in the Case-3 scenario, where the performance
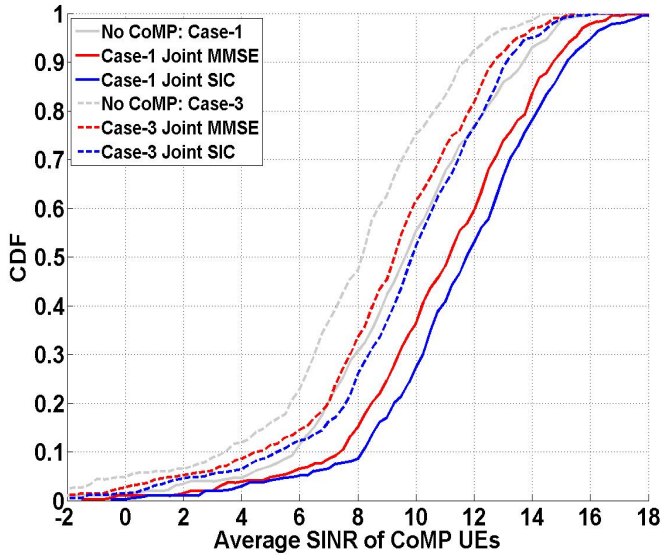
Figure 5.13: Average SINR Distribution in Limited Inter-Site Scenarios with $\alpha = 0.6$ and $P_0 = -58$ dBm
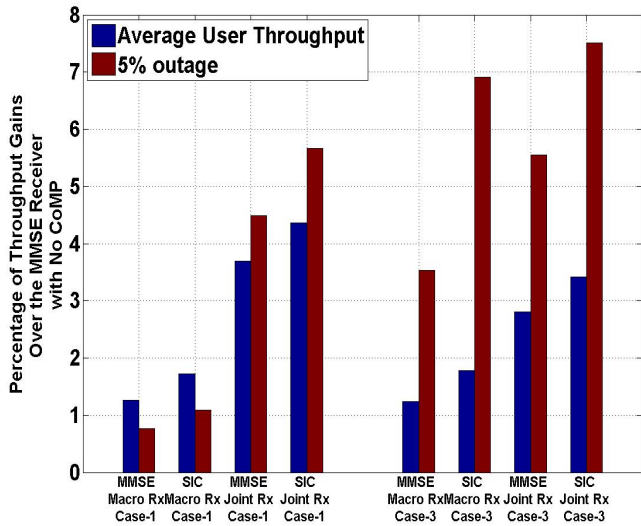

Figure 5.14: Limited Inter-Site Scenarios with $\alpha = 0.6$ and $P_0 = -58$ dBm

Table 5.4: Number of CoMP UEs out of the 5%-outage UEs
at Non-CoMP Case with 14° Downtilting

Scenario	Percentage of CoMP UEs in the overall 5%-outage
Intra-Site	11%
Inter-Site (Unlimited)	55%
Case-1 (Limited Inter-Site)	11%
Case-2 (Limited Inter-Site)	22%
Case-3 (Limited Inter-Site)	26%

gain in the Case-1 scenario can mainly be seen in the average user throughput.

It can also be seen that from Figure 5.14, to compare with the MMSE type of receiver, the MMSE-SIC receiver is more effective in the Case-3 scenario in terms of 5% outage throughput, because the cell-edge UEs with low SINR can gain more benefit from the interference cancellation than the high SINR UEs.

Comparing the CoMP joint reception with CoMP MRC macro diversity reception for both Case-1 and Case-3, the CoMP joint reception performs more efficiently in the Case-1 scenario with high SINR as shown in Figure 5.13. For the best case of MMSE-SIC receiver, the joint reception has about 5% gain in the 5% outage and 2% gain in the average user throughput over the MRC macro diversity reception. However, for the Case-3 scenario with low SINR, the joint reception only has 0.5% gain in the 5% outage and about 1% gain in the average user throughput over the MRC macro diversity reception.

By considering both the performance gain and capacity requirement of LTE X2-interface, the CoMP joint reception is a good choice for the Case-1/Intra-Site application. It can provide better overall performance than the CoMP macro diversity reception and without the need of large capacity X2-interface coordination. Whereas, the CoMP macro diversity reception with MMSE-SIC receiver is a good candidate for the cross-site, Case-3, type of application. It can give the sub-optimal performance gain close to the application of CoMP joint reception and demand relatively lower capacity requirement of X2-interface as discussed in Section 5.2.

5.6.3 CoMP Joint Reception with $\alpha = 1.0$

Based on the previous study in Section 3.5.2, the performance of CoMP joint reception with open-loop FPC parameter $\alpha = 1.0$ and $P_0 = -106$ dBm has also

been investigated in this study.

As shown in Figure 5.15, the average SINR distribution of unlimited Inter-Site CoMP UEs is shown by using the case of no CoMP with $\alpha = 0.6$ as a reference. As expected, compared with $\alpha = 0.6$, the utilization of $\alpha = 1.0$ optimizes the 5% outage cell-edge UE throughput by compromising the performance of cell-center UEs. The unlimited Inter-Site scenario still outperforms the Intra-Site scenario because large number of CoMP UEs are selected, and the MMSE-SIC receiver in both scenarios gives better gain than the MMSE receiver.
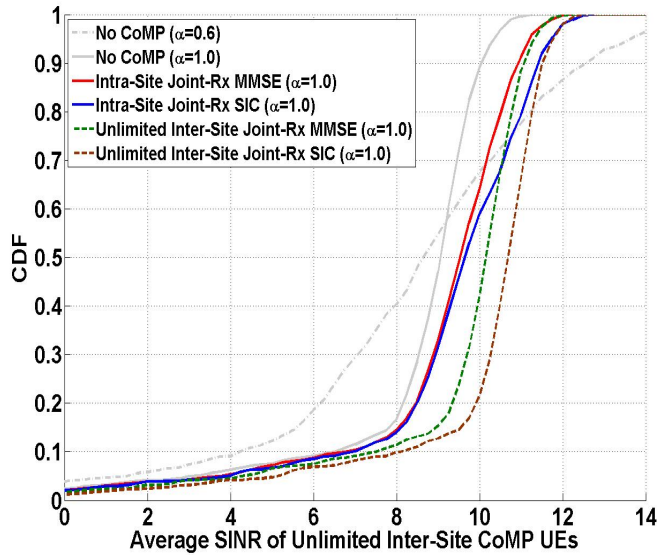

Figure 5.15: Average SINR of Inter-Site CoMP UEs in Intra-Site/Inter-Site Scenarios with $\alpha = 1.0$ and $P_0 = -106$ dBm

In Figure 5.16, the throughput gain plot over the no CoMP case with $\alpha = 1.0$ is presented. The cases of CoMP macro diversity with MRC reception are still used as a benchmark for the CoMP joint reception. Comparing with $\alpha = 0.6$, the MMSE-SIC receiver has shown marginal gain over the MMSE receiver in both Intra-Site and unlimited Inter-Site scenarios. This is due to the fact that, by using $\alpha = 1.0$, more cell-center UEs are transmitted with less power as shown in Figure 5.17, which results in low SINR as well. For those cell-center UEs with low SINR and being the pair of low SINR joint reception CoMP UEs, both UEs are quite hard to be detected and demodulated, which make it ineffective for the interference cancellation in order to improve the overall performance.
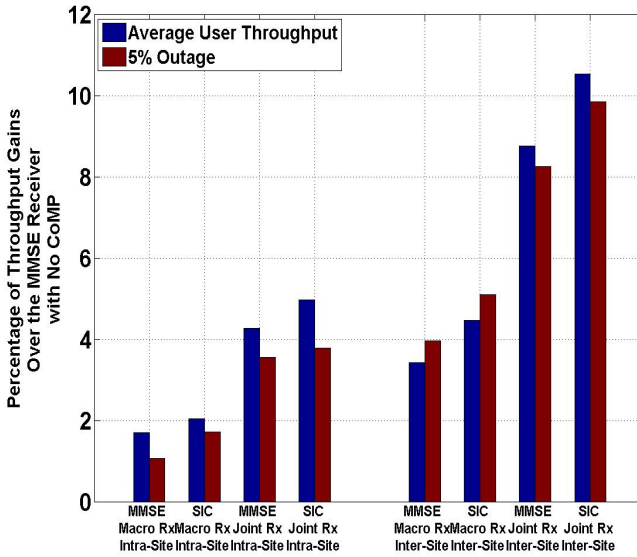
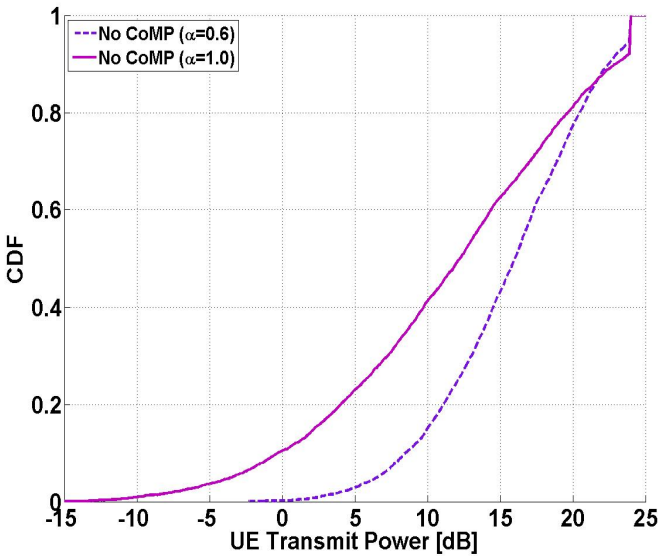Figure 5.16: Intra-Site and Inter-Site Scenarios with $\alpha = 1.0$ and $P_0 = -106$ dBm

Figure 5.17: UE Transmit Power Distribution of No CoMP scenario with $\alpha = 0.6$ vs. $\alpha = 1.0$

To compare the CoMP joint reception with MRC macro diversity reception, for the best case with MMSE-SIC receiver, there is about 3% and 2% gain for Intra-Site scenario and about 5% and 6% gain for unlimited Inter-Site scenario in terms of outage and average user throughput respectively.

5.6.4 CoMP Joint Reception with Close-loop FPC

As presented in Chapter 4, the application of close-loop FPC together with the IC-based macro diversity reception can provide further enhancement in both cell-edge and average user throughput compared with the standing alone IC-based macro diversity reception. In this study, the close-loop FPC scheme is also investigated for the CoMP joint reception with realistic MMSE/MMSE-SIC receiver.

In general, the exploited close-loop FPC scheme is to lower the transmit power of CoMP UEs, who normally generate high inter-cell interference to the other UEs, especially to the non-CoMP UEs. Because of less inter-cell interference received, the performance of non-CoMP UEs can be enhanced and the negative effect of powering down CoMP UEs is compensated by the CoMP joint reception gain.

The combination of CoMP joint reception and CLPC scheme with MMSE-SIC receiver has been evaluated under the unlimited Inter-Site scenario with the case of $\alpha = 0.6$ and $\alpha = 1.0$ as shown in Figure 5.18 and Figure 5.19 respectively. The case of 'No CLPC' presented in the previous Figure 5.12 and Figure 5.16 is utilized as the baseline for the CLPC cases. The CoMP MRC macro diversity reception is utilized as a reference to the CoMP joint reception.

Considering the CoMP joint reception with CLPC, for the case of $\alpha = 0.6$, the 5% outage throughput gain is optimized at *-1* dB. To compare with the no CLPC, it can provide further improvement of 4% gain in terms of 5% outage and only 1% gain in terms of average user throughput. Futher transmit power reduction of CoMP UE can still improve the average user throughput but with dramatically reduced cell-edge UE performances. For the case of $\alpha = 1.0$, with the optimal reduction at *-2* dB, the application of CLPC together with CoMP joint reception gives about 6% and 4% gain in terms of 5% outage and average user throughput respectively over the no CLPC.

In Figure 5.20, the performance of CLPC for MMSE-SIC receiver under the Intra-Site scenario is shown for both CoMP joint and MRC macro diversity reception with $\alpha = 0.6$ and $P_0 = -58$ dBm. As it can be seen, by reducing the transmit power of CoMP UEs, the Non-CoMP cell-edge UEs, who cannot get
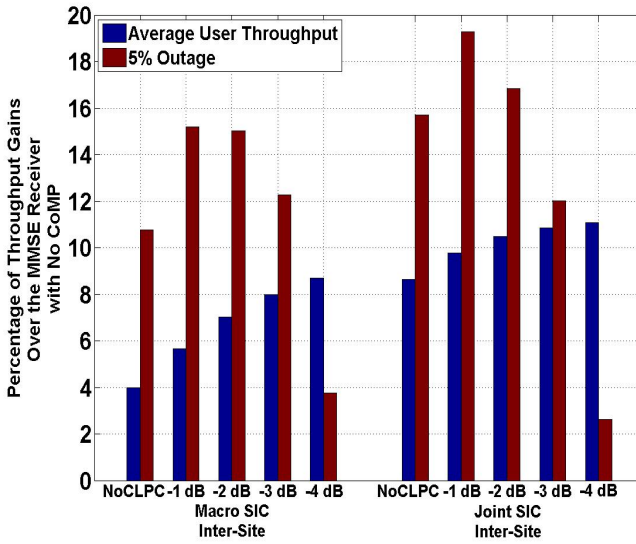
Figure 5.18: Inter-Site Scenarios for Macro vs. Joint SIC Receiver with $\alpha = 0.6$ and $P_0 = -58$ dBm
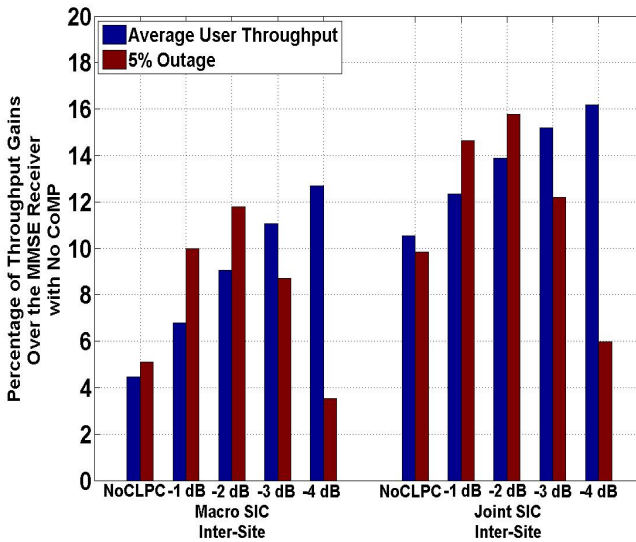

Figure 5.19: Inter-Site Scenarios for Macro vs. Joint SIC Receiver with $\alpha = 1.0$ and $P_0 = -106$ dBm
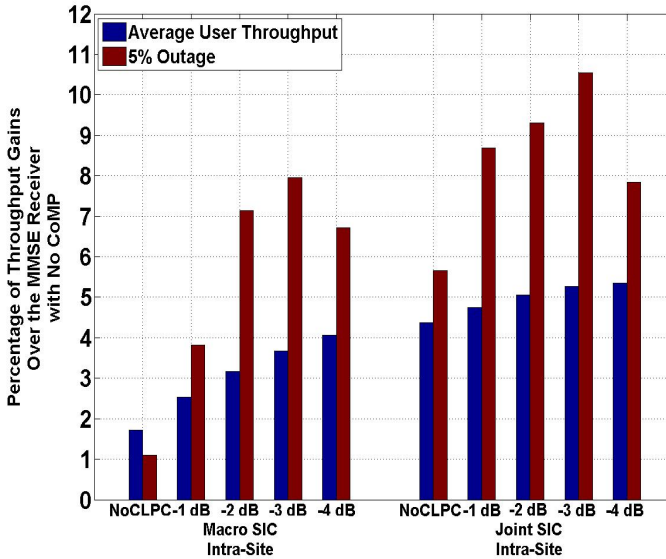
Figure 5.20: Intra-Site Scenarios for Macro vs. Joint SIC Receiver with $\alpha = 0.6$ and $P_0 = -58$ dBm

benefit from the CoMP reception, will get more opportunities to be scheduled in the PF frequency domain and further improve the overall 5% outage gain. Considering the CoMP joint reception, for the best case with optimal reduction of *-3* dB, there is about 11% gain and 5% gain over the baseline, Non-CoMP case, in terms of 5% outage and average user throughput respectively. To compare with the no CLPC case, there is a further enhancement of cell-edge user throughput by 5%.

5.7 Conclusions

In this chapter, the CoMP has been studied in the UL LTE in the form of joint reception. This study is carried out with MMSE/MMSE-SIC receiver and the investigations are performed in both Intra-Site and unlimited Inter-Site CoMP scenarios, where the unlimited Inter-Site scenario is further divided into Case-1 and Case-3 for detailed analysis. The open-loop FPC with $\alpha = 0.6$ and $P_0 = -58$ dBm is the main focus. The scheduled users are allocated by the packet scheduler performed in each individual cell and the selected CoMP UEs are paired with the corresponding co-channel UE scheduled in the coordination

cell to perform the CoMP joint detection. The two joint detection UEs can also be considered as paired by a random-fashion/independent PS algorithm.
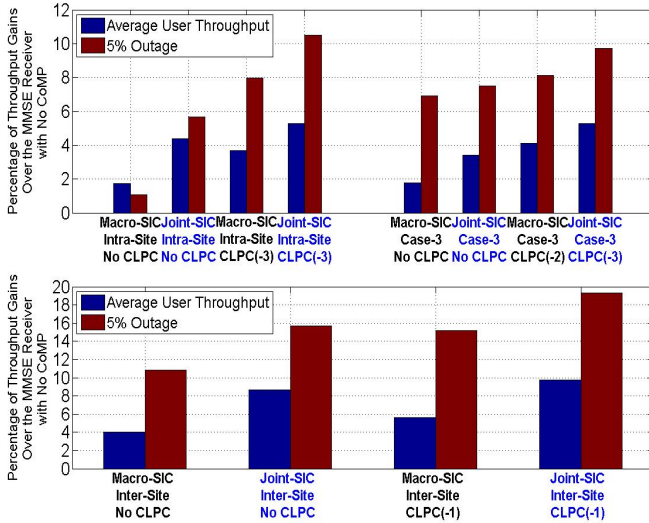
Figure 5.21: Macro vs. Joint SIC Receiver under the Intra- and Inter- Site Scenarios with $\alpha = 0.6$ and $P_0 = -58$ dBm

As a sum-up, the throughput gain plot over the no CoMP case is shown in Figure 5.21 with the MMSE-SIC receiver. As it can be seen in both Intra-Site and unlimited Inter-Site scenario, the CoMP joint reception outperforms the CoMP macro diversity with MRC reception, and the application of CLPC can further improve the overall performance. In the unlimited Inter-Site scenario, there is about 20% and 10% gain in terms of 5% outage and average user throughput respectively. Under the Intra-Site scenario, the performance of CoMP joint reception shows marginal gain in terms of both 5% outage and average user throughput. For the best case, there is about 10% and 5% gain in terms of outage and average user throughput respectively. The small improvement in the Intra-Site scenario is very much limited by the number of selected CoMP UEs.

Coordinated Packet Scheduling for CoMP Joint Reception

In Chapter 5, the performance of advanced (MMSE and MMSE-SIC) receiver for the CoMP application is investigated in the system-level without considering the multi-cell Coordinated Packet Scheduling (CPS). Under the CoMP Intra-Site scenario, the performance of CoMP joint reception shows marginal gain in terms of both 5% outage and average user throughput.

This chapter is the extension investigation of CoMP techniques from the previous chapter. The gain potential of multi-cell CPS is investigated under the Intra-Site scenario, where a cluster of Intra-Site cells jointly allocate the served UEs. The exploited CPS algorithm is based on the traditional PF scheduler and the orthogonality requirement is considered to pair the joint detection users. This study will focus on the joint MMSE-SIC detection which gave the optimal performance as presented in Section 5.3.2.

In Section 6.1, the multi-cell CoMP CPS is briefly introduced and the targeted study scenario is described. In Section 6.2, the studied multi-cell CPS algorithm is presented. In Section 6.3, the modeling assumption of the study is described and the performance evaluation results are presented in Section 6.4. In Section 6.5, the conclusion for the CoMP joint reception with CPS is made.

6.1   Multi-cell Coordinated Packet Scheduling

For the CoMP studies presented in Chapter 5, the Independent Packet Scheduling (IPS) was assumed, where each cell schedules its own serving UEs without considering the UE allocation in the other neighboring cells. To perform the CoMP joint detection, the allocated CoMP users were considered as paired in a random fashion with the co-channel user scheduled in the coordination cell. In this chapter, the potential of multi-cell Coordinated Packet Scheduling (CPS) is investigated together with the CoMP joint detection. By coordinating different cell sites in terms of the scheduling decision (PRB allocation) in the frequency domain, better joint detection pair could be allocated together to fully explore the CoMP multiuser detection gain. In general, the multi-cell CPS can be seen as an extension of the Inter-Cell Interference Coordination (ICIC) scheme already presented in the LTE network.

This study is focus on the Intra-Site CoMP, where the coordination cells are belong to the same BS site as described in Section 4.1. Compared with the Inter-Site CoMP, where the coordination cells are belong to different sites, it exhibits several advantages. First, the Intra-Site CoMP is not limited by the existing LTE network backhaul discussed in Section 5.2 since the coordination take place within the same physical location. The Intra-Site coordination cells can be coordinated via the equipment internal bus transfer. Therefore, there are basically no restrictions regarding to the amount of exchanged information and also the additional delay due to the CoMP coordination becomes almost negligible. Besides, the coordination cells belonging to the same site could be driven by the same clock, the synchronization of a certain UE to all coordination cells can be readily achieved. Finally, the intra-site coordination can be realized with the existing LTE Release 8 network since no backhaul signaling is involved and hence basically no further standardization is required for that purpose.

6.2   CPS Allocation Algorithm Design

Three-sector BS site is assumed in this study. The exploited CPS entity takes care of the physical resource allocation for all three intra-site cells. Therefore, three UEs will be allocated simultaneously on the same transmission frequency band by the CPS. An example is shown in Figure 6.1, *UE-A*, *UE-B* and *UE-C* are served respectively by the *Cell-1*, *Cell-2* and *Cell-3*, which are the coordination cells in one BS site/Intra-Site coordination cells. On a certain frequency band, *UE-A*, *UE-B* and *UE-C* will be jointly allocated by the CPS.
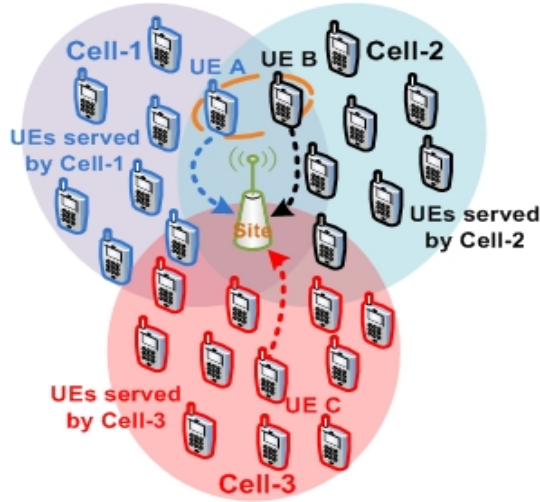
Figure 6.1: Scenario of CoMP Joint Reception with CPS

There are mainly two roles for the CPS algorithm investigated in this study, which are pairing and scheduling. The pairing makes sure that the best joint detection pair could be allocated together to fully explore the CoMP multiuser detection gain. Two scheduling algorithms are used jointly. The channel aware scheduling guarantees the QoS and the lowest path gain scheduling ensures the generated interference of allocated UE is minimized to the joint reception pair. Both pairing and channel aware scheduling rely on the available channel information. The pairing relies on the full spatial complex channel matrix (short-term) whereas the channel aware scheduling relies on the knowledge of SINR (long-term). In the following, the utilized pairing and scheduling criteria are defined.

6.2.1   CPS Pairing Algorithm

The theoretical work of [124] [125] shown that the MIMO capacity is influenced by the spatial correlation. With the independent channel fading between antennas, the capacity of the MIMO system grows proportionally to the minimum number of transmit and receive antenna, $min\left[N_t, N_r\right]$, for fixed transmit power. By exploiting the multiuser diversity, the CPS can allocate the joint reception UE pair with low channel correlation to minimize the mutual interference and therefore maximize the UL CoMP capacity. In this study, the defined channel

orthogonality $\lambda_{i,v}$ between UE i and UE v is expressed as:

$$\lambda_{i,v} = 1 - \frac{\left\langle \mathrm{H}_i^{\mathrm{H}}, \mathrm{H}_v \right\rangle}{\|\mathrm{H}_i\| \, \|\mathrm{H}_v\|}, \ 0 \leq \lambda_{i,v} \leq 1 \tag{6.1}$$

where H_i and H_v are the complex fast fading channel of *UE i* and *UE v*, and $\langle \bullet \rangle$ denotes the dot product. If the channel vector of the two UEs are orthogonal, the dot product in the nominator is zero and the defined channel orthogonality $\lambda_{i,v}$ between them is *1.0*, else is *0.0*.

The selection of best pairing UE is based on the maximum orthogonality in this study. For a CoMP *UE i*, the selected UE pair v can be expressed as:

$$v = \arg\max_{\substack{i,v \in \mathrm{V} \\ b(i) \neq b(v)}} \lambda_{i,v} \tag{6.2}$$

where V is all the users served in one site. i and v are the UEs from the same site but served in difference cell $b(i)$ and $b(v)$.

6.2.2　CPS Scheduling Algorithms

There are two scheduling algorithms considered in this study, which is the channel aware scheduling and lowest path gain scheduling.

The channel aware scheduling in this study only considered the FDPS with FTB as presented in Section 2.6. The PF scheduling algorithm is exploited. In a given serving cell b based on the maximum PF metric, the selected UE i transmits on PRB p at TTI t can be expressed as:

$$i_{b(i),p,t}^{\mathrm{PF}} = \arg\max_{i \in \mathrm{V}_{b(i)}} \left(\frac{\widehat{T}_{i,b(i),p,t}}{\overline{T}_{i,b(i),t}} \right) \tag{6.3}$$

where $\mathrm{V}_{b(i)}$ is all the users served in cell $b(i)$. $\widehat{T}_{i,b(i),p,t}$ is the estimated Layer-1 achievable throughput for UE i, served in cell $b(i)$, on PRB p and at scheduling instant time t. $\overline{T}_{i,b(i),t}$ is the past averaged Layer-1 acknowledge throughput

for UE i served in cell $b(i)$ at scheduling instant time t, which is calculated by using an exponential averaging filter:

$$\overline{T}_{i,b(i),t} = (1 - \xi)\overline{T}_{i,b(i),t-1} + \xi T_{i,b(i),t} \tag{6.4}$$

where $T_{i,b(i),t}$ is the Layer-1 acknowledged throughput for UE i served in cell $b(i)$ at scheduling instant time t and ξ is called the filter coefficient.

The lowest path gain scheduling exploited in this study ensures that the generated interference of allocated UE to the joint reception pair is minimized. With less received interference or higher received SINR, the CoMP joint detection gain can be further improved. For an allocated UE pair v and g transmit on PRB p at TTI t, the scheduled UE i based on the lowest path gain metric can be expressed as:

$$i^{\text{PG}}_{b(i),p,t} = \underset{\substack{i \in \text{V}_{b(i)} \\ b(i) \neq b(v) \neq b(g)}}{\arg\min} \left(-\text{L}_{i,b(i),p,t}\right) \tag{6.5}$$

where -L is the measured path gain of UE i in the serving cell $b(i)$ and the UE i, v and q are served in the Intra-Site cell $b(i)$, $b(v)$ and $b(q)$ respectively.

6.2.3   General Decision Flow of CPS

The general flow of CPS scheduler assumes that scheduling and pairing decisions are taken every TTI. For a certain frequency band, the decision flow is outlined as follows and the corresponding flow chart are shown in Figure 6.2:

1. Three UEs (*UE-A*, *UE-B* and *UE-C*) are selected from each Intra-Site cell according to the maximum PF metric which is presented in Equation 6.3 $\left(A^{\text{PF}}_{b(A),p,t}, B^{\text{PF}}_{b(B),p,t}, C^{\text{PF}}_{b(C),p,t}\right)$.

2. The selected three UEs are then sorted again according to the PF metric in descendant order and the output vector $\boldsymbol{\psi}^{\text{PF}}_{cells,p,t}$ can be expressed as:

$$\boldsymbol{\psi}^{\text{PF}}_{cells,p,t} = \text{Order}\left(A^{\text{PF}}_{b(A),p,t}, B^{\text{PF}}_{b(B),p,t}, C^{\text{PF}}_{b(C),p,t}\right) \tag{6.6}$$

where the first UE $\psi^{\text{PF,1st}}_{b(1st),p,t}$ has the highest allocation priority among the three UEs and the third UE $\psi^{\text{PF,3rd}}_{b(3rd),p,t}$ has the lowest.
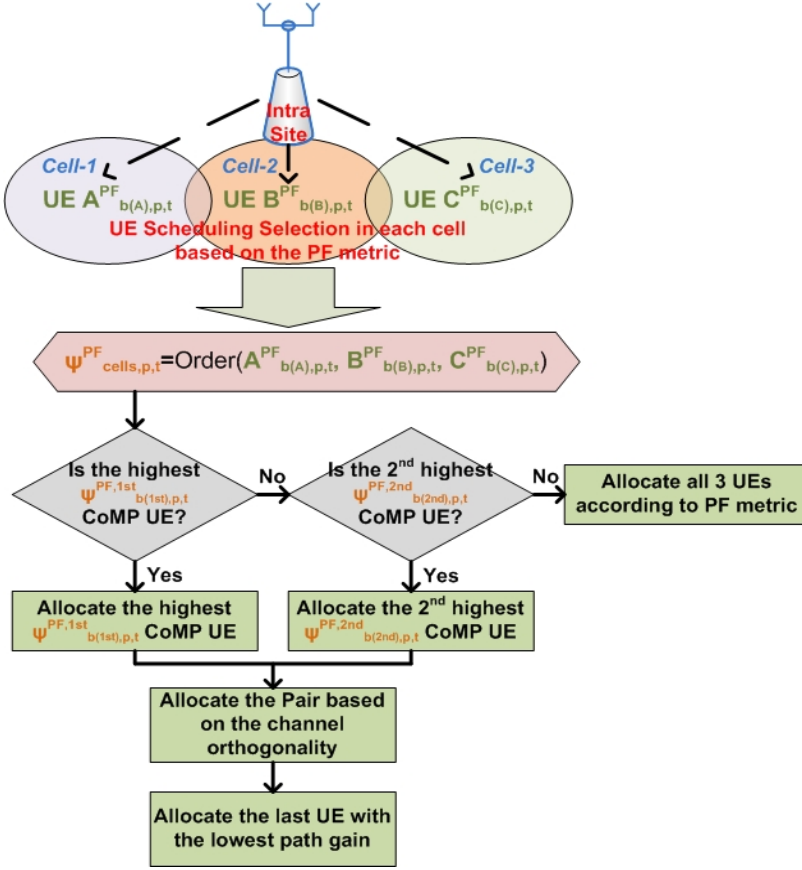
Figure 6.2: Flow Chart of Multi-cell CPS

3. Start from the highest priority UE $\psi_{b(1st),p,t}^{PF,1st}$, check if the UE is a CoMP UE:

   (a) If the UE $\psi_{b(1st),p,t}^{PF,1st}$ is a CoMP UE, allocate the UE $\psi_{b(1st),p,t}^{PF,1st}$ and find the best joint reception pair $\psi_{b(1stPair),p,t}^{PF,1stPair}$ based on the Equation 6.2. The allocation of last UE is selected based on the Equation 6.5, which has the lowest generated interference to the already allocated CoMP pair.

   (b) If the UE $\psi_{b(1st),p,t}^{PF,1st}$ is not a CoMP UE. But the second highest priority UE $\psi_{b(2nd),p,t}^{PF,2nd}$ is a CoMP UE. Allocate the UE $\psi_{b(2nd),p,t}^{PF,2nd}$ and find the best joint reception pair $\psi_{b(2ndPair),p,t}^{PF,2ndPair}$ based on the Equation 6.2. Still

by considering the lowest interference to the CoMP pair, the last UE is allocated based on Equation 6.5.

(c) If none of the UEs are CoMP UEs, then all three selected UEs are scheduled as expressed in Equation 6.3, which is corresponding to the independent PS performed in each cell.

Based on the above description, the algorithm generally needs to find two CoMP UEs and one non-CoMP UE. The pair of CoMP UE $\psi_{b(1\text{st}),p,t}^{\text{PF,1st}}$ or $\psi_{b(2\text{nd}),p,t}^{\text{PF,2nd}}$ can be selected by using Equation 6.2. If there is no pair found by using Equation 6.2, the algorithm is equivalent to the independent PS performed in each cell.

6.3 Simulation Assumptions

The main simulation assumptions for this UL CoMP CPS study are shown in Table 6.1:

Table 6.1: Simulation Assumptions of Multi-Cell Coordinated PS

Parameter	Assumptions
Deployment Scenario	Macro Case-1: ISD=500 m
Number of UEs	30 UEs/cell
OLPC P_0 and α value	-58 dBm and 0.6
CLPC P_{offset}	-1,-2,-3 or -4 dB
BS Antenna Pattern	Horizontal HPBW 70°
	Vertical HPBW 10°
BS Antenna Downtilting Angle	14°
Receiver Type	MMSE-SIC
Number of Joint Detection Cells	Max. 2 cells (1 serving + 1 coor. cell)
CPS Pairing Algorithm	Max. Orthogonality
CPS Scheduling Algorithm	PF or Lowest PG
CoMP UE Selection	RSRP-based, 3 dB window size
CoMP Scenario	Intra-Site
	(All 3 cells belong to the same site)

This study is still focus on the interference-limited Macro Case-1 scenario. 30 UEs are balance-loaded in each cell with spatially uniform distribution. The 3-D antenna pattern with 70° horizontal and 10° vertical HPBW patterns is exploited. Based on the investigation presented in Section 3.5.1, the eNB antenna is mechanically downtilted of 14° and the open-loop FPC parameter exploits $\alpha = 0.6$ and $P_0 = -58$ dBm.

The Intra-Site CoMP scenario is the main concentration for the investigated CPS algorithm. The CoMP UEs are selected based on the RSRP measurement as described in Section 4.2 and the selection criteria is defined in Equation 4.1. The CoMP joint reception with MMSE-SIC receiver is considered which gave the optimal performance in Chapter 5. A simple CLPC scheme is considered in this study by applying the P_{offset} to the joint reception CoMP UEs. The P_{offset} is equal to -1,-2,-3 or -4 dB in each study case.

6.4   Performance Evaluation

In this section, the simulation results of investigated CPS algorithm is presented. The corresponding study by using IPS, which is presented in the Chapter 5, is utilized as a reference.

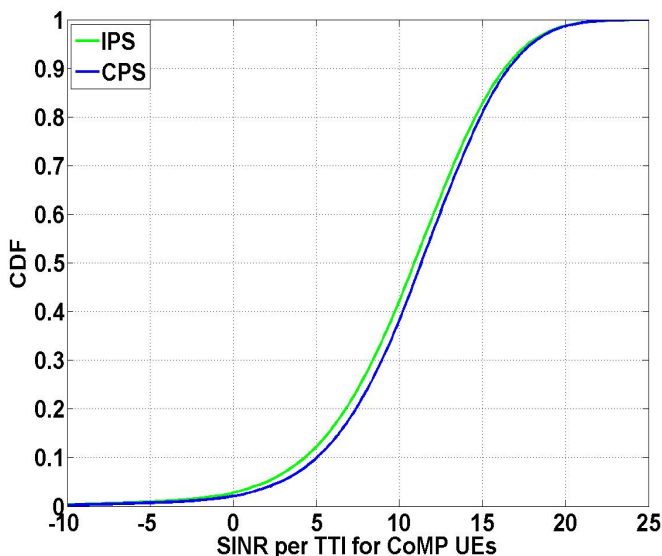Figure 6.3: SINR per TTI for Intra-Site CoMP UEs - IPS vs. CPS

In Figure 6.3, the SINR of CoMP UEs per TTI distribution is shown. Compared with IPS, the applied CPS algorithm improves the received SINR of CoMP UE for every TTI, but the improvement is quite marginal.

The throughput gain plot over the baseline, no-CoMP, case are shown in Figure 6.6. The case of IPS with MMSE-SIC receiver under the Intra-Site scenario
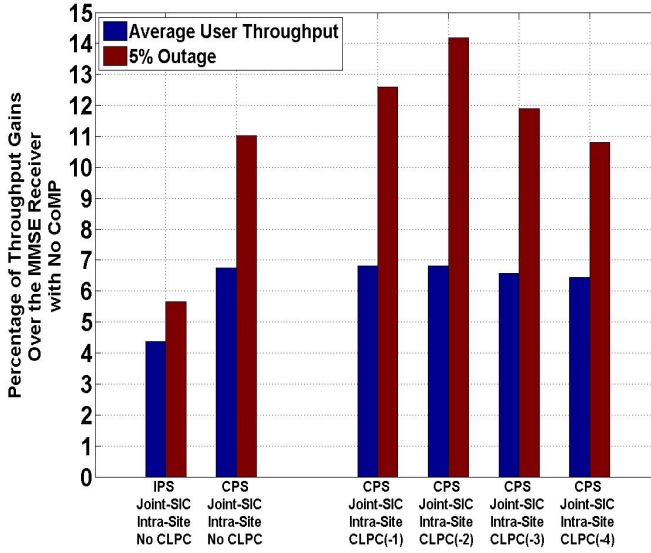
Figure 6.4: Throughput Gain Plot of Multi-Cell CPS with CLPC for Joint SIC reception under the Intra-Site scenario with $\alpha = 0.6$ and $P_0 = -58$ dBm

is shown as a reference, which is presented in Figure 5.12. Compared with IPS, both 5% outage and average user throughput are further improved when the multi-cell CPS are utilized. There are about 11% and 7% gain over the baseline case in terms of 5% outage and average user throughput respectively. By applying the close-loop FPC to power down the transmit power of CoMP UEs as described in Section 4.5, the 5% outage user throughput can be further optimized, and the negative effect of powering down CoMP UEs is compensated by the CoMP joint reception gain. In Figure 6.4, the combination performance of multi-cell CPS together with the close-loop FPC is shown. For the best case of powering down 2 dB, there are about another 3% gain for the cell-edge user throughput compared with the no CLPC case.

The CPS algorithm shown in Figure 6.2 only considers the pairing of the first two highest priority UEs $\psi_{b(\text{1st}),p,t}^{\text{PF,1st}}$ and $\psi_{b(\text{2nd}),p,t}^{\text{PF,2nd}}$. In Figure 6.5, another CPS algorithm is presented which also considers the pairing of the lowest priority UE $\psi_{b(\text{3rd}),p,t}^{\text{PF,3rd}}$. The throughput gain comparison of the two CPS algorithms over the baseline, no-CoMP, case are shown in Figure 6.6.

Compared with the first CPS algorithm, the second CPS algorithm shows the reduction of cell-edge user throughput from 11% to about 9%. This is because

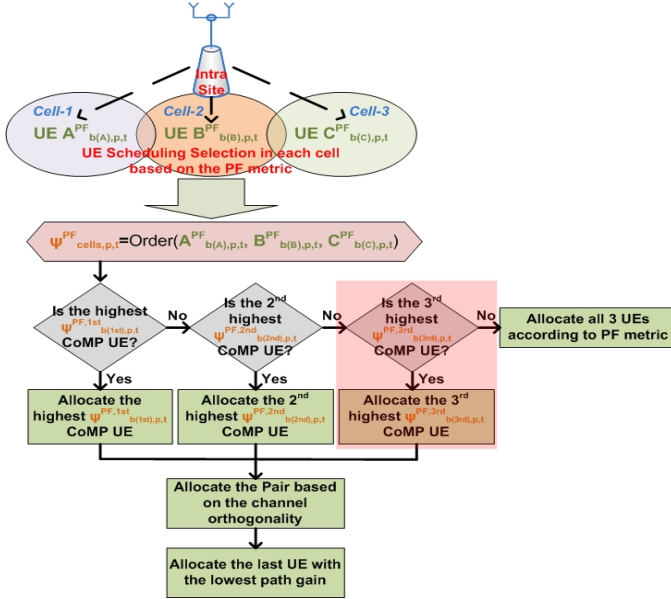Figure 6.5: Flow Chart of CPS: Pairing the lowest priority UE $\psi_{b(\text{3rd}),p,t}^{\text{PF},\text{3rd}}$
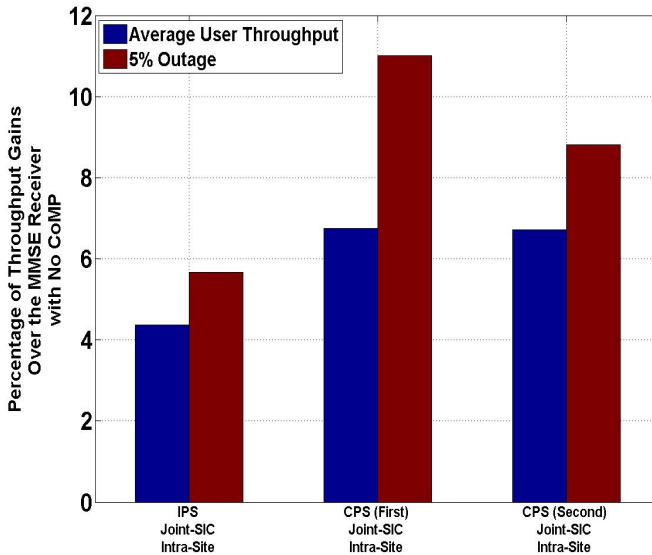

Figure 6.6: Throughput Gain Plot of Multi-Cell CPS vs IPS for Joint SIC reception under the Intra-Site scenario with $\alpha = 0.6$ and $P_0 = -58$ dBm

the second CPS algorithm gives too high priority to the CoMP UEs which results in the non-CoMP cell-edge UEs are less often scheduled. In the CoMP Intra-Site scenario, most of the non-CoMP cell-edge UEs locate at bore-sight cell-border region. In order to maintain the performance of those cell-edge users, they need to be allocated more often by the CPS scheduler. Low prioritization of them in the CPS domain will influence the overall 5% outage user throughput.

6.5 Conclusions

In this chapter, the multi-cell CoMP CPS has been studied. The CoMP Intra-Site scenario with MMSE-SIC joint reception is the main focus. The corresponding MMSE-SIC joint reception with IPS investigated in Chapter 5 is utilized as a reference.
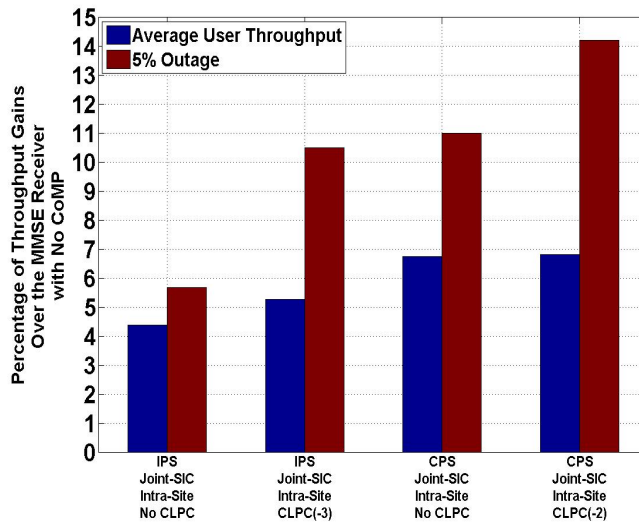
Figure 6.7: Multi-Cell CPS vs IPS for Joint SIC reception under the Intra-Site scenario with $\alpha = 0.6$ and $P_0 = -58$ dBm

As a sum-up, the comparison of multi-cell CPS with IPS is shown in Figure 6.7. The CPS can provide better throughput gain than the optimal IPS case even without the application of CLPC. The jointly applying the close-loop FPC with CPS can make further optimization in the CoMP Intra-Site scenario. For the best case of powering down 2 dB, there are about 14% and 7% gain over the

baseline, no CoMP, case in terms of 5% outage and average user throughput respectively.

The exploited CPS algorithm in this study has been investigated with the coordination of 3 neighboring Intra-Site cells. There are mainly two roles for the investigated CPS algorithm, which are pairing and scheduling. The pairing algorithm makes sure that the most orthogonal CoMP pair are allocated together to fully explore the CoMP multiuser detection gain, and the scheduling algorithm guarantees the QoS and the lowest generated interference to the scheduled CoMP pair. As presented in this study, in order to maintain the overall performance especially the cell-edge user performance, the user pairing and scheduling algorithms need to be jointly considered.

CHAPTER 7

Main Conclusion and Future Work Recommendations

The main object of this PhD thesis has been to study the potential multi-cell Radio Resource Management (RRM) techniques for limiting the impact of inter-cell interference in the Uplink (UL) LTE and further optimize the overall LTE network performance. Unlike the asynchronous UL WCDMA network, where the intra-cell interference and the near-far effect issue are the main interest, the frequency domain orthogonality of synchronous UL LTE network ideally removes the intra-cell interference. The inter-cell interference becomes the major concern with the frequency reuse factor of 1.

The conducted investigations have focused on the traditional mechanical antenna downtilting and the Coordinated Multi-Point (CoMP) feature proposed in the LTE-A study item. The CoMP techniques in the form of both macro diversity reception and joint reception have been studied. Besides, the multi-cell Coordinated Packet Scheduling (CPS) has also been studied with the CoMP joint reception. The other RRM functionalities, such as Adaptive Modulation and Coding (AMC), Outer Loop Link Adaptation (OLLA) and Hybrid Automatic Repeat reQuest (HARQ) have been considered in the analysis of results due to the interaction with the focused techniques.

The system-level simulator described in Appendix B has been used as the main tool for generation of study results. The simulator has been developed as part of the PhD project together with other colleagues from both Aalborg University and Nokia Siemens Networks (NSN). Along with the system-level designing, the development of the simulator has required a significant time investment in terms of modeling, software designing, implementation and testing. Part of the PhD study was also spend on the development of dynamic system-level simulator

described in Appendix A.5 which followed a different approach than the one presented in the main report.

The thesis is mainly divided into three parts where the first part addressed the topic of mechanical antenna downtilting and the interaction with the UL Fractional Power Control (FPC). The second part studied the CoMP technique in the form of macro diversity reception. Finally, the third part presented the UL CoMP joint reception and the coordinated packet scheduler design. In the following sections, a summary of the whole thesis is presented, and the main conclusions are drawn for the investigated topics. The recommendations for the future research are given at the end.

7.1   Antenna Tilting in Homogeneous UL LTE

In Chapter 3, the mechanical antenna downtilting has been investigated in the UL LTE. A simplified path loss model has been used to demonstrate the effect of antenna downtilting. The evaluations have been performed with the network-based mechanical antenna downtilting, where all the eNBs are mechanically downtilted with the same angle. The scenarios with different ISD have been investigated. Being an inter-cell interference mitigation technique, the mechanical downtilting performs efficiently under the interference-limited scenario. The optimal antenna downtilting angle for the interference-limited scenario with $ISD = 500$ m is 14°. A simple antenna downtilting method has been proposed by pointing the first notch of vertical antenna pattern to the boresight cell-edge area, and the cell-edge user throughput can be optimized in the UL LTE. Compared with the no downtilting case of 0°, there are about 296% gains in terms of cell coverage and about 147% increases in terms of cell capacity for downtilting angle of 14°. The application of antenna downtilting is less effective in the noise-limited scenario with $ISD = 1732$ m. The optimal antenna downtilting angle is about 2°. There is about 13% gains in terms of cell coverage and 4% increases in terms of cell capacity respctively compared with the no downtilting case of 0°.

The UL power control is an important technique to achieve the good UL LTE performance. The interaction of antenna downtilting together with UL open-loop FPC has also been analyzed in the interference-limited scenario. The study results have shown that the impact of mechanical antenna tilting to the chosen of open-loop FPC parameters can be neglected.

Furthermore, the antenna tilting is very sensitive to the narrow vertical antenna beamwidth. With narrow beam, both cell-edge user performance and average

user throughput are decreased dramatically after the optimal downtilting angle. By utilizing wider vertical antenna pattern, the overall network performance can be maintained over a certain downtilting angle range. Practically, it can also tolerate some extent of downtilting bias by installation or tuning defects. In 3GPP application, the vertical antenna pattern with HPBW equal to 10° is standardized.

7.2 UL CoMP in the Form of Macro Diversity Reception

CoMP is an advanced technique for interference mitigation which has been proposed in the LTE-A as one of the features to further reduce the impact of inter-cell interference. The UL CoMP involves the techniques such as CoMP reception and CPS. The CoMP reception implies the reception of UE transmitted signal at multiple geographically separated eNB antennas. In Chapter 4, CoMP reception in the form of macro diversity reception has been studied.

The study has been carried out in both Intra-Site and Inter-Site CoMP scenarios. The study results have shown that the CoMP macro diversity reception performs better in the Inter-Site scenario. The performance in the Intra-Site scenario is limited by the number of macro diversity UEs. In the Inter-Site scenario, both MRC and SC schemes have been studied, and as expected the MRC scheme performs better than the SC scheme.

It was also shown in the study that with standing alone macro diversity reception scheme, the overall improvement is very marginal. There is only about 2% average user throughput gain and 8% of 5% outage gain. By applying the CLPC scheme alone without the support of ideal IC in the coordination cell, the enhancement is very limited as well with only about 4% and 8% gain in terms of 5% outage and average user throughput respectively. By ideally canceling the strongest interference in the macro diversity link, the performance of both 5% outage and average user throughput can be largely enhanced by 14% and 8% gain, and by applying the CLPC scheme on the top of IC-based MRC reception, the 5% outage gain number can be nearly doubled together with another 4% gain in terms of average user throughput. So the combination of macro diversity reception together with IC and CLPC scheme is necessary in order to maximize the overall network enhancement.

Besides, the interaction of antenna downtilting angle together with macro diversity reception has shown the optimal performance for both outage and average user throughput at 14° downtilting. The study with non-ideal cell selection

scenario also demonstrated that, in the practical application, macro diversity reception can provide even higher gain than the simulated ideal cell selection assumption.

7.3   UL CoMP Joint Reception and Coordinated Packet Scheduling

In Chapter 5 and Chapter 6, the UL CoMP reception has also been investigated with joint reception processing, where the previous studied UL CoMP macro diversity reception is used as a reference.

For the Inter-Site CoMP scenario, the requirement of network backhaul is a key issue for the application of CoMP reception scheme. In this study the LTE network backhaul requirements for both CoMP reception schemes are first analyzed. Compared with the CoMP macro diversity reception, the backhaul requirement for the CoMP joint reception is about 10 times higher. Practically depends on the number of quantization bits and transmission overhead utilized, the backhaul requirement could be much higher for CoMP joint reception.

The study carried out in Chapter 5 is based on the realistic MMSE/MMSE-SIC receiver, where the multi-cell CPS is not exploited. The investigations are also evaluated in both Intra-Site and Inter-Site CoMP scenarios, and the Inter-Site scenario is further divided into Case-1 and Case-3 for detailed analysis. By considering the performance gain and capacity requirement of LTE X2-interface, the CoMP joint reception is a favorable choice for the Intra-Site application. It can provide better overall performance than the CoMP macro diversity reception without the need of large capacity X2-interface coordination. In general, there is about 10% cell-edge througput gain and 6% average user throughput gain compared with the no CoMP case. The CoMP macro diversity reception with MMSE-SIC receiver is a better candidate for the cross-site, Case-3, type of application. It can give the sub-optimal performance gain close to the application of CoMP joint reception and demand relatively much lower capacity requirement of X2-interface.

In Chapter 6, a multi-cell CPS algorithm is proposed and investigated in the Intra-Site scenario with 3 coordination cells. The study is focused on the MMSE-SIC joint reception. The exploited CPS utilizes the multiuser diversity to allocate better joint reception pair together to fully explore the multiuser detection gain. Compared with the corresponding Intra-Site scenario with no CoMP, the applied CPS algorithm makes further improvement in both cell-edge and average user throughput. The optimal case shows that there are about 14% gain in

terms of 5% outage and 7% gain in terms of average user throughput over the baseline, no CoMP, case.

Furthermore, compared with the theoretical CoMP investigations shown in the earlier literature, the achievable CoMP gain in this study is generally lower than the theoretical limits because of limited number of coordination eNBs and selected macro diversity UEs. In the realistic network, the overall CoMP performance may even be reduced due to the practical issues such as channel estimation errors, synchronization and latency challenges.

7.4 Overall Conclusion and Future Work Recommendations

In this study, the topic of multi-cell UL CoMP is the main focus. The overall results have shown that the UL CoMP gain in the Macro-cell scenario with three cell coordination is about 20% to 25% gain in terms of cell-edge user performance. Compared with the very high gain number reported in the earlier theoretical CoMP studies, the more realistic UL CoMP investigation presented in this study does not show considerable gains in terms of both cell-edge and average user throughput. One main reason for the presented small CoMP gain is the limited number of CoMP UEs. With larger CoMP UE selection window size, more users will be selected as the CoMP UEs and higher CoMP gain is expected. Besides, the study is limited to the CoMP scenario with 3 cells. In some TTIs, the strong interference might come from the cells outside the 3-cell coordination area. So larger CoMP coordination area is also expected to give better performance. Currently the study work is ongoing with larger CoMP coordination area. In this study the LTE X2-interface was considered ideally with unlimited transmission bandwidth and zero delay. For the larger area of CoMP coordination, the backhaul issues should be included for more realistic investigation. The potential gain of UL CoMP in the heterogeneous networks is another interesting topic which is ongoing to be investigated in the next step work. From the future implementation point of view, Macro-cell with remote radio head (RRH) scenario is showing a potential interests with CoMP application.

Performance of Integrator Handover Algorithm

The LTE network aims at increasing network capacity, lowering latencies and reducing network complexity [126]. It focuses on services in the packet-switched domain to minimize transmission latency and increase robustness of communication. An important requirement for LTE is to provide support for IP-based traffic with end to end QoS. Voice traffic will be supported mainly as Voice over Internet Protocol (VoIP) enabling better integration with other multimedia services [126]. For VoIP transmission to be intelligible to the receiver, voice packets should not be dropped, excessively delayed, or suffer varying delay/jitter. For mobile-to-mobile communication, the maximum tolerable one way (end-to-end) delay is 200 ms [127].

Handover/handoff (HO) is a critical procedure for QoS since it contains a so-called HO detach time, which is a gap in the data transmission. Typical values are in the range of 20 ms [126]. For the VoIP services, it is required to have a fast HO decision algorithm to avoid further delays and the risk of a call drop.

In this chapter, a HO decision algorithm is proposed for the LTE system. It is evaluated in the Manhattan scenario and compared with the traditional PBGT algorithm. As main Key Performance Indicator (KPI), the number of HOs and SINR before and after the HO are used. In Section A.1, the state of art for the DL LTE HO is presented. In Section A.2, the LTE intra-frequency HO procedure is briefly discussed. In Section A.4, both PBGT and integrator algorithm are introduced. In Section A.5, the system evaluation parameters and setup are shown. And the simulation results and conclusions are presented in Section A.6 and Section A.7 respectively.

A.1 DL LTE Handover

Handover is part of the LTE mobility management, and it is an important functionality for QoS provisioning, especially for the delay sensitive services [126]. LTE network aims at providing seamless access to voice and multimedia services, which is achieved by supporting HO from one cell, i.e. serving cell, to another, i.e. target cell. As presented in Section 2.1, the LTE has the decentralized network architecture, which facilitates the use of so-called hard HO[1]. In LTE Rel'8, the hard HO has been standardized for the DL LTE application [43], where the break-before-make type of connection makes the issue of serving seamless access even more critical.

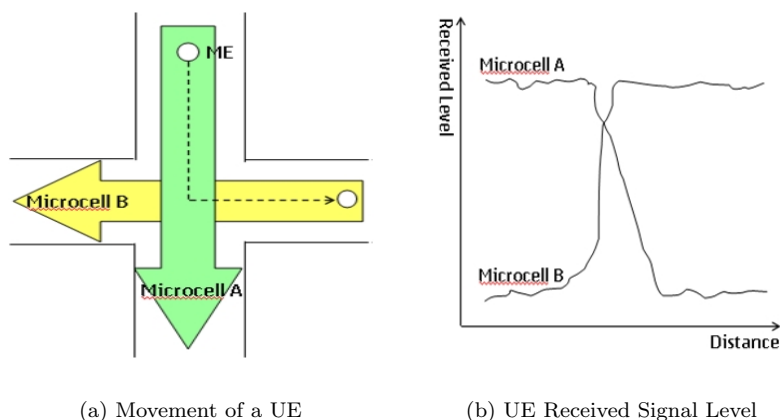(a) Movement of a UE　　　(b) UE Received Signal Level

Figure A.1: Corner effect or Manhattan scenario

One of the challenging environments for the hard HO is the corner turning effect in the Manhattan scenario as shown in Figure A.1. It happens due to the loss of the Line of Sight (LOS) component from the serving eNB to the UE, for example when a UE turns around a corner from one street to the other or a moving obstacle temporarily hinders the path between an eNB and a UE. The corner effect is very hard to predict, and it might cause a sudden large drop (e.g. 20-30 dB) in the UE signal strength.

In UMTS, the soft HO schemes can solve the corner effect quite efficiently compared with the hard HO schemes. Because the soft HO schemes are not

---

[1]A hard HO is defined as the link connection to the serving cell broken before the connection to the target cell, also known as break-before-make. On the contrary, a soft HO indicates that the link connection to the target cell is established before the serving link connection broken, also known as make-before-break.

supported in the LTE system, to deal with the corner effect, it requires fast hard HO decision algorithm. Otherwise the call or service quality will be decreased significantly, and a long gap may potentially lead to many lost packets or even a lost HO command which leads to a potential call drop. For the real time services, such as VoIP application, in order to keep the QoS criteria, it is quite important for the fast HO decision algorithm to be implemented to avoid the call or service drop. It is also desired that the fast hard HO decision algorithm can deal with all the environment scenarios, such as the moving obstacles temporarily hindering the path between an eNB and a UE which resembles the corner effect.

In general, the LTE HO can be divided into intra-LTE HO and inter-Radio Access Technology (RAT) HO, where the inter-RAT HO contains the applications such as the HO from LTE to the 2G networks or other 3G networks. In this study, the focus is on the DL hard HO for the intra-LTE application.

A.2 DL LTE Hard Handover Procedure

The hard intra-frequency HO in DL LTE is network-initiated, network-controlled and UE-assisted [128], where, as shown in Figure A.2, the hard HO procedure in DL LTE typically consists of three phases: Initialization, Preparation and Decision [126].

The initialization phase contains three main steps which are UE measurements, UE processing and UE reporting [19]. Firstly, the UE measures the DL RS from both serving cell and target cells. The processing of measurements is also performed in UE in order to filter out the effect of fast fading and measurement/estimation imperfections. At the end, the processed measurements are reported from the UE to the serving eNB in a periodic or event based manner. In the network side, the preparation phase contains two main steps which are the serving eNB HO decision and the serving eNB negotiation with target eNB. If the HO is granted by the serving eNB, the execution phase contains two main steps as well which are the serving eNB temporary forwarding packets to the target eNB and path switch in aGW [19].

A.3 Modeling of HO Measurement in DL LTE

The Reference Signal Received Power (RSRP) is standardized as the DL measurement in LTE. A single RSRP observation is defined as the mean measured power per RS observed over a single sub-frame or TTI, as shown in Figure
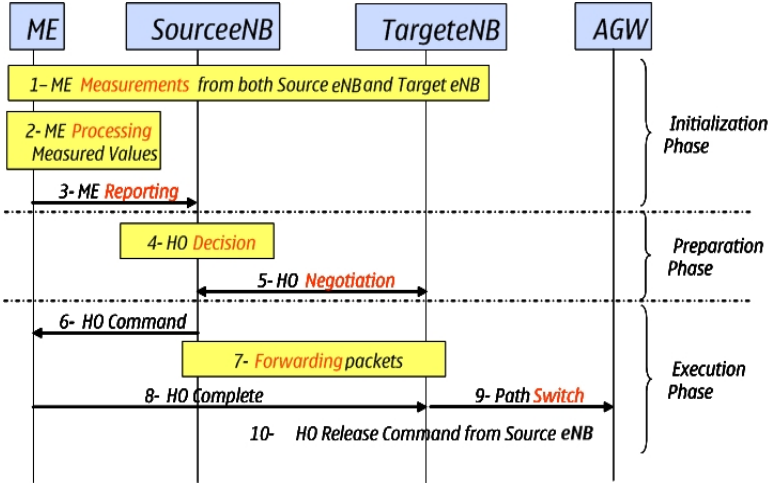
Figure A.2: Intra-LTE HO Procedure

A.3. One or several such observations may be combined to form an RSRP measurement report in accordance with the specified frequency and time domain filtering procedure [129].

As discussed in Chapter 2, the LTE utilizes the scalable bandwidth up to 20 MHz. The application of scalable bandwidth in LTE also allows to perform the HO measurement with different bandwidth. Depending on the RSRP measurement bandwidth, the frequency selective fading will have impact on the HO performance. With wide-band signal measurements, the impact is marginal because of the measurement averaging in the frequency domain [129]. However, for the narrow-band signal measurements, the multi-path fading can cause the signal power to drop rapidly, which seriously impacts the HO performance.

As shown in Figure A.3, there are a total of eight DL reference symbols per PRB at each antenna port. This limited number of RS for the HO RSRP measurements introduces the measurement errors according to different measurement bandwidth. In this study, the measurement error is modeled as uncorrelated and normally distributed in dB with zero mean and σ dB standard deviation as shown in Equation A.1 [55]:

$$\triangle Q \sim N(0, \sigma^2) \text{ [dB]} \tag{A.1}$$

where Q is the error measured in dB.
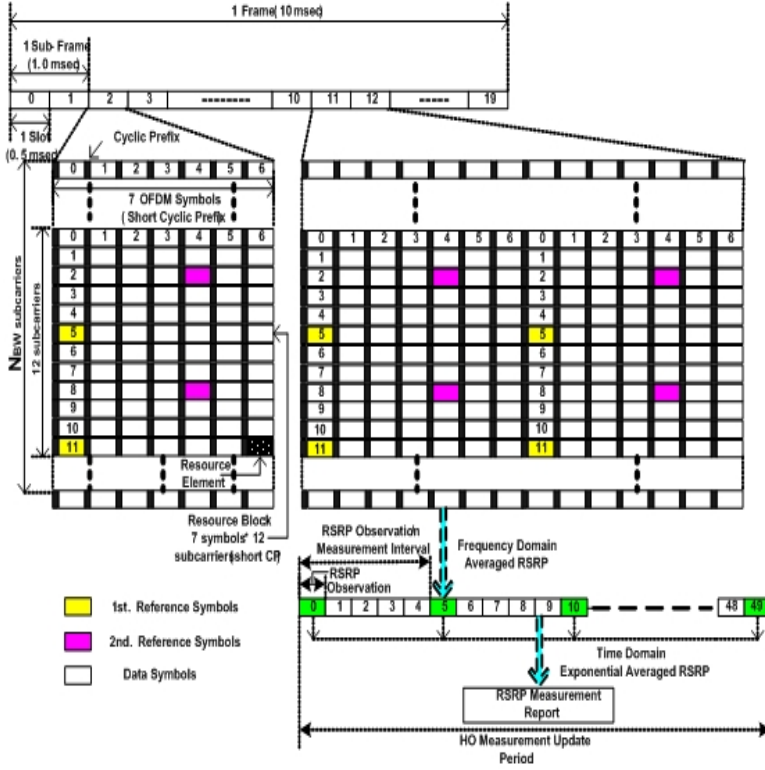
Figure A.3: RS Structure in DL LTE

As shown in Table A.1, more measurement errors are expected for the smaller RSRP measurement bandwidth which contains less number of RSs, i.e. with the measurement bandwidth of 1.25 MHz for 6 PRBs, the corresponding measurement error standard deviation σ is 0.8 dB.

Table A.1: Standard Deviation of Measurement Error [55]

Measurement Bandwidth [MHz]	Number of PRBs	σ [dB]
1.25	6	0.8
2.5	12	0.6
5	25	0.45
10	50	0.35

A.4 DL LTE Hard Handover Decision Algorithm

Two HO decision algorithms are evaluated in this study, the PBGT algorithm and the integrator algorithm.

A.4.1 Power Budget (PBGT) Algorithm

The PBGT algorithm uses both HO margin (HOM) and Time-to-Trigger (TTT) timer to make the HO decision, as shown in Figure A.4. A HO is triggered when the triggering condition, $RSRP_T > RSRP_S + HOM$, is fulfilled during TTT, where $RSRP_S/RSRP_T$ are the serving/target cell RSRP measurements.
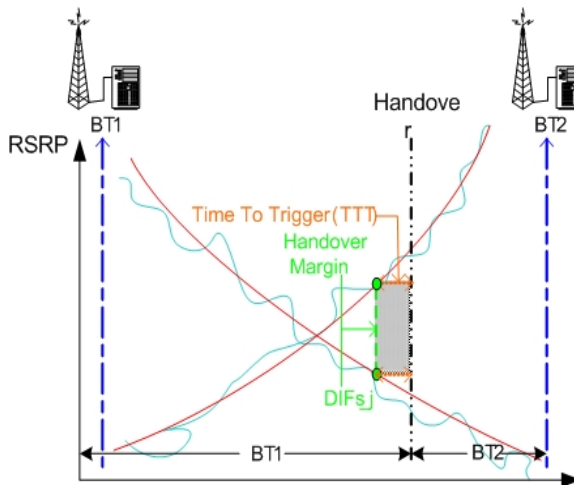
Figure A.4: HO Decision Algorithms

A.4.2 Integrator Algorithm

The integrator algorithm considers both a triggering threshold and a forgetting factor to make the HO decision. The general idea of integrator algorithm is to integrate the RSRP differences of the serving and target cell, as shown in the shaded area in Figure A.4, by using an Infinite Impulse Response (IIR) filter. The HO decision is made according to the triggering condition between the filtered RSRP differences and the triggering threshold.

In this study a special case of the first order auto regressive moving average (ARMA) filter is used and shown below:

$$
\begin{aligned}
FDIF_{s\_j}(t) &= (1-\alpha)FDIF_{s\_j}(t-1) + \alpha DIF_{s\_j}(t) & \text{(A.2)} \\
DIF_{s\_j}(t) &= RSRP_T(t) - RSRP_S(t) & \text{(A.3)}
\end{aligned}
$$

where $DIF_{s\_j}(t)$ is the difference of DL RSRP measurement between the received signal level of the serving cell 's' and the target cell 'j' at the time t. $FDIF_{s\_j}(t)$ and $FDIF_{s\_j}(t-1)$ are the filtered $DIF_{s\_j}(t)$ and $DIF_{s\_j}(t-1)$ value at the time t between the serving cell s and the neighboring cell j. α is known as the forgetting factor or smoothing constant ($0 \leq \alpha \leq 1$).

$FDIF_{Threshold}$ is the HO triggering threshold. If $FDIF_{s\_j}(t) > FDIF_{Threshold}$, then the HO is triggered immediately. The $FDIF_{s\_j}(t)$ value is influenced by the choice of the α value. If the choice of α value is equal to or close to 1, it would result in the $FDIF_{s\_j}(t)$ value more likely being reflected by the most recent $DIF_{s\_j}(t)$ value. The value of the $FDIF_{s\_j}(t)$ will be very instantaneous or responsive. Else, if the choice of α value is equal to or close to 0, it would result in the $FDIF_{s\_j}(t)$ value more likely being reflected by the averaged past $FDIF_{s\_j}(t)$ value. The value of the $FDIF_{s\_j}(t)$ would be very constant or unresponsive to the actual $DIF_{s\_j}(t)$ change.

The initial value of $FDIF_{s\_j}(t-1)$ can be defined either by averaging several early periods of $DIF_{s\_j}(t)$ values or simply the first observed value of $DIF_{s\_j}(t)$. In this study, the defined initial value is set at zero.

A.5   Simulation Assumptions

A dynamic system-level simulator for the DL LTE application is used to evaluate the proposed integration algorithm [130]. The Manhattan scenario with micro cells is used as the network model. In Figure A.5, the Manhattan scenario setup is shown. The Manhattan grid setup has 28 eNBs, which are located below the roof top, with the block size of 200 m and street width size of 30 m. The eNB antennas are omi-directional. The statistics are only collected from the central cells.

In Table 1, the detailed simulation parameters and their values are shown. The active UEs are uniformly distributed over the network area, and the UEs are allowed to move forward, backwards and turning corners (no wrap-around) with
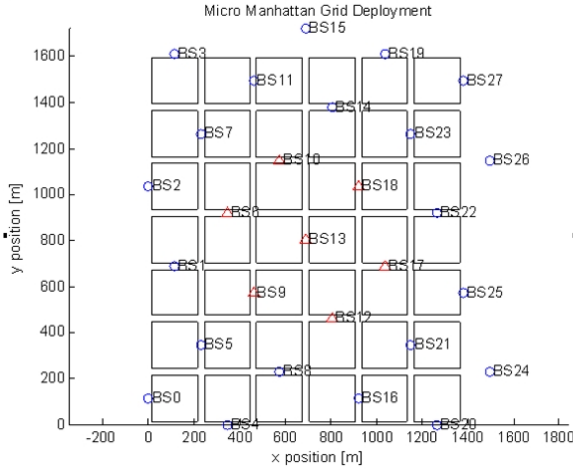
Figure A.5: Micro Scenario Setup

a constant speed during the whole simulation time. When the UEs reach the simulation border, they will simply turn around and move in the reverse direction.

As the traffic model, a standard VoIP model is used with 30 byte of packet size and 6 byte of full header size. The RR packet scheduler is assumed during the simulations. Path loss, shadow fading, and frequency selective fast fading have been included in the simulation. The shadow fading is modeled as log-normal distributed with a mean value of 0 dB and a standard deviation of 6 dB. The spatial de-correlation distance parameter used to describe the spatial correlation function of the shadow fading is set at 50 m. The frequency selective fast fading is modeled by using the 3GPP standard Pedestrian (3 kmph) or Vehicular-A model (30 kmph/120 kmph) depending on the UE moving speed.

For the RSRP measurements, the RSs are not explicitly modeled. The RS values in one TTI are assumed to be highly correlated in both time and frequency directions and are represented by one path loss plus fading value per PRB. According to the 3GPP definition, the RSRP observations are only made for the given N central PRBs, which are then averaged in frequency domain. The 3GPP defined minimum measurement bandwidth is 1.25 MHz. During the simulation, the measurement bandwidth is chosen to be 1.25 MHz and the corresponding central number of PRBs to be measured is 6. The 6 PRB values are measured independently and linear averaged afterwards. The UE sampling of the RSRP measurement is set to be 5 ms. An RSRP value is reported to the serving eNB every 500 ms. One report contains the exponential average in time of 100 RSRP

Table A.2: Micro-Scenario Simulation Parameters in DL LTE

Parameter	Assumptions
Network Layout	Micro Cells, Manhattan Grid
	(Block Size-200 m,Street Size-30 m)
Number of eNBs	28
Number of UEs	1400
Average number of UEs per cell	50
Inter-eNB Distance	200 m
eNB Height	10 m (below roof top level)
UE Location	Outdoors
eNB Antenna	Omi-directional with linear gain=1
UE Move Speed	3 kmph, 30 kmph, 120 kmph)
Duration of simulation	90 sec.
System Bandwidth	5 MHz
RSRP Measurement Bandwidth	1.25 MHz or 6 PRBs
RSRP Measurement Period	5 ms
Measurement Error σ	0.8
Sliding Window Size	500 ms

samples. The exponential smoothing filter uses a forgetting factor of 0.1.

In order to evaluate the performance of the proposed HO algorithms, two KPIs: Number of HOs and SINR have been used during the investigation of the proposed algorithms.

- The Number of HOs show what the average number of HOs per UE is by using of the proposed HO algorithms. Every HO comes with a risk of an HO failure. In general, by lowering the number of HOs, the HO burden to the network can be reduced and the potential degradation in QoS due to the detach time gap introduced by the HOs can be minimized as well. However, the number of HOs cannot be infinitely minimized. There is always a tradeoff between the number of HOs and the signal quality parameter.

- The signal quality is evaluated by the scheduled SINR per UE. During the evaluation the SINR is divided into SINR before HO and SINR after HO. The SINR before HO tells the signal quality level before making the HO and the SINR after HO tells us the signal quality level after making the HO. In our simulation the observation time for SINR before and after HO is 500 ms.

A.6 Performance Evaluation

In the simulations, the influences of forgetting factor α and $FDIF_{Threshold}$ to the proposed integrator algorithm are evaluated first, and followed by the performance comparison with the PBGT algorithm.

In order to evaluate the influence of α to the integrator algorithm, the value of $FDIF_{Threshold}$ is fixed to be -5. The forgetting factor varies between 0.25, 0.5, and 1.

According to the theory, when $\alpha=1$, it means that all the past FDIF values will be forgotten, and the HO only depends on the present instantaneous DIF value. The filtered or integrated instantaneous DIF value can also easily reach the $FDIF_{Threshold}$ to trigger the HO. So it is expected that there is a larger number of HOs for $\alpha=1$ than lower values of α.

As shown in Figure A.6, the case of $\alpha=1$ has the highest number of HOs, and the number of HOs are decreasing when α is getting smaller. In Figure A.7, all the SINR after HO are improved compared to the SINR before HO for all the varying α cases. Before making the HO, $\alpha=1$ has the best SINR since it can make the HO without any delay in the serving eNB with declining RSRP measurement, and there is about 5 dB difference at cdf probability 70% to compare with $\alpha=0.25$. After the HO, it shows that $\alpha=1$ has the lowest SINR.

To evaluate the influence of $FDIF_{Threshold}$ to the integrator algorithm, the α value is fixed to be 0.5. The $FDIF_{Threshold}$ varies between -0.1 dB, -5 dB and -10 dB.

Theoretically higher values of the $FDIF_{Threshold}$ correspond to a larger Handover Margin (HOM) value in PBGT algorithm. So a lower number of HOs are expected with a higher value of $FDIF_{Threshold}$. As it can be seen in Figure A.8, $FDIF_{Threshold}=-0.1$ dB has the highest number of HOs and $FDIF_{Threshold}=-10$ dB has the lowest number of HOs.

As shown in Figure A.9, in general, all the SINR values after HO are improved compared to the SINR before HO for all cases. The best SINR before HO is achieved for $FDIF_{Threshold}$ equal to -0.1 dB. This is due to the fact that this setting leads to the fastest HO decision while the slowest HO decision ($FDIF_{Threshold}=-10$ dB) leads to the worst SINR before HO. With the same cdf probability at 70%, there is about 5 dB difference in SINR between them. However, after making the HO, there is a big improvement for $FDIF_{Threshold}=-10$ dB in SINR, and the improvement for $FDIF_{Threshold}=-0.1$ dB is quite small.
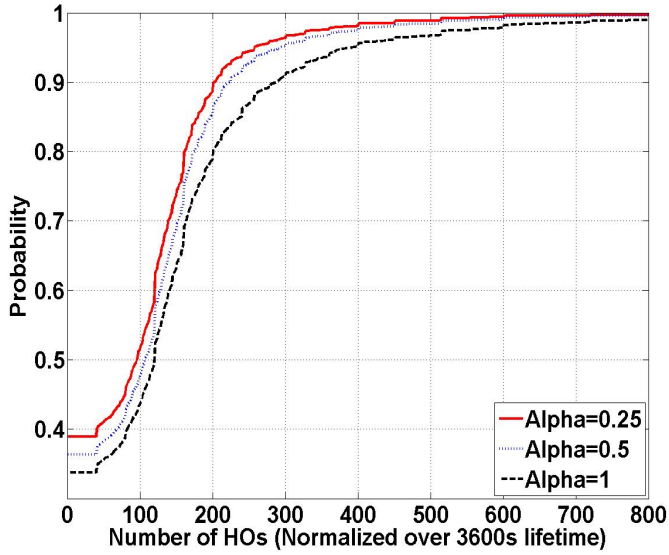
Figure A.6: Number of HOs: Varying α Values with $FDIF_{Threshold} = -5dB$
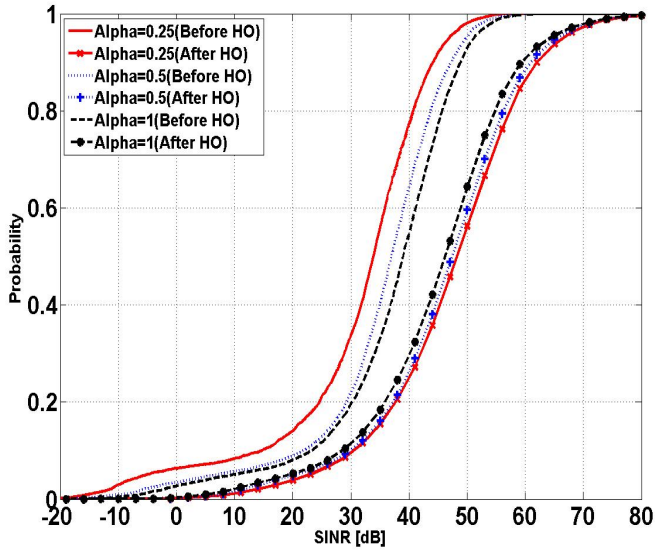

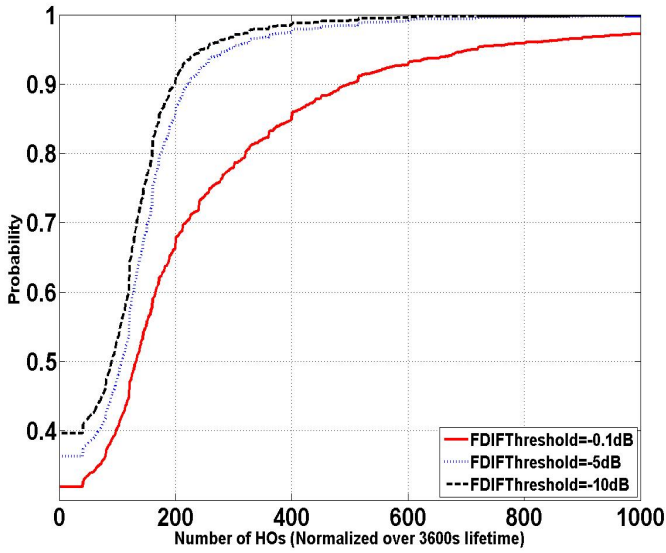Figure A.7: SINR: Varying α Values with $FDIF_{Threshold} = -5dB$

Figure A.8: Number of HOs: Varying $FDIF_{Threshold}$ with α=0.5
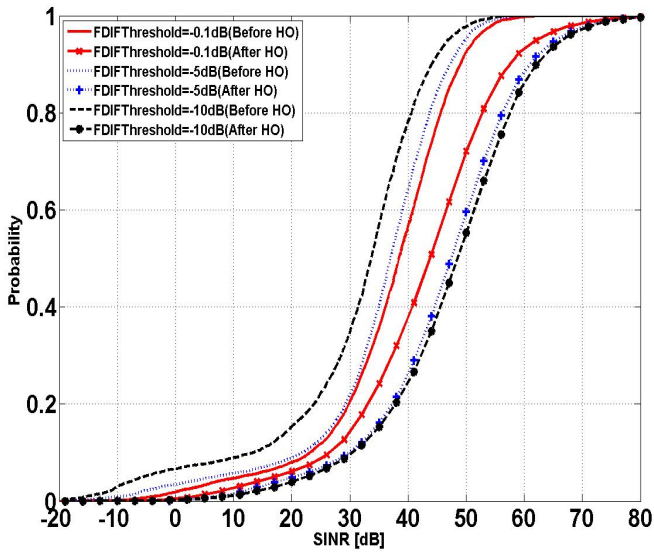

Figure A.9: SINR: Varying $FDIF_{Threshold}$ with α=0.5

Based on the above evaluations of the integrator algorithm, comparisons of the integrator algorithm with the traditional PBGT algorithm are made. The comparisons are performed in two steps.

In the first step, special parameters are used in both algorithms. For the integrator algorithm with $\alpha = 1$, the HO decision depends only on the $FDIF_{Threshold}$. For the PBGT algorithm with TTT=0 ms, the HO triggering relies only on the HOM. We set the value of $FDIF_{Threshold}$ equal to the HOM. It is expected that both algorithms are identical since HOM=$FDIF_{Threshold}$=$RSRP_s(t)$ - $RSRP_T(t)$. As shown in Figure A.10 and A.11 the two algorithms are performed identically.

In the second step, more realistic parameters are chosen based on the first step evaluation. HOM=5 dB and TTT=500 ms are used in the PBGT version algorithm, and $FDIF_{Threshold}$=-5db and Forgetting Factor=0.5 are used in the integrator algorithm for comparison at the speed 3 kmph, 30 kmph and 120 kmph.

As it can be seen in Figure A.10 and A.11, with this specific parameter setup, the integrator and PBGT algorithms have also the same performances in both Numbers of HOs and SINR before and after HO evaluations at different UE speeds, and as expected the higher speed has a higher number of HOs.

A.7   Conclusions

In this paper, the integrator handover decision algorithm is proposed and studied. The general idea of this algorithm is to integrate the RSRP differences of the serving and target cell.

Two parameters, FDIF threshold and Forgetting Factor α, have been studied respectively, which can be used to tune the integrator algorithm. The performances of integrator algorithm are also evaluated and compared with the traditional PBGT algorithm in the LTE network.

The simulation results show that the integrator algorithm has the same performance as the PBGT algorithm based on the Number of HO analysis and SINR before and SINR after HO evaluations at different UE speeds.
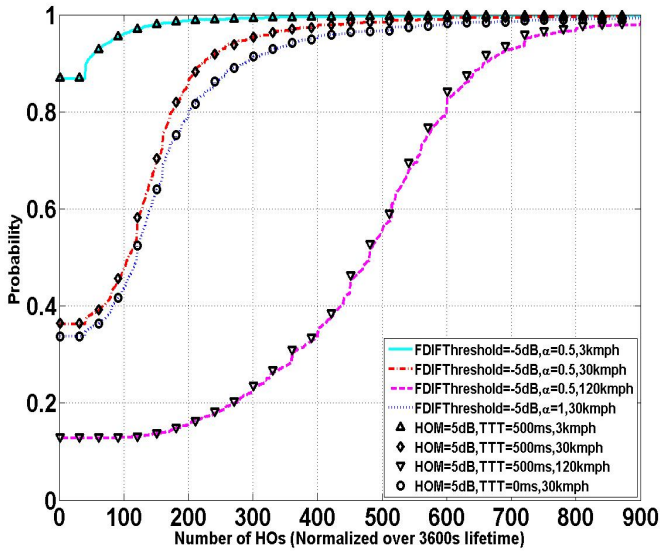
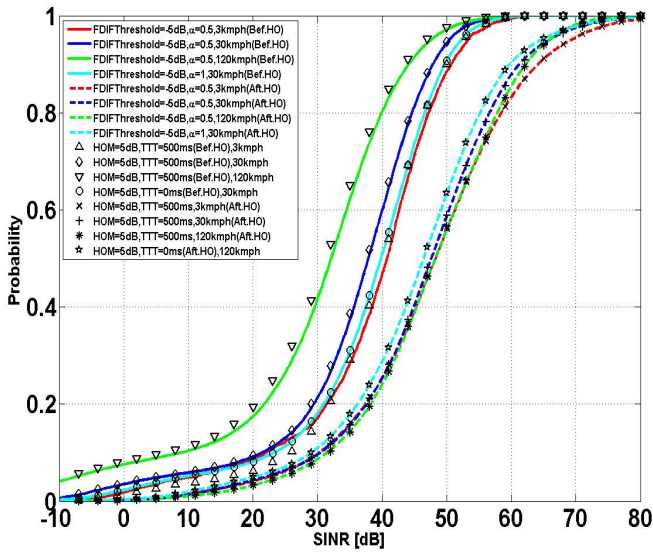Figure A.10: Number of HOs - Comparison

Figure A.11: SINR - Comparison

System-Level Simulator Description

A semi-static system-level simulator has been used in this study for the performance assessment of the designed algorithms presented in Chapter 3, 4, 5, and 6. In Section B.1, the models used in the system-level simulator are described. In Section B.2, the mostly used KPIs are defined. And the default simulation assumptions and parameters are listed in Section B.3.

B.1   System-Level Simulator

The performance evaluation is made by using a multi-cell system-level simulator, which contains 19 BSs with 3 sectors per BS (in total 57 cells) as shown in Figure B.1. A hexagonal shape per sector has been simulated. The orientation of antenna main lobe is indicated by the red-dashed line in Figure B.1. The 3-D antenna pattern with 70° horizontal HPBW and 10° vertical HPBW is exploited. Wrap-around is applied to eliminate the network edge effect and generate accurate simulation results.

The deployment scenario is defined according to [78], where Macro case-1 scenario is characterized by small cell radius with ISD of 500 m, and Macro case-3 scenario is indicated by a large cell radius with ISD of 1732 m. BS antenna is located at the roof top with the height of 32 m above ground.

The propagation modeling consists of path-loss, shadowing and fast fading. A 20 dB outdoor-to-indoor penetration loss is included in the path-loss model for
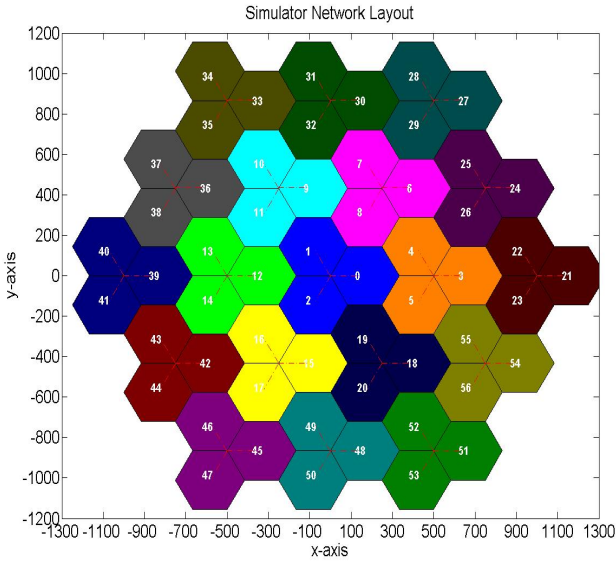
Figure B.1: System Level Simulator Network Layout

the Macro cell scenario [131]. Shadowing is fully correlated between cells of the same site, while the correlation is 0.5 between different site cells. The fast fading can be simulated with either Typical Urban (TU) power delay profile for UE speed of 3 kmph or SCMC channel model. The TU model is a tapped delay line implementation with uncorrelated Rayleigh fading path [132]. The SCMC channel model is a tapped delay-line model for multiple antennas with correlation parameters derived from fixed angular parameters and assumed antenna configurations. It can be used for simulating full MIMO channels of size up to 4x4 [133].

The UE creation or arrival process depends on the traffic model deployed. For the full/infinite buffer traffic model, the UEs are dropped in the system at the start of a simulation run and remain in the network until the end of the run. One simulation consists of several simulation runs. For the finite buffer traffic model, the UEs are generated at the beginning of the simulation. Once the UE buffer is emptied, the UE is killed and replaced by a new UE at different network location. The finite buffer traffic model can also be combined with AC, where the UEs are generated in the network according to a Poisson arrival process. If a certain AC decision criteria is fulfilled, the UE is admitted, otherwise the UE is rejected or blocked.

For the best effort services with variable bit rate, the full buffer UEs experience

different channel conditions, which result in different data rates by transmitting a different amount of data in the same simulation time, whereas the finite buffer UEs will transmit the same amount of data and the session time is terminated once the buffer is emptied. In this case, the cell-edge UEs will stay longer in the network due to low data rate compared to the cell-center UEs.

The distribution of the UEs depends on whether the load is balanced or unbalanced. The network is called balanced-load if the UEs are uniformly generated in each cell and also each cell contains the same number of UE. Else if the UEs are uniformly distributed in the whole network region with different number of UEs in each cell, then it is called unbalanced-load network.

For each UE, the fast fading component is time varying at every TTI, while the PL and shadowing components are assumed to be constant during a packet call. The serving cell is selected according to the lowest total path-loss including distance dependent path-loss, shadowing, and effective antenna gains.

The RRM functionalities such as LA, PS and HARQ are also accurately modeled in the simulator for each cell. As presented in Section 2.4, the LA is modeled as the fast AMC based on the CSI measurement. In order to maintain the BLER target of the first transmission, the OLLA offset is used to bias the CSI before using it for MCS selection. The dynamic PS is modeled as decoupled TD and FD scheduler as presented in Section 2.6. With the transmission bandwidth of 10 MHz in LTE, there are in total 50 PRBs where 48 PRBs are used for data transmission and 2 PRBs are utilized for control signaling transmission. Fixed transmission bandwidth with 6 PRBs is the main focus in this study. Therefore in each TTI, 8 UEs will be scheduled in the frequency domain in each cell according to the applied scheduling algorithm. The system model also includes synchronous adaptive HARQ with ideal chase combining as presented in Section 2.3. The UL Power Control (PC) is implemented according to the standardized formula presented in Equation 2.5, where both OLPC and CLPC components are considered.

The single simulator approach, which includes everything from single-cell link-level processing to multi-cell network management, is too high for the required simulation resolution [7]. Therefore, separated link-level and system-level simulators are desired. The link-to-system performance mapping function is used to connect the separated link and system level simulations. At system-level simulation, the mapping function can be used to predict the instantaneous BLER without performing detailed link-level processing steps. The mapping function is estimated from the link-level simulations, which considers the facts such as the MCS format, receiver type and channel state. The generated mapping function should be general enough to cover different transceiver types and antenna techniques. In this study, the Actual Value Interface (AVI) method is used for the

link-to-system mapping [134]. The AVI tables constructed from an extensive link-level simulations are used to map the average received SINR to the corresponding BLEP. Besides, the compressed SINR to symbol variance mapping presented in Section 5.3.2 is used for the multiuser detection with MMSE-SIC receiver.

B.2   Key Performance Indicator - KPI

For the study in the system-level, the KPIs used to evaluate the performance are as follows:

1. The average cell throughput $\overline{\text{TP}}_{cell}$ is defined as the ratio between the total correctly decoded bits per cell and the total simulation time

$$\overline{\text{TP}}_{cell} = \frac{\text{Total correctly received bits per cell}}{\text{Simulation Time}} \qquad \text{(B.1)}$$

2. The corresponding spectral efficiency is given by the ratio of total cell throughput divided by the bandwidth occupied:

$$\text{Spectral Efficiency} = \frac{\overline{\text{TP}}_{cell}}{\text{Bandwidth}} \qquad \text{(B.2)}$$

3. The average user throughput for the ith active user is defined as:

$$\text{TP}_{i} = \frac{\text{Correctly received bits from user } i}{\text{Session Time}} \qquad \text{(B.3)}$$

Coverage, denoted by $\text{TP}_{\text{coverage}}$, is determined from the CDF curve of the average user throughput taken over all the completed sessions. Coverage is defined as the data rate corresponding to the 5% quantile in the CDF curve, i.e., 95% of the users experience a higher average data rate than the rate specified by the coverage parameter. This KPI indicates data rate experienced by users around the cell edge. Further, it can be used to differentiate packet scheduler in terms of fairness in the distribution of throughput among users.

B.3   Simulation Assumptions

The default simulation assumptions and parameters are listed in Table B.1:

Table B.1: Simulation Assumptions of Mechanical Antenna Downtilting

Parameter	Assumptions
Simulation Time	5 runs, 5 s/run, 2 s/run (WarmUp)
System Carrier Frequency	2 GHz
System Bandwidth	10 MHz (50 PRBs)
Number of PRBs for Data/Control	48 PRBs / 2 PRBs
Frequency Reuse Factor	1
Number of sub-carriers per PRB	12
TTI	1 ms
PRBs per UE per TTI	6 PRBs
Deployment Scenario	Macro Case-1: ISD=500 m
	Macro Case-3: ISD=1732 m
Minimum UE to BS Distance	35 m
BS / UE Height	32 m / 1.5 m
Number of UE/BS Antennas	1-UE Tx / 2-BS Rx Antenna
Receiver Type	MRC/MMSE/SIC
BS Antenna HPBW	Horizontal: 70°
	Vertical: 10°
BS Antenna Gain	14 dBi
UE Antenna Gain	0 dBi
Max UE Transmit Power	24 dBm (250 mW)
FPC P_0 and α value	Macro case-1: -58 dBm and 0.6
	Macro case-1: -106 dBm and 1.0
Distance dependent Path-Loss	$128.1 + 37.6log_{10}(d[km])$
Log-normal Shadowing	Standard deviation: 8 dB
	Correlation distance: 50 m
	Correlation bet. cells/sites: 1.0/0.5
CSI Log-normal Err. Std. Dev.	1 dB
CSI Resolution	2
OLLA Offset	0.5 dB
OLLA Offset Range	[-4.0,4.0] dB
Control channel overhead	3/14 symbols

Bibliography

[1] Editors Desk, "Mobile web: Latest facts and stats forecast a rosy outlook," http://mobithinking.com/blog/latest-mobile-stats.htm, August 2009.

[2] "2008 global broadband phenomena - executive summary," Sandvine, October 2008.

[3] Hans Beijner, "Ran evolution: An introduction to evo ran," Ericsson, September 2009.

[4] 3G Americas, "The mobile broadband future - hspa+ and lte: An educational feature brought to you by 3g americas and wireless week," 3G Americas Wireless Communications, 2008.

[5] Chandra D and Harris R. J. and Shenoy N., "Tcp performance for future ip-based wireless networks," 3rd. IASTED International Conference on Wireless and Optical Communication (WOC2003), Banff Canada, July, 2003.

[6] M. Døttling, W. Mohr, and A. Osseiran, Radio Technologies and Concepts for IMT-Advanced. John Wiley & Sons Ltd, 2009.

[7] H. Holma and A. Toskala, WCDMA for UMTS: Radio Access for Third Generation Mobile Communication, 3rd edition. John Wiley & Sons Ltd, 2004.

[8] ——, HSDPA/HSUPA for UMTS: High Speed Radio Access for Mobile Communication. John Wiley & Sons Ltd, 2006.

[9] QUALCOMM, "Hspa+ rel-8 and rel-9," http://russia.qualcomm.com/common/documents/articles/HSPAplus_R8andR9_Benefits_081109.pdf, September 2009.

[10] H. Holma and A. Toskala, <u>WCDMA for UMTS: HSPA Evolution and LTE</u>. John Wiley & Sons Ltd, 2007.

[11] Ericsson, "Evo ran: 3 generation, 1 network," http://www.ericsson.com/ericsson/corpinfo/publications/review/technology_update/archive/2009/issue_2/articles/evoran.shtml, February 2009.

[12] 3GPP Technical Specifications 36.101, "Evolved universal terrestrial radio access (e-utra), user equipment (ue) radio transmission and reception (release 8), version 8.2.0," <u>3GPP</u>, 2008.

[13] 3GPP Technical Specifications 36.104, "Evolved universal terrestrial radio access (e-utra), base station (bs) radio transmission and reception (release 8), version 8.2.0," <u>3GPP</u>, 2008.

[14] 3GPP Technical Report 25.913, "Requirements for evolved utra (e-utra) and evolved utran (e-utran), version 7.3.0," <u>3GPP</u>, March 2006.

[15] H. Holma, A. Toskala, K. Pajukoski, and E. Tiirola, "Utran long term evolution in 3gpp," <u>in proceeding of the IEEE international symposium on personal, indoor and mobile radio communication (PIMRC), Helsinki, Finland</u>, 2006.

[16] E. Dahlman, S. Parkvall, J. Skold, and P. Beming, <u>3G Evolution: HSPA and LTE for Mobile Broadband</u>. Elsevier Science, 2008.

[17] H. Schulze and C. Lueders, <u>Theory and Applications of OFDMA and CDMA: Wideband Wireless Communication</u>. John Wiley & Sons Ltd, 2005.

[18] S. Sesia, I. Toufik, and M. Baker, <u>LTE, The UMTS Long Term Evolution: From Theory to Practice</u>. John Wiley & Sons Ltd, 2008.

[19] H. Holma and A. Toskala, <u>LTE for UMTS: OFDMA and SC-FDMA Based Radio Access</u>. John Wiley & Sons Ltd, 2007.

[20] H. G. Myung, J. Lim, and D. J. Goodman, "Single carrier fdma for uplink wireless transmission," <u>IEEE Vehicular Technology Magazine</u>, vol. 1, pp. 30–38, Sep.2008.

[21] D. Tse and P. Viswanath, <u>Fundamentals of Wireless Communication</u>, 1st ed. Cambridge University Press, 2005.

[22] E. Dahlman, H. Ekstrom, A. Furuskar, Y. Jading, J. Karlsson, M. Lundevall, and S. Parkvall, "The 3g long-term evolution - radio interface concepts and performance evaluation," <u>in proceeding of the IEEE vehicular technology conference (VTC), Melbourne, Australia</u>, vol. 1, May 2006.

[23] ITU-R, "Itu-r imt.[rest], requirements, evaluation criteria and submission templates for the development of imtadvanced," http://www.itu.int/md/R07-SG05-C-0068/en, 2007.

[24] S. Kumar, "Techniques for efficient spectrum usage for next generation mobile communication networks: An lte and lte-a case study," Ph.D. dissertation, Department of Electronic Systems, Aalborg University, 2009.

[25] 3GPP Technical Report 36.913, "Requirements for further advancements for e-utra (lte-advanced)," 3GPP, June 2008.

[26] P. E. Mogensen, T. Koivisto, K. I. Pedersen, I. Z. Kovács, B. Raaf, K. Pajukoski, and M. J. Rinne, "Lte-advanced: The path towards gigabit/s in wireless mobile communications," Wireless VITAE 2009, pp. liv–cxiv, May 2009.

[27] E. Seidel, "Progress on 'lte advanced - the new 4g standard," Nomor Research GmbH, July, 2008.

[28] S. Parkvall and D. Astely, "The evolution of lte towards imtadvanced," Journal of Communications, vol. 4, p. 3, April 2009.

[29] C. U. Castellanos, D. L. Villa, C. Rosa, K. I. Pedersen, F. D. Calabrese, P. H. Michaelsen, and J. Michel, "Performance of uplink fractional power control in utran lte," in Proceedings of the IEEE Vehicular Technology Conference (VTC) Singapore, pp. 2517–2521, May 2008.

[30] S. Hussain, "Dynamic radio resource management in 3gpp lte," Ph.D. dissertation, Department of Applied Signal Processing, Blekings Institute of Technology, January 2009.

[31] "Performance enhancement in a frequency hopping gsm network, howpublished=Kluwer Academic Publisher, year=2000."

[32] 3GPP Technical Report 25.814, "Physical layer aspect for evolved universal terrestrial radio access (utra)," 3GPP, September 2006.

[33] jarmo niemela, tero isotalo, and jukka lempiainen, "Optimum antenna downtilt angels for macrocellular wcdma networks," EURASIP Journal on Wireless Communications and Networking, issue 5, pp. 816-827, 2005.

[34] A. Wacker, K. Sipila, and A. Kuurne, "Automated and remotely optimization of antenna subsystem based on radio network performance," WPMC pp. 752-756, October 2002.

[35] F. L., H. C., and G. R., "Distributed uplink macro diversity for cooperating base stations," IEEE International Conference on ICC Workshops, June 2009.

[36] P. Marsch, S. Khattak, and G. Fettweis, "A framework for determining realistic capacity bounds for distributed antenna systems," in Proceedings of IEEE Information Theory Workshop, Chengdu, China, pp. 22-26, October 2006.

[37] S. Venkatesan, "coordinating base stations for greater uplink spectral efficiency in a cellular systems," In Proceeding of IEEE symposium, personal, indoor and mobile radio communication, September 2007.

[38] M. N. Bacha, J. S. Evans, and S. V. Hanly, "On the capacity of mimo cellular networks with macrodiversity," in Proceedings of the IEEE Australian Theory Workshop, 7th, 2006.

[39] H. Zhang and H. Dai, "Cochannel interference mitigation and cooperative processing in downlink multicell multiuser mimo networks," EURASIP Journal Wireless Communication and Networking, vol.2004, no.2, pp.222-235, December 2004.

[40] N.H.Dawod, I.D.Marsland, and R.H.M.Hafez, "Improved transmit null steering for mimo-ofdm downlinks with distributed base station antenna arrays," IEEE Journal Selected Areas Communication vol.24, no.3, pp.419-426, March 2006.

[41] M. Karakayali, G.J.Foschini, and R.A.Valenzuela, "Network coordination for spectrally efficient communications in cellular systems," IEEE Wireless Communication, vol.13, no.4, pp.56-61, August 2006.

[42] Redl, S. M., Weber, M. K., Oliphant, and M. W., An introduction to GSM. Artech House, Boston, 1995.

[43] 3GPP Technical Specifications 36.300, "Evolved universal terrestrial radio access (e-utra) and evolved universal terrestrial radio access network (e-utran), overall description, version 8.3.0," 3GPP, January 2008.

[44] Ericsson, "Ericsson review, no. 03," http://www.ericsson.com/ericsson/corpinfo/publications/review/2007_03/05.shtml, 2007.

[45] 3GPP Technical Specifications 36.420, "Evolved universal terrestrial radio access (e-utra): X2 general aspects and principals," 3GPP, 2008.

[46] 3GPP Technical Specifications 36.421, "Evolved universal terrestrial radio access (e-utra): X2 layer 1," 3GPP, 2008.

[47] 3GPP Technical Specifications 36.422, "Evolved universal terrestrial radio access (e-utra): X2 signaling transport," 3GPP, 2008.

[48] 3GPP Technical Specifications 36.423, "Evolved universal terrestrial radio access (e-utra): X2 application protocol (x2ap)," 3GPP, 2008.

[49] F. D. Calabrese, "Scheduling and link adaptation for uplink sc-fdma systems: An lte case study," Ph.D. dissertation, Department of Electronic Systems, Aalborg University, 2009.

[50] Frank Rayal, "The essential aspects of lte phy - part 2," http://www.eetindia.co.in/STATIC/PDF/201006/EEIOL_2010JUN29_RFD_TA_01.pdf?SOURCES=DOWNLOAD, 2010.

[51] C. Rosa, D. L. Villa, C. U. Castellanos, F. D. Calabrese, P. H. Michaelsen, K. I. Pedersen, and P. Skov, "Performance of fast amc in e-utran uplink," in Proceedings of the IEEE International Conference on Communications (ICC) Beijing China, pp. 4973–4977, May 2008.

[52] A. Pokhariyal, "Downlink frequency-domain adaptation and scheduling," Ph.D. dissertation, Department of Electronic Systems, Aalborg University, 2007.

[53] K. C. Beh, A. Doufexi, and S. Armour, "Performance evaluation of hybrid arq schemes of 3gpp lte ofdma system," in Proceedings of the 18th Annual IEEE International Symposium on Personal, Indoor and Mobile Radio Communications (PIMRC), 2007.

[54] B. Priyanto, H. Codina, S. Rene, T. Sorensen, and P. Mogensen, "Initial performance evaluation of dft-spread ofdm based sc-fdma for utra lte uplink," in Proceedings of the IEEE Vehicular Technology Conference (VTC) Dublin Irland, pp. 1550–2252, April 2007.

[55] M. Anas, "Uplink radio resource management for qos provisioning in long term evolution," Ph.D. dissertation, Department of Electronic Systems, Aalborg University, 2009.

[56] K. I. Pedersen, F. F., T. E. Kolding, L. T. F., and P. E. Mogensen, "Performance of high-speed downlink packet access in coexistence with dedicated channels," in Proceedings of the IEEE Vehicular Technology Conference (VTC), 2007.

[57] Klaus I. Pedersen and Akhilesh Pokhariyal, "Outter loop link adaptation for uprise lte dl version 1.4," NSN Internal Document, 2006.

[58] Claudio Rosa and Carlos Ubeda and Francesco Calabrese, "Lte uplink rrm: Concept document," NSN Internal Document, 2007.

[59] 3GPP Technical Specifications 36.213, "Evolved universal terrestrial radio access (e-utra): Physical layer procedure, version 8.2.0," 3GPP, 2008.

[60] M. Boussif, N. Quinteroand, F. D. Calabrese, C. Rosa, and J. Wigard, "Interference based power control performance in lte uplink," in Proceedings of the IEEE International Symposium on Wireless Communications Systems (ISWCS) Reykjavik Iceland, pp. 698–702, October 2008.

[61] D. Lee and C. Xu, "Mechanical antenna downtilt and its impact on system design," in Proceedings of the IEEE 47th Vehicular Technology Conference, 1997.

[62] "Technical information and new products - kathrein antennen electronic," Kathrein, September 2000.

[63] P. Zanier, "Automated wcdma antenna tilt optimization based on network measurements," Nokia Siemens Network - Internal Slides, Version 0.0.6, January, 2009.

[64] 3GPP, "Default enb antenna tilt values for lte-advanced evaluations," R1-084314, November 2008.

[65] U. Türke and M. Koonert, "Advanced site configuration techniques for automatic umts radio network design," in Proceedings of the IEEE Vehicular Technology Conference Spring, 2005.

[66] J. Niemela and J. Lempiainen, "Impact of mechanical antenna downtilt on performance of wcdma cellular network," in Proceedings of the IEEE Vehicular Technology Conference (VTC), Spring, 2004.

[67] U. Turke and M. Koonert, "Advanced site configuration techniques for automatic umts radio network design," in Proceedings of the IEEE Vehicular Technology Conference (VTC), Spring, 2005.

[68] F. Gunnarsson, M. N. Johansson, A. Furuskar, M. Lundevall, A. Simonsson, C. Tidestav, and M. Blomgren, "Downtilted base station antennas - a simulation model proposal and impact on hspa and lte performance," in Proceedings of the IEEE Vehicular Technology Conference (VTC), Spring, 2008.

[69] K. Pedersen, I. Z. Kovacs, T. Sørensen, and P. Mogensen, "Review of antenna technologies for macro cells," Nokia Siemens Network - Internal Document, 1H 2009.

[70] 3GPP Technical Report 25.996, "Technical specification group radio access network - spatial channel model for multiple input multiple output (mimo) simulations," 3GPP, September 2003.

[71] L. Thiele, T. Wirth, K. Borner, M. Olbrich, and V. Jungnickel, "Modeling of 3d field patterns of downtilted antennas and their impact on cellular systems," International ITG workshop on Smart Antennas WSA Berlin Germany, February 2009.

[72] F. Gil, A. Claro, J. Ferreira, C. Pardelinha, and L. Correia, "A 3d interpolation method for base station antenna radiation patterns," IEEE Antennas and Propagation Magazine 43(2), April 2001.

[73] T. Vasiliadis, A. Dimitriou, and G. Sergiadis, "A novel technique for the approximation of 3-d antenna radiation patterns," IEEE Transactions on Antennas and Propagation, 53(7), July 2005.

[74] H. Asplund, J.-H. Berg, and T. Sørensen, "The influence of base station antenna tilt on path loss," Nordisk Radio Symposium (NRS), Lund, Sweden, November 1999.

[75] M. A. F, F. Josef, and B. Ernst, "Pattern distortion of mobile radio base station antennas by antenna masts and roofs," Microwave Conference, 25th European, September 1995.

[76] 3GPP, "Default enb antenna tilt values for lte-advanced evaluations, r1-084314," 3GPP.

[77] ——, "Selection procedures for the choice of radio transmission technologies of the umts technical requirement, tr 101 112 (umts 30.03)," 3GPP, April,1998.

[78] 3GPP Technical Report, "Universal mobile telecommunication system (umts), selection procedure for the choice of radio transmission technologies of the umts," 3GPP, April 1998.

[79] P. Komulainen and M. Boldi, "Initial report on advanced multiple antenna systems, celtic / cp5-026," Ph.D. dissertation, CELTIC Telecommunication Solutions, 2009.

[80] V. Kotzsch and G. Fettweis, "Interference analysis in time and frequency asynchronous network mimo ofdm systems," in Proceedings of the IEEE Wireless Communications and Networking Conference (WCNC'2010), Sydney, Australia, 18.-21., April 2010.

[81] Nokia Siemens Networks and Nokia, "Setup of comp cooperation areas, r1-091354," 3GPP, 2009.

[82] A. Tolli, "Resource management in cooperative mimo-ofdm cellular systems," Ph.D. dissertation, University of Oulu, 2008.

[83] L. Thiele, T. Wirth, M. Schellmann, Y. Hadisusanto, and V. Jungnickel, "Mu-mimo with localized donwlink base station cooperation and downtilted antennas," IEEE International workshop on LTE evolution, June 2009.

[84] J.Jin, W.QiXing, G.Liu, H.Yang, B.Li, and D.Yang, "A novel cooperative nulti-cell mimo scheme for the downlink of lte-advanced system," IEEE International workshop on LTE evolution, June 2009.

[85] 3GPP, "Performance evaluation of coherent su and mu comp for lte-a," TSG-RAN1 57bis R1-092430, Jule 2009.

[86] ——, "Preliminary comp gains for itu micro scenario," TSG-RAN1 57bis R1-092691, Jule 2009.

[87] ——, "Performance evaluation of downlink comp," TSG-RAN1 57bis R1-092777, Jule 2009.

[88] ——, "Performance estimate on comp joint transmission," TSG-RAN1 57bis R1-092479, Jule 2009.

[89] ——, "Evaluation of dl comp gain considering rs overhead for lte-advanced," TSG-RAN1 56bis, March 2009.

[90] M. Andreas, F. Philipp, and S. Joachim, "Performance of the lte uplink with intra-site joint detection and joint link adaptation," in Proceedings of the IEEE Vehicular Technology Conference (VTC), Spring, May 2010.

[91] V. Stencel, A. Muller, and P. Frank, "Lte advanced-a further evolutionary step for next generation mobile networks," IEEE 20th International Conference Radioelektronika, 2010.

[92] G. M., M. P., Z. Rong, and F. G., "Field trial results for a coordinated multi-point uplink in cellular systems," IEEE Smart Antennas (WSA), 2010 International ITG Workshop, February 2010.

[93] 3GPP Technical Specifications 36.214, "Evolved universal terrestrial radio access (e-utra) and evolved universal terrestrial radio access network (e-utran),physical layer measurements, version 8.0.0," 3GPP, September 2009.

[94] M. Lalam, R. Visoz, and A. Berthet, "A fast prediction method to optimize link adaptation for ic receivers," in Proceedings of the IEEE ISWCS Reykjavik Iceland, October 2008.

[95] Klaus I. Pedersen and Akhilesh Pokhariyal, "Non-ideal serving cell selection for uprise lte dl," NSN Internal Document, 2006.

[96] Naizheng Zheng and Claudio Rosa and Jeroen Wigard, "Intra-site sector macro combining with interference management in uplink lte networks," NSN Internal Document, 2008.

[97] Mohit Garg, "Multi-user detection," http://www.mohrahit.in/find/multi-user-detection.pdf, 2000.

[98] L. Z., X. P., S. T. B., and V. B., "Spatial frequency scheduling for uplink sc-fdma based linearly precoded lte multiuser mimo systems," in Proceedings of the European Transactions on Telecommunications, pp. 11, 2010.

[99] A. E. Gamal and T. Cover, "Multiple user information theory," In Proceeding of IEEE, vol.68, no.12, pp. 1466-1483, December 1980.

[100] R. Lupas and S. Verdu, "Linear multiuser detectors for synchronous code-division multiple-access channels," IEEE Transaction Information Theory, vol.35, pp.123-136, January 1989.

[101] U. Madhow and M. L. Honig, "Mmse interference suppression for direct-sequence spread-spectrum cdma," IEEE Transaction Communications, vol.42, pp.3178-3188, December 1994.

[102] A. D. Hallen, "Decorrelating decision-feedback multiuser detector for synchronous code-division multiple-access channels," IEEE Transaction Communications, vol.41, pp.285-290, February 1993.

[103] M. K. Varanasi and B. Aazhang, "Near-optimum detection in synchronous code-division multiple-access systems," IEEE Transaction Communications, vol.39, pp.725-736, May 1991.

[104] ——, "Multistage detection in asynchronous code-division multiple-access communications," IEEE Transaction Communications, vol.38, pp.509-519, April 1990.

[105] P. Patel and J. Holtzman, "Analysis of a simple successive interference cancellation scheme in a ds/cdma system," IEEE Journal Selection Areas Communications, vol.12, pp.796-807, June 1994.

[106] D. Gesbert, M. Kountouris, R. W. H. Jr., C.-B. Chae, and T. Salzer, "From single user to multiuser communications: Shifting the mimo paradigm," IEEE Signal Processing Magazine, 2007.

[107] N. Chiurtu and J. Ayadi, "Multi-user multiple antenna systems in uplink ofdm communications," 16th IEEE International Conference on Electronics, Circuits, and Systems (ICECS), December 2009.

[108] L. Thiele, M. Schellmann, T. Wirth, and V. Jungnickel, "Cooperative multi-user mimo based on limited feedback in downlink ofdm systems," Signals, Systems and Computers, 42nd, Asilomar Conference, October 2008.

[109] J. G. Andrews, "Interference cancellation for cellular systems: A contemporary overview," IEEE Wireless Communication, April 2005.

[110] R. Prasad, M. I. Rahman, S. S. Das, and N. Marchetti, Single- and Multi-Carrier MIMO Transmission for Broadband Wireless Systems. River Publisher, 2008.

[111] K. C. Beh, A. Doufexi, and S. Armour, "Performance evaluation of hybrid arq schemes of 3gpp lte ofdma system," IEEE International Symposium on Personal, Indoor and Mobile Radio Communications (PIMRC), 2007.

[112] B. Zhu, N. Ansari, and Z. Siveski, "Convergence and stability analysis of a synchronous adaptive cdma receiver," IEEE Transaction on Communications, December 1995.

[113] R. Sandra, D. Fernando, B. Carmen, P. Gema, G. Alberto, and A. Vicenç, "Recent advances in mimo wireless systems," Waves, pp.115-123, 2009.

[114] J. Shen and Z. Ding, "Blind mmse cdma detection in multipath channels," IEEE Workshop on Signal Processing Advances in Wireless Communications, SPAWC, 1999.

[115] G. Berardinelli, L. A. M. R. de Temino, S. Frattasi, T. B. Sorensen, P. Mogensen, and K. Pajukoski, "On the feasibility of precoded single user mimo for lte-a uplink," Journal of Communications, Vol 4, No 3 (2009), pp. 155–163, April 2009.

[116] M. Schellmann, L. Thiele, T. Haustein, and V. Jungnickel, "Spatial transmission mode switching in multi-user mimo-ofdm systems with user fairness," IEEE Transactions on Vehicular Technology, 2009.

[117] H. Yuan and P. Skov, "Ul multi-user mimo implementation," Nokia Siemens Network - Internal Document, 2009.

[118] G. Berardinelli, B. E. Priyanto, T. B. Sørensen, and P. Mogensen, "Improving sc-fdma performance by turbo equalization in utra lte uplink," in Proceedings of the IEEE Vehicular Technology Conference (VTC) Singapore, pp. 2557–2561, May 2008.

[119] Fernando H. Gregorio, "Multiuser detection for sdma ofdm," http://www.comlab.hut.fi/opetus/333/2004_2005_slides/Multiuser_detection_text.pdf, 2004.

[120] V. Kuhn, "Linear and nonlinear multi-user detection in coded ofdm-cdma systems," International Conference on Telecommunications (ICC 01), Vol.5,Bucharest,Romania, July 2001.

[121] R. Visoz, A. Berthet, and M. Lalam, "A novel fast semi-analytical performance prediction method for iterative mmse-ic multiuser mimo joint decoding," in Proceedings of GLOBECOM 2008, 2008.

[122] Orange, "R1-090395, performance prediction of turbo-sic receivers for system-level simulations," 3GPP, 2009.

[123] K. I. Pedersen, A. Toskala, and P. E. Mogensen, "Mobility management and capacity analysis for high speed downlink packet access in wcdma," in Proceedings of the IEEE Vehicular Technology Conference, VTC-Fall, 60th, 2004.

[124] E. Telatar, "Capacity of multi-antenna gaussian channels," european Transactions on Telecommunications 10(6), pp 585-569, 1999.

[125] G. Foschini and M. Gans, "On limits of wireless communications in a fading environment when using multiple antennas," Wireless Personal Communications 6(3), pp 311-335, 1998.

[126] Ulrich Barth, "3gpp long -term evolution/system architecture evolution overview," Alcatel, September 2006.

[127] NGMN, "Next generation mobile networks radio access performance evaluation methodology," NGMN, 2006.

[128] Leping Huang, "Handover and ue measurement modeling in freac," Internal Nokia, 2006.

[129] Jean Aicard Fabien, "3gpp tsg ran wg4 r4-070440: Ls on lte measurement supporting mobility," 3GPP, 2006.

[130] Siemens, "Mobile radio simulation environment, requirement specification version 1.0.1 ius," Internal Document, 2006.

[131] 3GPP Technical Report 25.943, "Deployment aspects (release 5), version 5.1.0," 3GPP, 2002.

[132] T. B. Sorensen, P. E. Mogensen, and F. Frederiksen, "Extension of the itu channel models for wideband (ofdm) systems," in Proceedings of the IEEE VTC Dallas Texas USA, September 2005.

[133] H. Asplund, J. Medbo, B. Goransson, J. Karlsson, and J. Skold, "A simplified approach to applying the 3gpp spatial channel model," The 17th Annual IEEE International Symposium on Personal, Indoor and Mobile Radio Communications (PIMRC), 2006.

[134] S. Hamalainen, P. Slanina, M. Hartman, A. Lappetelainen, H. Holma, and O. Salonaho, "a novel interface between link and system level simulations," in Proceedings of ACTS Summit, Aalborg, Denmark, pp. 599-604, October, 1997.